NRL Memorandum Report 3341

12

DARPA-NRL Laser Program

Semiannual Technical Report to Defense Advanced Research Projects Agency 1 July 1975 to 31 December 1975

Laser Physics Branch
Optical Sciences Division

August 1976

NAVAL RESEARCH LABORATORY
Washington, D.C.

SECURITY CLASSIFICATION OF THIS PAGE (When Data Entered)

REPORT DOCUMENTATION PAGE

READ INSTRUCTIONS BEFORE COMPLETING FORM

1. REPORT NUMBER: NRL ~~Memorandum Report~~ 3341	2. GOVT ACCESSION NO.
3. RECIPIENT'S CATALOG NUMBER	
4. TITLE (and Subtitle): DARPA-NRL LASER PROGRAM — SEMIANNUAL TECHNICAL REPORT TO DEFENSE ADVANCED RESEARCH PROJECTS AGENCY — 1 July 1975 to 31 December 1975	5. TYPE OF REPORT & PERIOD COVERED: Interim report on a continuing NRL problem.
	6. PERFORMING ORG. REPORT NUMBER
7. AUTHOR(s): Laser Physics Branch	8. CONTRACT OR GRANT NUMBER(s): DARPA Order-2062
9. PERFORMING ORGANIZATION NAME AND ADDRESS: Naval Research Laboratory, Washington, D.C. 20375	10. PROGRAM ELEMENT, PROJECT, TASK AREA & WORK UNIT NUMBERS: NRL Problems N01-48 & K03-53, ~~Project 5E20~~
11. CONTROLLING OFFICE NAME AND ADDRESS: Defense Advanced Research Projects Agency, Arlington, Virginia 22209	12. REPORT DATE: August 1976
	13. NUMBER OF PAGES: 174
14. MONITORING AGENCY NAME & ADDRESS (if different from Controlling Office)	15. SECURITY CLASS. (of this report): UNCLASSIFIED
	15a. DECLASSIFICATION/DOWNGRADING SCHEDULE

16. DISTRIBUTION STATEMENT (of this Report)
Approved for public release; distribution unlimited.

17. DISTRIBUTION STATEMENT (of the abstract entered in Block 20, if different from Report)

18. SUPPLEMENTARY NOTES

19. KEY WORDS (Continue on reverse side if necessary and identify by block number)

Lasers	Chemical kinetics
Electrical lasers	Electronic state lifetimes
Chemical lasers	Energy transfer
Laser diagnostics	Chemiluminescence
Electronic state lasers	

20. ABSTRACT (Continue on reverse side if necessary and identify by block number)

The DARPA-NRL Laser Program is concerned with the development of laser technology in three project areas: chemical infrared lasers, electrical infrared lasers and electronic-state lasers. The chemical infrared laser program includes studies of pulsed HCl laser systems and molecular energy transfer processes. Data have been collected which suggests that intramolecular energy transfer occurs in SF_6 at a rate 10^8 times the gas kinetic collision rate.

The electrical infrared program emphasizes electric-discharge gasdynamic lasers and electron-beam pumping of potential laser systems in the mid-infrared. Several new energy transfer lasers

(Continues)

DD FORM 1 JAN 73 1473 EDITION OF 1 NOV 65 IS OBSOLETE
S/N 0102-014-6601

SECURITY CLASSIFICATION OF THIS PAGE (When Data Entered)

20. Abstract (Continued)

have been discovered and a detailed discussion of the study of direct excitation HCl lasers is given.

A numer of excitation approaches are being evaluated for application to electronic state gas lasers. A most important step in the development of rare-gas halide lasers is the reporting here of the operation of XeF and KrF lasers in self-sustained discharges. Chemical pumping of atomic states is shown to lead to sufficient population for lasing and related quenching studies are described. Transverse discharge excitation of metal vapor lasers has been reduced to practice and coherent anti-Stokes Raman spectroscopy is being developed for probing the number density and vibrational temperature of gaseous species in a lasing medium.

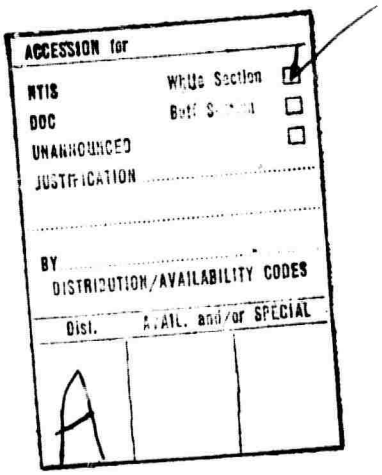

TABLE OF CONTENTS

APPENDICES

FOREWORD

The Laser Physics Branch of the Optical Sciences Division, Naval Research Laboratory, Washington, D. C., prepared this semiannual report on work sponsored by the Defense Advanced Research Projects Agency, DARPA Order 2062. Co-authors of the report were J. R. Airey, R. Burnham, L. Champagne, N. Djeu, J. Eversole, J. G. Eden, D. Frankel, N. W. Harris, G. A. Hart, A. L. Harvey, M. C. Lin, T. J. Manuccia, S. K. Searles, J. A. Stregack, W. S. Watt, and B. Wexler.

SEMIANNUAL TECHNICAL REPORT

REPORTING PERIOD

1 July 1975 - 31 December 1975

1.	DARPA Order	2062, Amendment No. 5
2.	Program Code Number	5E20
3.	Name of Contractor	Naval Research Laboratory
4.	Effective Date of Contract	1 July 1972
5.	Contract Expiration Date	30 June 1976
6.	Amount of Contract	$550,000
7.	Contract Number	62301E
8.	Principal Investigator	J. R. Airey
9.	Telephone Number	(202) 767-3217
10.	Project Scientist	W. S. Watt
11.	Telephone Number	(202) 767-2074
12.	Title of Work	DARPA/NRL Laser Technology Program

SPONSORED BY

DEFENSE ADVANCED RESEARCH PROJECTS AGENCY

DARPA Order No. 2062

DARPA-NRL LASER PROGRAM
SEMIANNUAL TECHNICAL REPORT
TO DEFENSE ADVANCED RESEARCH PROJECTS AGENCY
1 July 1975 to 31 December 1975
CHEMICAL INFRARED LASERS

1. Pulsed HCl Chemical Laser

The initial small-scale experiments to evaluate fuels for pulsed HCl chemical lasers have been described previously.[1] During this period the effort has been directed toward the testing of the best candidates in a larger volume e-beam sustainer apparatus.

As a result of difficulties which arose (see later) in the electrically-excited HCl laser studies, the progress to date has been entirely in the design and construction of an improved laser chamber. This chamber is made from monel to minimize attack by HCl, includes features to allow uniform cooling of the gases and allows extensive diagnostics of the e-beam characteristics.

Since it is also anticipated that rare-gas halide laser systems will be studied in this apparatus, safety features necessary for the use and disposal of fluorine have been installed.

The chamber fabrication is nearing completion and will be installed in the next several weeks. After beam diagnostic studies, experiments related to pulsed HCl laser systems will be undertaken.

2. Polyatomic Energy Transfer

During this reporting period, efforts were continued to measure vibrational energy transfer (V-V) rates in polyatomic molecules. Most of the essential apparatus was on hand prior to July and has been

described previously. However, the detectors available were found to have a risetime which was too long to utilize the full speed of the nanosecond pumping pulses. This problem was eliminated by the procurement of a new detector from the Santa Barbara Research Corporation. This detector, a Ge:Hg photoconductor mounted in a Model 9145-2HS high speed liquid helium dewar, was tested and found to have a response time better than that of the measuring system and sensitivity about 10^3 greater than that of the original detectors.

The apparatus was modified to incorporate a 1,000 torr pressure sensing head in the sample system which, in conjunction with the 10 torr head, permits the entire pressure range of interest to be covered without gas contact with mercury and maintains 4-digit precision. In addition, a lens pair was inserted into the probe laser beam path between the sample cell and detector. This arrangement increased the optical collection efficiency to nearly 100%. The apparatus is sketched in Fig. 1.

A shutter was placed in front of the probe laser so that the sample and detector were illuminated for only several milliseconds before and after the arrival of the pumping pulse. This reduces the boil-off rate of liquid helium in the detector dewar, minimizes heating effects in the sample, and provides a trigger signal to the nanosecond laser.

Energy transfer data were obtained by pumping SF_6 with a 2 ns pulse (FWHM) of CO_2 P(20) radiation while probing with any CO_2 transition from P(20) to P(36). These probe measurements indicate the

presence of molecules in excited levels other than the $v_3 = 1$ level which is filled by the pumping pulse. Because the results indicated a very fast nonexponential risetime which did not get faster as the gas pressure was increased, it was thought that perhaps the transit time through the 76 cm long cell could be a limitation. This possibility was rejected when substitution of a 10 cm long cell produced identical results. A schematic energy level diagram of the double resonance effect is shown in Fig. 2.

The measured transmission intensities were not exponential but were almost linear over most of their duration. While the amplitude varied with gas pressure, the shape of the absorption curve was invariant with pressure and mixture composition and was observed to be an integral of the pumping laser pulse itself. This is illustrated in Fig. 3a, which shows the double resonance signal when probing on the P(28) line of the CO_2 10 μ transition. For comparison, a trace of a pumping pulse as well as the detector's response to a small fraction of such a pulse were obtained on previous "shots" and are shown in Fig. 4.

For the double resonance signal to be an integral of the pumping pulse nearly steady state pumping conditions must exist, i.e., the lower pumped level must be replenished, and the upper pumped level depleted at a high enough rate so that saturation effects do not become important. The onset of saturation would be seen by the double-resonance signal ceasing to rise before the end of the pulse. Another indication that saturation is not reached is illustrated in Fig. 3b,

which shows the double resonance signal obtained by probing the pumped transition. There is in this case a rapid rise in transmission followed by a return to equilibrium, due predominantly to rotational relaxation of the ground state, at a rate (τ = 2.9 ns) near the detector's own recovery rate. Under the conditions of the experiment this gives a value of - 3 x 10^9 s^{-1} $torr^{-1}$ as the rate at which the lower level being pumped returns to equilibrium. A lower limit to the rate at which molecules in the upper pumped levels undergo energy transfer and appear in the excited vibrational manifold is 10^{10} s^{-1} $torr^{-1}$, which is 10^3 times the gas kinetic collision rate.

This extremely fast V-V energy transfer rate is difficult to explain in the framework of conventional theories of energy transfer. The most reasonable explanation is that the high infrared fields cause sufficient mixing of the wavefunctions of the vibrational fundamentals of SF_6 that they are effectively coupled together. The high density of vibrational levels near 1,000 cm^{-1} and above presumably contribute to this effect while the lower lying fundamental and overtone levels of SF_6 have considerable population at 300 K. High resolution diode-laser spectra show that the highly overlapped absorption features give rise to a continuum which underlies the discrete, highly complex ground state absorption features. A theoretical approach to energy transfer is needed which takes these aspects of the problem into account. Experiments to further investigate this intriguing phenomenon are continuing.

In December, progress was being made toward creating a low power laser absorption apparatus for the purpose of measuring absorption coefficients of molecular gases at CO_2 laser wavelengths. This measurement will identify molecules which may be useful in an isolation cell of a multistage CO_2 laser oscillator-amplifier system. A lock-in amplifier with a ratio electronics option was purchased and finally accepted after adjustments by the manufacturer. This lock-in with ratio option is to be the primary instrument in the absorption measurements, since it can compensate for laser power variation and yield percent transmission data directly. Much of the rest of the apparatus was on hand and fabrication of the remaining pieces is nearing completion. It is estimated that final assembly will be completed in one month and that preliminary experiments with a variety of molecules will begin at that time.

One other effort, related to that mentioned above, was begun in December. This is the construction of a gas handling apparatus in which the mixed deuterium isotopes of ammonia, NHD_2 and NH_2D can be synthesized. These molecules will be studied as possible gain suppressors in large, high gain, CO_2 laser amplifiers. Construction and testing were nearly complete by the end of the month. Synthesis and evaluation of the products will begin soon after testing is complete.

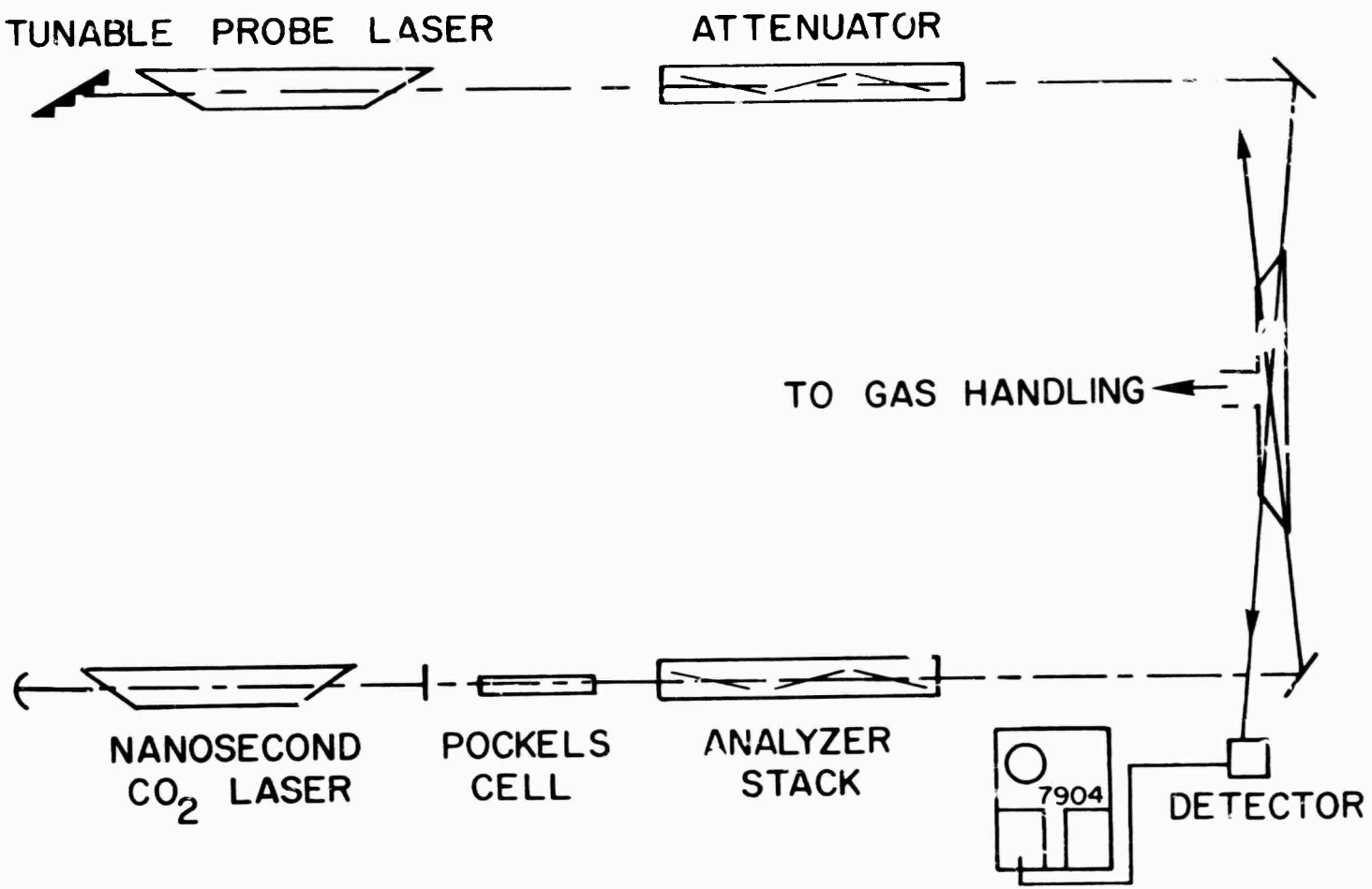

Fig. 1 — Infrared double resonance apparatus. Not shown is a lens pair in the probe laser beampath between the sample cell and detector.

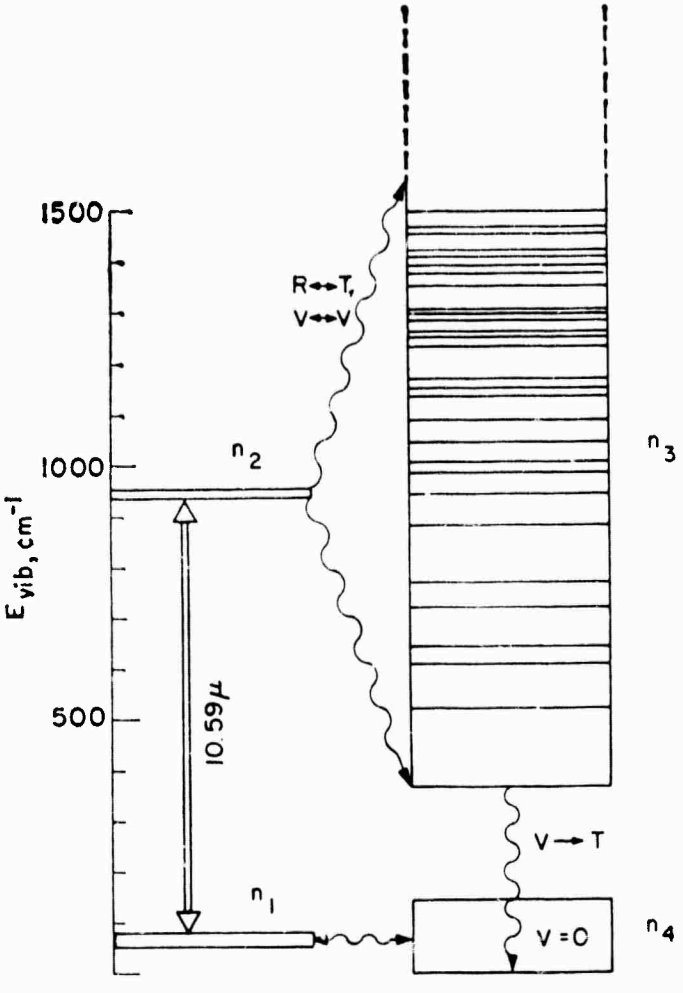

Fig. 2 — Energy level diagram of SF_6. The double arrow represents pumping by the nanosecond laser. The levels in the upper right hand part of the diagram are in rapid equilibrium with each other. The V-T relaxation step occurs on a microsecond time scale and does not concern us here.

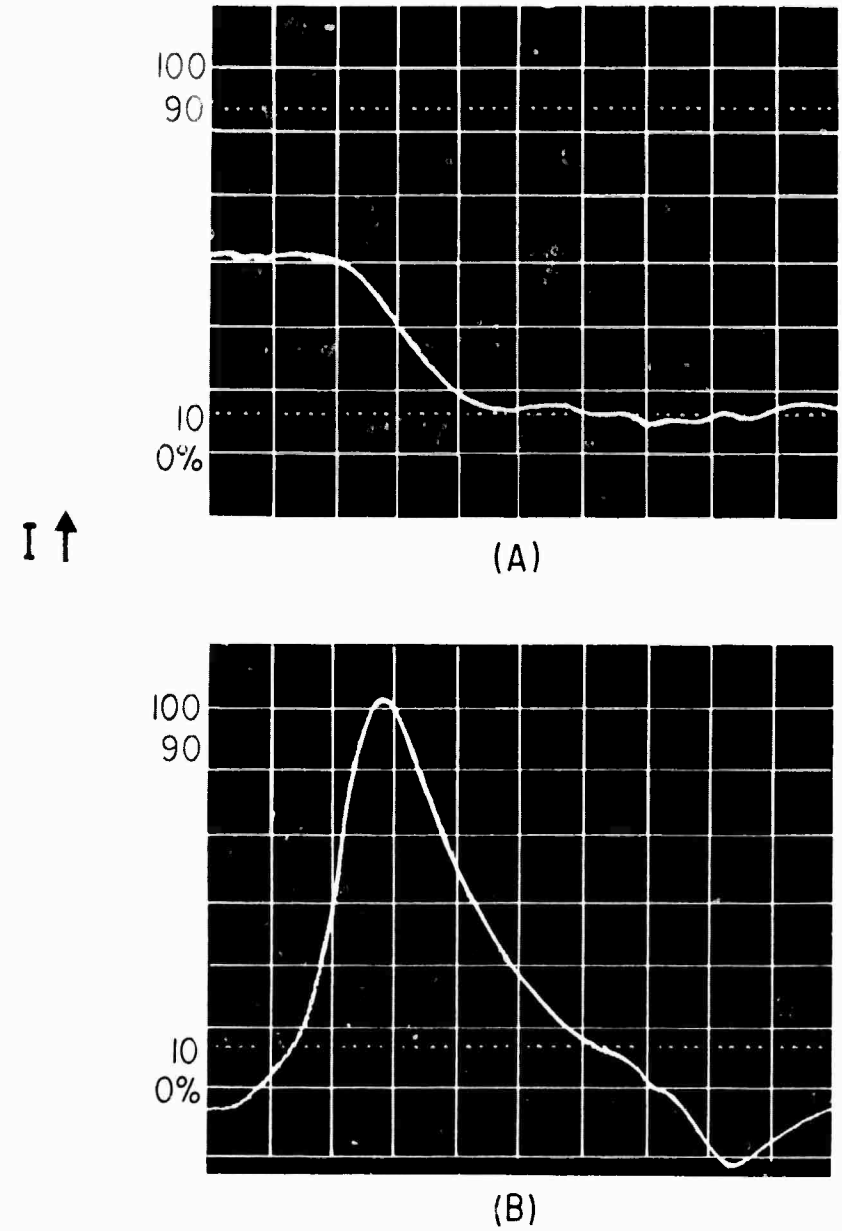

Fig. 3 — Infrared double resonance signals. (A) probed at P(28), horizontal axis 2 ns/div; (B) probed at P(20), horizontal axis 2 ns/div. The indicated intensity is that reaching the detector, so that A indicates induced abosrption in the sample, while B shows partial saturation of the transition being pumped.

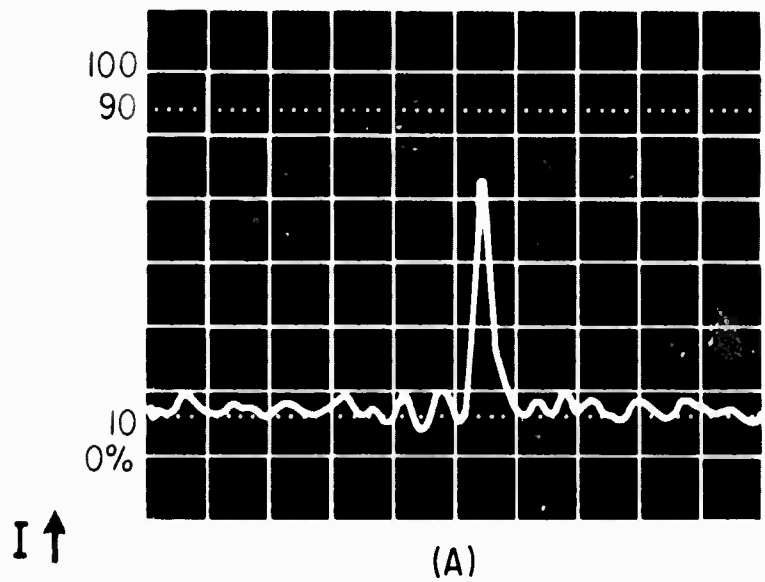

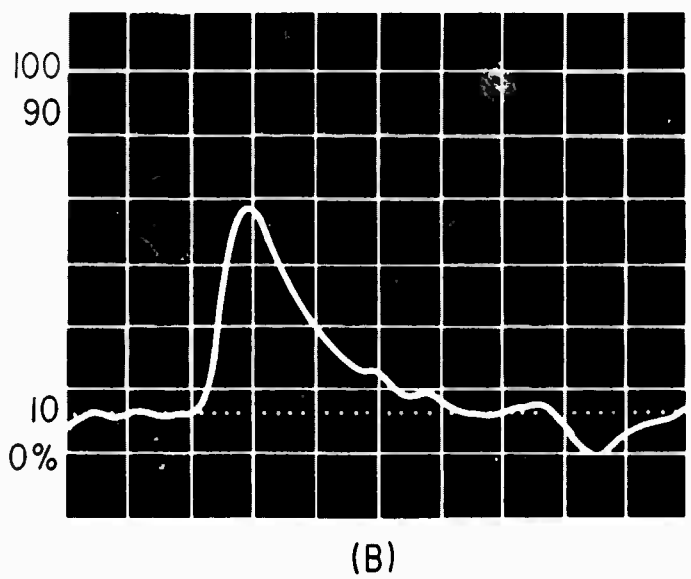

Fig. 4 — Nanosecond laser pulse detected with: (A) photon drag detector, horizontal scale 5 ns/div; (B) signal detector, horizontal scale 2 ns/div

ELECTRICAL INFRARED LASERS

1. Electric Discharge Gasdynamic Lasers

In the Electric Discharge Gasdynamic Laser (EDGDL) facility, experiments are aimed at producing new and efficient cw electrical lasers. While primary interest is in the 3-5 micron region, potential new lasers in other regions of the infrared are also being investigated. Since several attractive candidate molecules have not been made to lase by direct electron impact, attempts are being made to produce inversions by energy transfer from selected diatomic molecules (deuterium, hydrogen, nitrogen or carbon monoxide) excited in an electric discharge.

A description of the EDGDL facility has been given in previous reports.[1-4] During this reporting period four new cw electrical laser systems were demonstrated. N_2O was made to lase via vibrational energy transfer from both CO and D_2, and transfer from CO was used to produce both CS_2 and C_2H_2 lasers. In addition, the apparatus was modified in order to achieve arc-free glow discharges at plenum pressures up to 200 torr. The computer model for the D_2-HCl system has been completed and used to both explain existing data and to provide guidance for future experiments.

Operating characteristics of the new laser systems are described in two publications[5,6] (see Appendices 1 and 2). This work was

performed before the apparatus was modified and, therefore, utilized He diluent. Because of the difficulty in maintaining a stable arc-free glow discharge in Argon-diatom mixtures as well as in the CO-He mixtures, it was decided to modify the excitation plenum. The rectangular pyrex plenum with twenty-six individually ballasted electrodes was redesigned and now consists of ten pyrex tubes. At the downstream end of the plenum, the tubes connect into a lucite block which serves as a transition section to match up to the nozzle array. On the upstream end the tubes extend into another lucite block. Each tube is terminated by a nylon cap through which both the gas enters and the electrode is inserted into the tube. A pin which has been rounded on the end extends through the back plate of the lucite chamber and through the back of the nylon cap. These pins are individually ballasted (200 KΩ) and serve as the cathodes.

A series of holes have been drilled into the cylindrical walls of the nylon caps such that they are offset from the radial direction. The premixed plenum gas is injected through these holes in such a manner as to induce a swirling flow in the gas. This has helped to sustain arc-free operation and hence better laser performance.

Using the new plenum, stable glow discharges were run in both argon and helium mixtures of deuterium, nitrogen, and carbon monoxide up to the current capacity limit (500 ma) of the power supply. During some of these experiments individual 8 henry chokes were connected in series to each pin to further prevent arcing.

C_2H_2 laser experiments using the new plenum produced 0.5 watts coupled out of the cavity through a 0.5 mm hole which has a geometric outcoupling of approximately 0.1 percent. These results represent a five-fold increase in outcoupled power compared to the low current results previously reported.[6] The intracavity flux is of the order of 1 kw which demonstrates the energy storage capability of C_2H_2.

The computer model for the D_2-HCl system prepared by Physical Sciences, Inc. of Wakefield, MA, has been completed. The model assumes an instantaneously mixed gas at specified conditions (pressure, vibrational temperatures, gas temperature, etc.) and takes into account the gasdynamic and kinetic proceeses that occur in the EDGDL. Two sets of computer runs have been made to date; the first set is to examine the potential of a D_2-HCl e-beam sustained EDGDL operating from a 1 atmosphere plenum, while the second is to examine the predicted properties for actual experimental conditions achieved in the present apparatus. Figures 5 and 6 give predicted maximum gains in a given HCl vibrational band at one atmosphere pressure starting from initial D_2 vibrational temperatures of 1250 K and 1500 K. These are characteristic of the D_2 vibrational temperatures inferred from the earlier low pressure D_2-CO_2 gain studies[4]. It should be noted that the rotational line for maximum gain in a given vibrational band changes along the flow direction of the EDGDL. Figure 7 shows the predicted peak gain of any individual line as a function of initial D_2 vibrational temperature and demonstrates the desirability of obtaining as high an initial D_2 vibrational temperature as possible. Figures 8 and 9 show the predicted gains for a 700 torr plenum case

which is close to conditions actually run in the EDGDL with initial D_2 vibrational temperatures of 1250 K and 1500 K. For the 1500 K temperature case the predicted gain is sufficient to sustain lasing in the EDGDL, while for the 1250 K case, lasing would be marginal. Subject to the 500 ma limit of the power supply, experiments were performed both at 160 torr and 198 torr plenum pressures and HCl fluorescence was monitored at wavelengths greater than 4.1 microns. The fluorescence from the lower plenum pressure experiments was the greater, from which it is inferred that insufficient current was available to excite the additional D_2 used in the higher plenum pressure case and hence that the effect of the additional D_2 is to lower the effective D_2 vibrational temperature. The earlier estimate of a D_2 vibrational temperature of 1500 K was at still lower plenum pressures, approximately 60 torr. Therefore, at these elevated pressure (160-200 torr) and limited current conditions the vibrational temperatures achieved would appear to be substantially lower than 1500 K and hence preclude lasing.

In order to gain confidence in the model, HCl fluorescence scans were taken far downstream of the nozzles to minimize any effects of mixing in the EDGDL. The measured fluorescence was found to qualitatively follow the predictions of the model.

In order to increase the D_2 vibrational temperature two experimental approaches will be taken. The first will be to attempt to lower the ballast resistance on each pin so that a lower voltage but higher current (6 amps) power supply can be used. The second will be to use an e-beam sustained discharge. A sustainer chamber has

been fitted to the e-beam and voltage breakdown experiments performed. For the mixtures of interest, the E/N predicted for optimum vibrational excitation are achievable.

Present plans call for improving the discharge in order to increase the plenum vibrational temperature. Nozzles will be designed and fabricated to use with the e-beam sustained discharge in order to operate at higher plenum pressures. With the present apparatus further study in order to better characterize the previously demonstrated laser systems will be performed in addition to undertaking the investigation of several new potential cw laser systems.

References

1. NRL-ARPA Laser Program Semiannual Technical Report, 1 July-31 December 1973, NRL Memorandum Report 2846.

2. NRL-DARPA Laser Program Semiannual Technical Report, 1 January-30 June 1974, NRL Memorandum Report 3005.

3. NRL-DARPA Laser Program Semiannual Technical Report, 1 July-31 December 1974, NRL Memorandum Report 3084.

4. NRL-DARPA Laser Program Semiannual Technical Report, 1 January-30 June 1975, NRL Memorandum Report 3217.

5. J.A. Stregack, B.L. Wexler, and G.A. Hart, Appl. Phys. Lett. 27, 670 (1975).

6. J.A. Stregack, B.L. Wexler, and G.A. Hart, Appl. Phys. Lett. 28, 137 (1976).

7. R. McCleary and W.E.K. Gibbs, IEEE J. Quantum Electron. QE-9, 828 (1973).

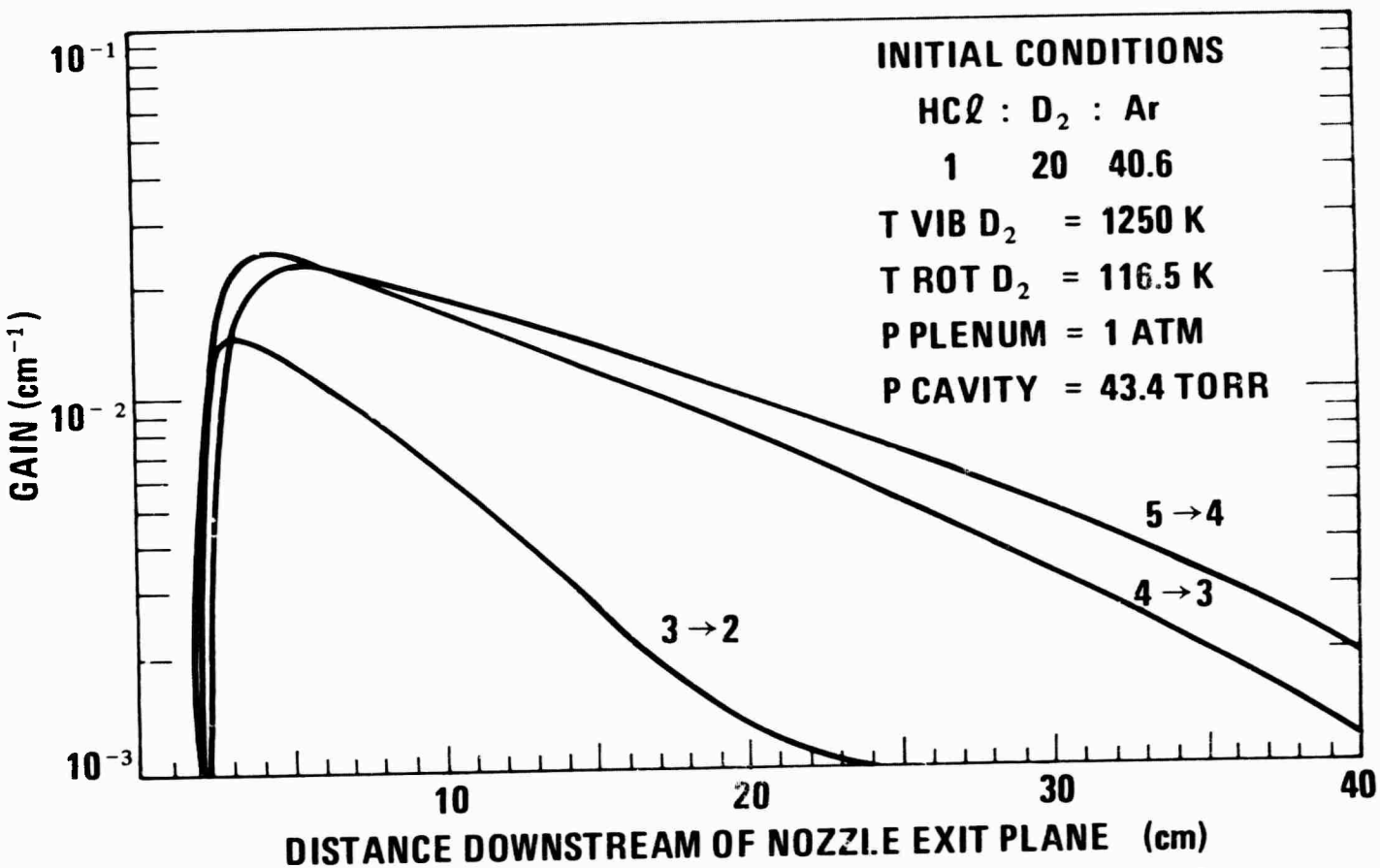

Fig. 5 — Computed maximum gain in the given HCl vibrational bands for a one atmosphere plenum pressure and an initial D_2 vibrational temperature of 1250 K

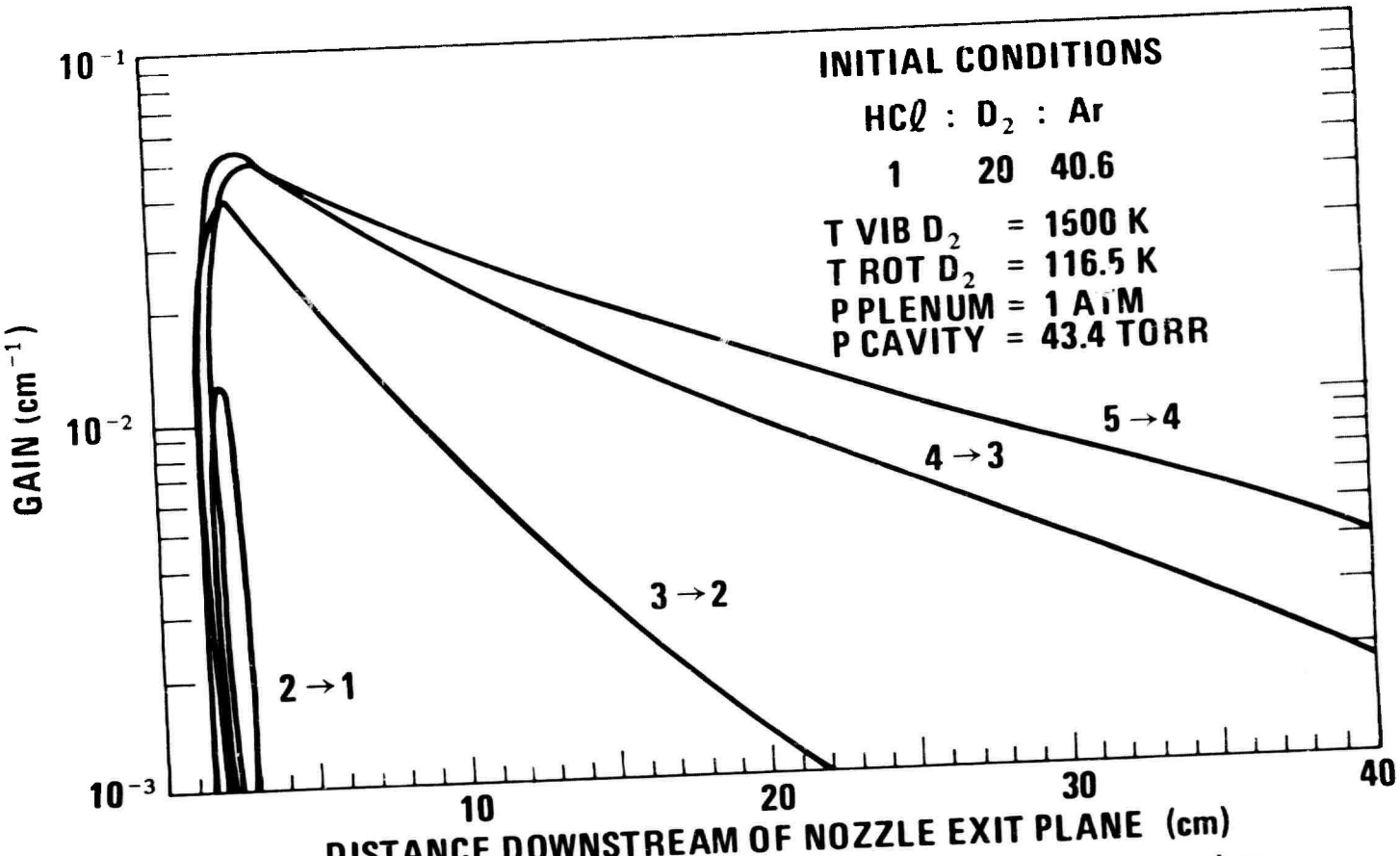

Fig. 6 — Computed maximum gain in the given HCl vibrational bands for a one atmosphere plenum pressure and an initial D_2 vibrational temperature of 1500 K

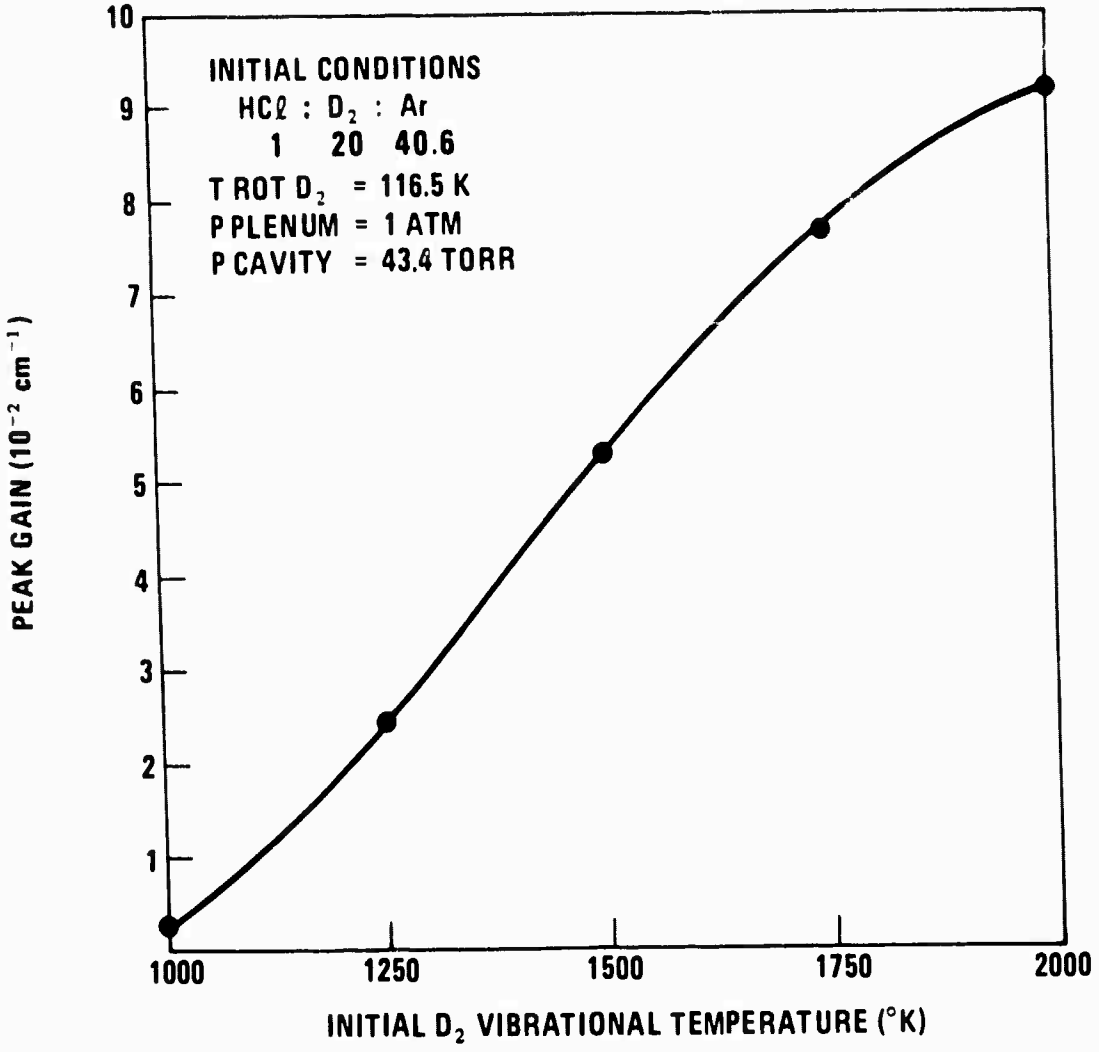

Fig. 7 — Predicted peak gain as a function of initial D_2 vibrational temperature for a one atmosphere plenum pressure

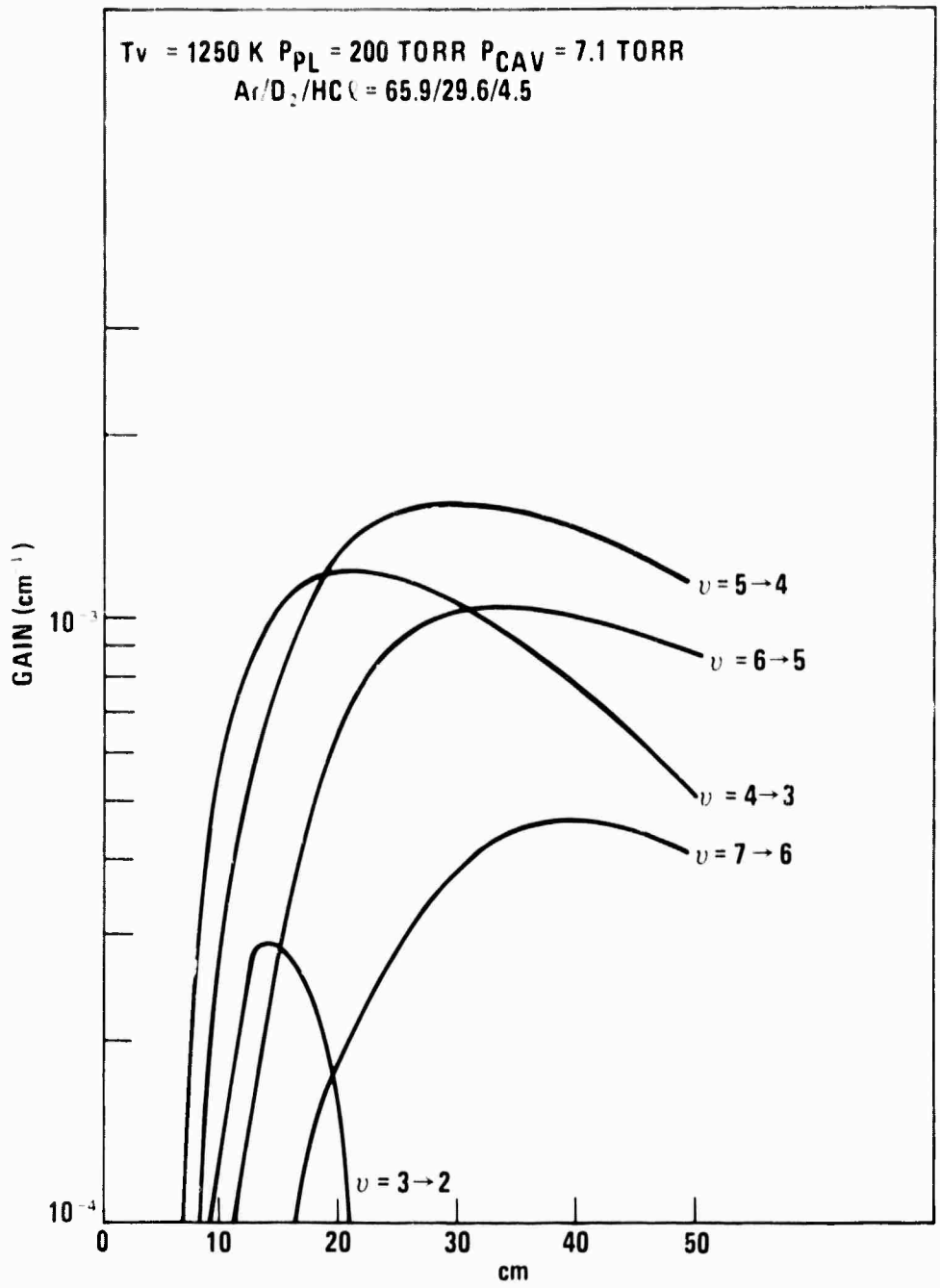

Fig. 8 — Computed maximum gain in the given HCl vibrational bands for a 200 torr plenum pressure and an initial D_2 vibrational temperature of 1250 K

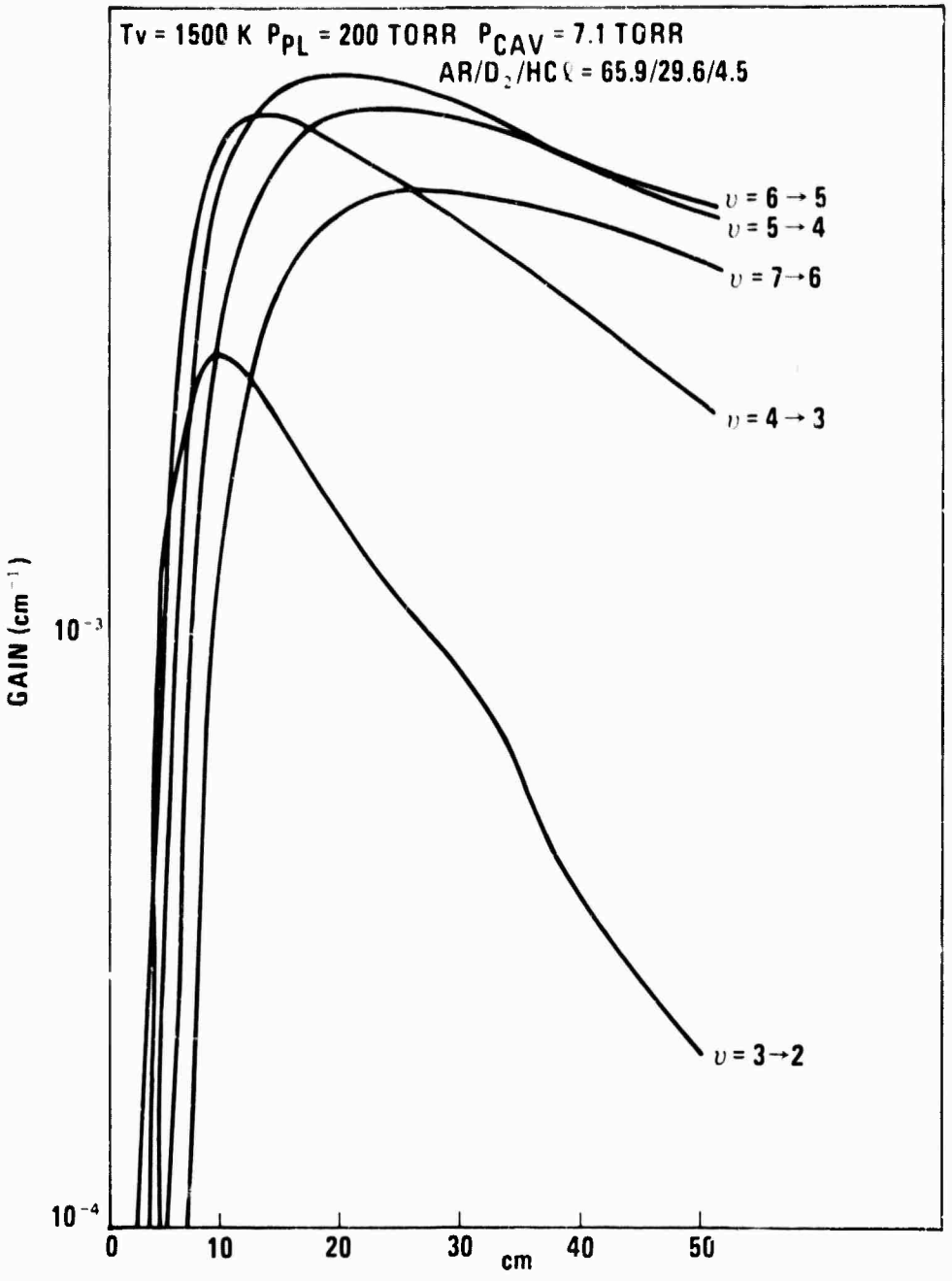

Fig. 9 — Computed maximum gain in the given HCl vibrational bands for a 200 torr plenum pressure and an initial D_2 vibrational temperature of 1500 K

2. E-Beam Sustainer Pumped HCl Laser

The objective of the HCl pulsed electrical infrared laser program for this reporting period was to determine if the ~1%/cm gain predicted by a kinetic model of the e-beam sustainer pumped HCl system could be observed. Negative results encountered in these experiments indicated that at least one, and possibly more, important processes not included in the kinetic model strongly influenced the electrical behavior of the discharge. This prompted a series of experiments to be conducted to quantitatively characterize the performance of the NRL Maxwell cold cathode e-beam/sustainer. These measurements were made both with and without gases for which the transport properties are known in the discharge chamber. The results of these experiments indicated that this particular program should be terminated and established important guidelines for the implementation of any similar program in the future.

2.1 Kinetic Model Calculations

a. Electron-HCl Cross Sections

Early in this reporting period efforts to generate an accurate set of electron-HCl collisional interaction cross-sections and to use these cross-sections as input to a kinetic model of the proposed HCl electric discharge laser produced significant results. In conjunction with the experimental study being conducted at NRL the electron-HCl transport data of Bailey and Duncanson[1] was used by Physical Sciences Incorporated (PSI) to construct a self-consistent set of cross sections for HCl. From the Bailey and Duncanson[1]

data it is possible to obtain an estimate of the electron drift velocity v_d and characteristic electron energy ε_K as a function of the Townsend parameter E/N[2]. This swarm data can then be used in the Frost and Phelps[3] analytical method to solve the Boltzmann equation for the HCl cross sections. Table I shows the agreement between the drift velocities derived from the Bailey and Duncanson[1] data and those predicted from the PSI cross section set. Table II draws the same comparison for the characteristic electron energy. Figure 10 displays the electron-HCl cross section set that produces these results. Shown in the figure are the overall momentum transfer cross section and the various contributions to this cross section; the resonant cross sections for HCl vibrational excitation into v = 1 and v = 2, the dissociative attachment cross section, the electronic excitation cross section and the ionization cross section. The shape and magnitude (1.3×10^{-15} cm^{-2} peak) of the HCl (v = 1) vibrational excitation cross section shown in Figure 10 are those reported by Rohr and Linder[4]. This cross section is in good agreement with the electron impact vibrational excitation rate constant measurements of Center and Chen[5] for HCl, when their experimental data is corrected for the error introduced by assuming that the HCl(v = 1) population had reached steady state during a sustainer pulse of 100 microseconds[6]. The HCl(v = 2) vibrational excitation cross section was also obtained by using the basic shape of the Rohr and Linder[4] cross section. The cross section was shifted to higher electron energies to reflect the difference between the v = 1 threshold of 0.357 eV and the v = 2 threshold of 0.703 eV. The

magnitude of the major peak in the v = 2 cross section was determined from the height of the v = 1 peak using the 2:19 ratio that Ziesel, Nenner, and Schulz[7] had determined for this near threshold peak region. The Rohr and Linder[4] v = 1 and v = 2 energy loss data for monoenergetic 3 eV electrons was used to establish the ratio of the two cross sections at that energy. This 17:4 ratio of the v = 1 to v = 2 cross section was assumed to hold for all electron energies more than 0.1 eV in excess of the v = 2 resonsnce energy at 0.703 eV.

Although these vibrational cross sections are of primary importance in determining the maximum gain and efficiency achievable in an electric discharge HCl laser, the other cross sections calculated by PS1 establish the extent to which other important kinetic processes occur. The cross sections for elastic scattering and rotational excitation determine what fraction of the energy delivered to the gas by the discharge will appear as gas heating as opposed to vibrational excitation. Large fractional power transfer to gas heating degrades potential HCl laser performance by reducing the rate of the anharmonic pumping process and thereby decreasing the partial inversion. The dissociative attachment cross section is important because the dissociation products can deactivate vibrationally excited HCl two to three hundred times more rapidly than the already fast HCl self-deactivation process.

$$HCl(v=1) + HCl \rightarrow HCl(v=0) + HCl, \quad k = 2.4 \times 10^{-14} cm^3/sec \text{ [8]} \qquad (1)$$

$$HCl(v=1) + Cl \rightarrow HCl(v=0) + Cl, \quad k = 8.5 \times 10^{-12} cm^3/sec \text{ [9]} \qquad (2)$$

$$HCl(v=1) + H \rightarrow HCl(v=0) + H, \quad k = 6.5 \times 10^{-12} cm^3/sec \text{ [10]} \qquad (3)$$

The extent of dissociative attachment at the E/N values where vibrational excitation is efficiently promoted is clearly a critical factor because of the rapidity of these atomic quenching reactions. The cross section for electronic excitation of HCl to the $A^1\pi$ state is also important because dissociation into H and Cl atoms occurs from this state. The ionization cross section sets an upper limit on the E/N range usable before arcing occurs. The shape of the Rohr and Linder[4] cross section increases the importance of the electronic excitation and ionization cross sections. The low energy peak of the vibrational cross section shown in Figure 10 is narrower than that previously estimated by United Technologies Research Center (UTRC)[11], having about one-third the width of the UTRC cross section in the 0-1 eV region. This unfavorable narrowing is offset by the appearance of a broad secondary peak from 0.45 to 2 eV shown in Figure 10. However to utilize the electrons in the 0.5 to 2 eV region it is necessary to increase the applied E/N_{HCl} from the 8×10^{-16} V-cm^2 that interacts most strongly with 0.4 - 0.7 eV electrons to a value of 1.2×10^{-15} V-cm^2. Going to this higher E/N_{HCl} increases the electron characteristic energy ε_K from 0.25 eV to 0.73 eV. Consequently the high energy tail of the electron energy distribution would be expected to increase ten orders of magnitude in the 10 eV region for the case of a Maxwellian distribution. For this reason the electronic excitation and ionization cross sections must be considered despite their large threshold energies. A detailed picture of the electron energy distribution is required to determine the effect of these processes as a function of E/N_{HCl}.

Because of the importance of these cross sections it should be emphasized that the PSI effort did not produce an exact duplicate of the cross section set that UTRC calculated which is shown in Figure 11. The UTRC results served as a starting point in developing the PSI HCl cross-section package. The most important difference is the previously discussed narrower vibrational excitation peak in the 0.4 - 0.7 eV region and the appearance of a second broad peak from 0.45 to 2 eV. This not only requires the application of a higher E/N_{HCl} but also means that the electron-HCl vibrational excitation cross section is no longer roughly three orders of magnitude larger than the dissociative attachment cross section. Another significant difference is that the PSI cross section for HCl excitation into v = 2 is more comparable to the v = 1 cross section than is the case for the UTRC cross sections.

The importance of the differences between the PSI and UTRC cross sections can best be assessed by comparing the calculated electron-molecule rate coefficients which result when the computed electron energy distributions are integrated with the loss process cross sections. Figure 12 shows the UTRC results for a 10% HCl mixture in helium diluent at various E/N values. Similar results for 9:1 Ar:HCl mixtures as calculated by PSI are shown in Figure 13. Since the diluent gases only make a slight elastic collision contribution to electron energy loss in the mixtures, the results can be compared. The most noticeable differences are the significantly greater rates for HCl (v=0) to HCl (v=2) excitation and HCl dissociative attachment predicted by PSI.

PSI also calculated the fractional energy transfer into vibrational, rotational, and electronic excitation as shown in Figure 14. These results indicate that 87% of the discharge energy can be channeled into vibrational excitation for an E/N_{Total} of 1.2×10^{-16} V-cm^2 or an E/N_{HCl} of 1.2×10^{-15} V-cm^2.

Similar calculations carried out by PSI for a 3.33% HCl mixture in argon diluent are shown in Figure 15 and Figure 16. The shape of the 10% and 3.33% HCl curves are very similar with the only major difference being the E/N_{Total} values responsible for the observed rates and percent energy allocation values. Figure 17 superimposes the calculated electron-molecule rate coefficients for 10% and 3.33% HCl mixtures as a function of E/N_{HCl}. With the exception of the electronic excitation rate constants, the two sets of curves are almost identical. Consequently, superimposing the fractional power transfer curves as a function of E/N_{HCl} again produces near identical curves in Figure 18. This similarity leads to the important conclusion that to a great extent E/N_{HCl} is the parameter which predominantly determines the behavior of the discharge. This conclusion is strongly reinforced by comparing the calculated drift velocity and characteristic energy for 100%, 10% and 3.33% HCl mixtures in argon diluent as a function of E/N_{HCl}. Figure 19, which displays the calculated drift velocities for these three mixtures as a function of E/N_{HCl} illustrates that up to an E/N_{HCl} of 1×10^{-15} V-cm^2 the three drift velocities differ by no more than 10%. Figure 20 shows that the characteristic electron energies as a function of E/N_{HCl} are again similar for the three mixtures. However, in this case a

significant difference between the 3.33% and 10% mixtures does appear at higher E/N_{HCl} values such as 1.8×10^{-15} V-cm^2. This is reflected in the noticeably higher electronic excitation rate coefficient for the 10% mixture compared to the 3.33% mixture in Figure 17. The greater fractional power transfer into electronic excitation at the expense of vibrational excitation is shown in Figure 18. This demonstrates the importance of the previously discussed electronic excitation cross section as the fraction of electrons in the high energy tail increases with increasing E/N_{HCl}.

b. HCl Gain Predictions

Using the electron-molecule rate coefficients derived from the PSI cross sections for HCl, predictions of the gain realizable in the NRL Maxwell e-beam sustainer were calculated. Input required for such calculations included the total pressure of the Ar:HCl mixture, the partial pressure of HCl, the sustainer current density J_s, the discharge pulse length, and the temperature of the gas mixture. Calculations were carried out for several sets of initial conditions using an anharmonic oscillator code developed at PSI which includes all relevant anharmonic pumping reactions as well as quenching and radiative processes. The temperature dependence of all the rate constants used is built into the code. This is an important refinement because of the marked dependence of both the anharmonic pumping reactions[12] and HCl self-deactivation[8] on the translational temperature of the gas.

The inputs for the first case considered were: Ar:HCl 29:1, three atmosphere total pressure mixture at room temperature with a

3 microsecond, $6A/cm^2$ sustainer current pulse. The energy density was chosen because, for the same partial pressure of HCl, 76 torr, in a one atmosphere mixture with Ar, a current of $6A/cm^2$ had been achieved. Since both the three and the one atmosphere mixtures with 76 torr HCl should be dissociative attachment dominated the electron number density production equation determining the peak current attainable is:

$$\frac{dn_e}{dt} = 0 = S - k_a [HCl] n_e \qquad (4)$$

$$n_e = S/k_a [HCl].$$

S, the term denoting the ion production rate of the electron beam used as a source of electrons in the discharge, would be expected to increase linearly with pressure between one and three atmospheres in the NRL device. Consequently the electron number density and sustainer current would be expected to also increase by a factor of three in going to three atmospheres. The choice of $6A/cm^2$ thus represented an extremely conservative estimate of the current to be achieved for three atmosphere operation. The initial reason for choosing to study the three atmosphere case was that if in fact the current tripled, the rate of HCl (v = 1) production from electron impact on HCl molecules would also triple. This in turn would greatly accelerate the key anharmonic pumping step:

$$HCl(v=1) + HCl(v=1) \rightarrow HCl(v=2) + HCl(v=0). \qquad (6)$$

For this set of gas mixture and discharge parameters, peak gains

of 1%/cm, 1%/cm and 1.2%/cm were predicted on P-branch transitions in the 4-3, 5-4 and 6-5 bands. For each of these bands the onset of gain would begin ~3 μsec after the start of the sustainer current pulse and continue for 7 to 12 μsec. It should be noted that at the time these gain prediction calculations for the three atmosphere case were first carried out the complete PSI cross section set had not reached its final form. Consequently, the electron-molecule rate constants plotted in Figure 17 were not available. Instead it was assumed that the rate coefficient for vibrational excitation of HCl into v = 1 would be 1.5×10^{-8} cm^3/sec at the E/N_{HCl} chosen for consideration, 8×10^{-16} V-cm^2. As Figure 17 indicates, a rate constant of 8.5×10^{-9} cm^3/sec is now calculated for this E/N_{HCl} so that the rate coefficient used was too large by a factor of two leading to overoptimistic gain values. To some extent this optimistic value was offset by the absence of any direct pumping of HCl(v=2) by the discharge in the kinetic model used in these preliminary calculations.

When the HCl cross section set was completed and the necessary electron-molecule rate constants computed, more rigorous gain calculations were carried out for a one atmosphere Ar:HCl mixture at room temperature. The same HCl partial pressure of 76 torr was used with a 3 μsec sustainer current pulse of 6A/cm^2, and an E/N_{HCl} of 1.2×10^{-15} V-cm^2. This E/N_{HCl} was chosen because results of PSI fractional power transfer calculations indicated that fractional power transfer to HCl vibrational excitation is a maximum at this value. Figure 21 shows the predicted gain on the four lines with the largest partial inversions.

At first inspection these predicted room temperature peak gains 1-2%/cm seem surprisingly large compared to those calculated in the three atmosphere case with the same partial pressure of HCl. However for a sustainer current of $6A/cm^2$ the one atmosphere case with an E/N_{HCl} of $1.2x10^{-15}V\text{-}cm^2$ has a drift velocity of $5.5x10^6$ cm/sec while the three atmosphere $8x10^{-16}V\text{-}cm^2$ case has a drift velocity of $4.9x10^6$ cm/sec. Consequently at one atmosphere $n_e = 6.82x10^{12}/cm^3$ while at three atmospheres $n_e = 7.65x10^{12}/cm^3$. Coupled with the assumed electron-molecule v = 1 pumping rate constant in the three atmosphere case of $1.5x10^{-9}cm^3/sec$ and the calculated one atmosphere rate constant of $1.3x10^{-9}cm^3/sec$ it would be expected that the three atmosphere case would have significantly higher gain. However, the more than tripled pressure of the argon diluent increases the HCl radiative linewidths enough to negate the effect of this assumed stronger pumping.

The predicted room temperature gains of 1-2%/cm, if realizable, would ensure lasing in the NRL 100 cm path length device. Indeed, even if these predictions were overoptimistic by a factor of ten, stimulated emission should still be observable using a 0.5% transmitting mirror as an output coupler and a total reflector as the second mirror.

These gain predictions were in fact overoptimistic because they did not include important HCl deactivation processes involving H and Cl atoms. These had initially been neglected because preliminary current measurements had been interpreted to indicate that the electron production term for the e-beam source was $3x10^{20}/cm^3$-sec. For this

source term any HCl deactivation caused by the maximum atom concentrations produced would have been negligible when compared to HCl self-deactivation. However, subsequent measurements of the e-beam current transmitted by the foil as well as sustainer currents determined for pure nitrogen at one atmosphere indicated that the actual source term was $2\text{-}3\times10^{21}/cm^3\text{-sec}$. A 3 μsec e-beam pulse would thus produce at least $6\times10^{15}/cm^3$ Ar^+ ions and electrons. For a 9:1 Ar:HCl mixture at an E/N_{HCl} of 1.2×10^{-15} V-cm^2 most of the electrons produced would undergo dissociative attachment within a few nanoseconds via

$$e^- + HCl \longrightarrow Cl^- + H\,, \quad k_a = 1.4\times10^{-10}cm^3/sec\,, \tag{7}$$

where $1/k_a[HCl] = 2.9\times10^{-9}$ sec. With the time dependence of the electron number density given by

$$\frac{dn_e}{dt} = S - k_a n_e [HCl]\,, \tag{8}$$

or

$$n_e = \frac{S}{k_a[HCl]}\left(1 - e^{-k_a[HCl]t}\right)\,, \tag{9}$$

the electron number density at the end of the e-beam pulse is $5.8\times10^{12}/cm^3$. Thus all but 0.1% of the electrons produced by the e-beam immediately react with HCl to yield Cl^- and H.

The Ar^+ produced by the e-beam pulse takes part in one of the following two reactions within a few nanoseconds

$$Ar^+ + HCl \longrightarrow ArH^+ + Cl\,, \quad k \geq 1.3\times10^{-10}cm^3/sec^{(13)}, \tag{10}$$

$$Ar^+ + 2Ar \longrightarrow Ar_2^+ + Ar\,, \quad k = 2\times10^{-31}cm^6/sec^{(14)}\,. \tag{11}$$

More than three quarters of the $6x10^{15}/cm^3$ Ar^+ produced will dissociate HCl according to reaction 10, yielding a Cl atom concentration of $4.6x10^{15}/cm^3$. The products of such reactions must be considered, because a rate constant of $\sim 1x10^{-7} cm^3/sec$ would be expected for the bimolecular ion recombination reaction of Cl^- with either ArH^+ or Ar_2^+. Recombination with Ar_2^+ would yield an additional Cl atom concentration of $1.4x10^{15}/cm^3$. Recombination with ArH^+ could yield either H and Cl as atomic neutrals or HCl as a molecular neutral. It is not necessary for a stable molecule to be formed as an electron is transferred from Cl^- to H^+. Lacking experimental data concerning the actual mechanism of this reaction the assumption is made that half of the Cl^- undergoing this reaction is released as an atomic chlorine concentration of $2.3x10^{15}/cm^3$.

For this 9:1 Ar:HCl mixture at 1 atmosphere and an E/N_{HCl} of $1.2x10^{-15}$ V-cm^2 the rate constant for electronic excitation of HCl by electron impact is $1.4x10^{-11} cm^3/sec$. Consequently, $6x10^{14}/cm^3$ HCl molecules are excited to the A $^1\Pi$ state by a 3 μsec discharge with $n_e = 5.8x10^{12}/cm^3$. Again, the assumption is made that half of these excited molecules subsequently dissociate producing H and Cl atom concentrations of $3x10^{14}/cm^3$. It should be noted that this contribution, although not entirely negligible compared to other atom sources, is only approximately one-thirtieth of the total atom concentration. The assumption of 50 percent channeling into dissociation products is not critical.

Adding the contributions of the various reactions considered yields total H and Cl concentrations of $8.6x10^{15}/cm^3$. H and Cl

can subsequently serve as highly efficient V-T deactivators

$$HCl(v=1) + H \longrightarrow HCl(v=0) + H, \quad k = 6.5 \pm 2.2\times10^{-12} cm^3/sec^{(10)}, \qquad (12)$$

$$HCl(v=1) + Cl \longrightarrow HCl(v=0) + Cl, \quad k = 8.5 \pm 2.5\times10^{-12} cm^3/sec.^{(9)} \qquad (13)$$

The rates given are for room temperature. Using H and Cl concentrations of $8.6\times10^{15}/cm^3$ yields $\tau_{V\text{-}T,atoms} = 7.75$ μsec. The comparable relaxstion time for HCl self-deactivation

$$HCl(v=1) + HCl \longrightarrow HCl(v=0) + HCl \quad k = 2.4\times10^{-14} cm^3/sec^{(8)} \qquad (14)$$

with a HCl concentration of $2.45\times10^{18}/cm^3$ is $\tau_{V\text{-}T,HCl} = 16.9$ μsec. Thus atom production serves to increase the effective V-T deactivation rate by a factor of 3.2.

To reflect this increased quenching a second gain calculation was made in which the effect of atom production was taken into account by increasing the rate constant for HCl self-deactivation by a factor of three. Figure 22 shows that the gains predicted in this case are an order of magnitude smaller than those calculated neglecting atom quenching. The gain predicted is still sufficient to produce observable stimulated emission in the 100 cm NRL device, but the actual chances for success become much more marginal because there is no longer a factor of ten leeway between the predicted gain and that necessary to overcome cavity losses.

3. Stimulated Emission Experiments

a. Room Temperature Measurements

Since the initial PSI gain predictions for a 9:1 Ar:HCl mixture at room temperature not including atom effects had been so favorable an attempt was made to observe lasing in the NRL 100 cm e-beam

sustainer. Even the calculations which include atomic quenching of HCl still indicate a single pass gain of 20% would be achievable at room temperature. These room temperature experiments would be far simpler to accomplish than those requiring cooling of the gases and the sustainer chamber. Ease of operation was an important consideration because a scan of the key parameters including sustainer voltage, mole fraction HCl and total pressure was judged advisable. It would be extremely difficult and costly to make such a parameter scan with a cooled system. At room temperature, even if laser action were not observed useful information concerning the behavior of the discharge as a function of the experimental parameters could be gathered and compared with the PSI electron-molecule rate constant calculations.

A 2.5 cm diameter optical cavity was constructed with Brewster-angle windows and external mirrors. One mirror was a gold coated totally reflecting flat and the other was a gold coated output coupler with a 10 meter radius of curvature. Light passing through this partial reflector was focussed by a 2.5 cm diameter ZnSe lens of focal length 12.5 cm onto a 1 mm diameter Spectronics Model SD 8720 indium antimonide photovoltaic detector (In:Sb(PV)). The detector was modified to operate in the zero bias mode to provide the highest possible detectivity, was r.f. shielded from noise produced by the electron beam and lead shielded from x-rays. Signals from the detector were monitored on a Tektronix Model 555 oscilloscope equipped with a Model 1A7A differential amplifier. The sustainer current was also displayed on this oscilloscope. Also monitored were the

sustainer voltage, e-beam voltage, and e-beam current out of the capacitor bank.

HCl partial pressures of 50, 75, 100, and 125 torr were used, the gas being Air Products Technical Grade (99.99%). For each of these HCl partial pressures 99.975% pure argon supplied by Burdett was used as a diluent to achieve total pressures of 0.5, 1, 2 and 3 atmospheres. The principal impurity in this argon was moisture since it was water pumped. To remove this water a trap was installed in the feed lines from the argon cylinders. All chamber pressures up to 800 torr were measured on a Wallace and Tiernan 62A-4D-0800X 303 stainless steel differential pressure gauge.

For each of these sixteen mixtures, an examination was made of the E/N_{HCl} region predicted to achieve maximum power transfer into vibrational excitation, $1.0\text{-}1.4\times10^{-15}$ V-cm^2. Successively higher sustainer voltages were applied to a given mixture until breakdown occurred. Lower E/N_{HCl} values in the $4\text{-}8\times10^{-16}$ V-cm^2 range were also investigated both in the hope of achieving laser emission and to gather discharge voltage and current data.

This scan of E/N_{HCl} values was prompted by a reanalysis of the electron-molecule rate constants, drift velocities, and characteristic energies calculated by PSI. Fractional power transfer is the obvious initial guidepost in selecting an E/N to investigate. However it is usually instructive to determine the actual energy transferred to the channel of interest at various E/N as well as the magnitude of the temperature increase that can be expected due to translational and rotational excitation. This can be determined by multiplying the

applied electric field by the current density to arrive at a predicted value of the power/cm^3 delivered. The current density needed for this calculation is provided by taking the product of the previously computed electron number density and drift velocity. When this power density figure is multiplied by the pulse length and fractional power factors the energy density transferred to various forms of excitation is obtained. This calculation also furnishes a prediction of the current vs E/N behavior to be observed which provides a useful test of the accuracy that can be expected from a given model.

The first step in the procedure is to solve for the steady state electron number density. For the case of a 9:1 Ar:HCl mixture this can be written as

$$\frac{dn_e}{dt} = 0 = S + k_i n_e [HCl] - k_a n_e [HCl] - \alpha n_e^2 \qquad (15)$$

where S is the source term for production of electrons by the e-beam, k_a is the rate constant for dissociative attachment in HCl, k_i is the rate constant for ionization of HCl, and α is the dissociative recombination rate constant for argon dimer ions. Solving Eq. 15 for n_e yields

$$n_e = \frac{-(k_a - k_i)[HCl] + \sqrt{(k_a - k_i)^2 [HCl]^2 + 4S\alpha}}{2\alpha} \qquad (16)$$

PSI had calculated k_a and k_i vs E/N_{HCl} and had found k_i to be negligable in comparison to k_a over the range of E/N_{HCl} considered. From the PSI computed values of the characteristic electron energy,

ϵ_K, vs E/N_{HCL} an approximation to α can be obtained by using the Mehr and Biondi[15] relation,

$$\alpha = 8.8\times10^{-7} \cdot \left(\frac{300^{o}K}{T_e}\right)^{0.67} \text{ cm}^3/\text{sec}, \qquad (17)$$

or

$$\alpha = 8.8\times10^{-7} \cdot \left(\frac{0.0258 \text{ eV}}{\epsilon_K}\right)^{0.67} \text{ cm}^3/\text{sec} . \qquad (18)$$

Table III shows the results of such calculations and used the PSI computed drift velocities to predict sustainer current density versus E/N_{HCl} using a source term of $2\times10^{21}/\text{cm}^3\text{-sec}$. Also shown in Table III is the total energy density resulting from a 3 μsec pulse at the voltage corresponding to the specified E/N_{HCl}. It is of interest to note that at an E/N_{HCl} of 6×10^{-16} V-cm^2 the loss term due to HCl dissociative attachment is approximately equal to that of Ar_2^+ dissociative recombination. At higher E/N_{HCl} values the discharge in this mixture is attachment dominated.

Table IV lists the electron-molecule rate constants for HCl v = 1 and v = 2 excitation calculated by PSI. These can be used together with the PSI drift velocities to calculate the fractional power transfer to v = 1 and v = 2 excitation. The fraction of energy being channeled into v = 1 is given by

$$f_{v=1} = \frac{k_{v=1} \cdot n_e \cdot [HCl] \cdot 2885.90 \cdot hc}{v_d \cdot n_e \cdot V \cdot 1.6\times10^{-19}} , \qquad (19)$$

or equivalently

$$f_{v=1} = 0.3585\, k_{v=1}/(v_d \cdot E/N_{HCl}) . \qquad (20)$$

Note that this expression is independent of n_e and hence $f_{v=1}$ does not depend on the method used to calculate n_e. Similarly the fraction of energy transferred to HCl(v=2) is given by

$$f_{v=2} = 1.964 \cdot 0.3585\, k_{v=2}/(v_d \cdot E/N_{HCl}) , \qquad (21)$$

where 1.964 is the ratio between the v=2 and v=1 vibrational energies. Table IV shows the fractions calculated in this fashion together with the energy density channeled into v=1 alone as wellas into v=2 taken together. Because energy channeled into v=2 is more effective in promoting the necessary anharmonic pumping a better criteria for selecting optimum operating conditions would be to add the energy transferred to v=1 to that transferred directly to v=2.

This makes the assumption that all the v=1 produced reacts according to

$$HCl(v=1) + HCl(v=1) \longrightarrow HCl(v=2) + HCl(v=0) \quad . \qquad (22)$$

Because of the large rate constant for this process[16], $5.1\pm0.5\times10^{-12}$ cm^3/sec and the number density of HCl(v=1) produced in all the cases considered, $HCl(v=1) \geq 5.6\times10^{17}$, loss by any other processes, including HCl self-deactivation is negligible as a first approximation. The energy defect for this anharmonic pumping reaction, $103.8cm^{-1}$, is less than two percent of the energy being channeled from v=1 to v=2. Consequently th $E_{v=1,2}$ figures given in the ninth column of Table IV accurately reflect the energy being channeled into HCl(v=2). This approach was used by PSI in constructing the fractional power transfer curves shown in Figures 5 and 7.

Also shown in Table IV is the expected temperature rise using a

gas constant for the mixture of 1.6R. This was calculated on the assumption that the energy not transferred into vibrational excitation went into gas heating. A correction to this was necessary for the four highest E/N_{HCl} values where 1.5, 4, 9 and 16% of the available energy goes into electronic excitation.

In Table IV there is no clear cut optimum E/N_{HCl} value which maximizes the energy channeled into v=2 and minimizes the temperature rise without leading to discharge breakdown (as in the case of the two largest E/N_{HCl} values). An approach to assessing the trade-off between more effective pumping and the corresponding temperature rise is provided by the results of previous UTRC gain calculations for He:HCl mixtures[17]. There it was found that the gain decreased an order of magnitude for each 100 K increase in temperature between 150 K and 300 K. The UTRC calculations also indicated that the maximum gain was directly proportional to each of the three factors responsible for v=1 pumping: electron number density, HCl partial pressure, and current pulse lengths. Applying these estimation techniques to the data in Table IV, and using the energy transferred into v=1 as the most representative measure of pumping strength, it turns out that E/N_{HCl} values from 8 to 14×10^{-16} V-cm^2 are equally favorable.

Multiple experiments were made at each set of mixture and voltage parameters to determine shot to shot reproducibility. This approach made it clear that it was necessary to change the gas fill every two or three shots. The sustainer chamber was flushed with argon between mixture fills to remove dissociation

products. The chamber was also pumped out thoroughly each night and weekends in an attempt to minimize the amount of chlorine that might adhere to the chamber walls.

The 300 kV e-beam was fired for 3 μsec with the cathode spaced 9 cm from the 0.0025 cm titanium foil. As will be discussed in a later section this cathode-foil spacing and pulse length was found to produce the greatest electron number density in the sustainer chamber.

Laser emission was not observed in any of these experiments. The observed sustainer current density (J_s) dependence on E/N_{HCl}, HCl partial pressure, and mixture total pressure did not follow, even qualitatively, the predictions based upon the PSI calculations. Since this represented a setback for the HCl EDL program these J_s measurements warrant further discussion.

The predicted J_s values are shown in Table III for a 9:1 Ar:HCl 1 atm mixture at room temperature as a function of E/N_{HCl}. Originally J_s was calculated for an e-beam source term of $2\times10^{21}/cm^3$-sec. J_s was recomputed for a source term of $3\times10^{21}/cm^3$-sec which was subsequently established for the NRL Maxwell e-beam using J_s values measured in pure nitrogen. This value also agrees with an energy deposition calculation based on the $5A/cm^2$ e-beam current measured on the discharge region side of the foil using a Faraday cup. The recalculated J_s values for the Ar:HCl mixture are shown in Figure 23 together with the experimental J_s values. The predicted J_s values are between a factor of 2 and 7 too large. Furthermore the predicted J_s decreases by a factor of 2.5 when the E/N_{HCl} increases from 6×10^{16} V-cm^2 to 9×10^{-16} V-cm^2 whereas the observed J_s actually increases by a factor of 1.4.

Equally poor agreement is observed in other cases where a direct comparison can be made between experimental J_s values and those calculated using the drift velocities, characteristic energies, and HCl dissociative attachment cross-sections calculated by PSI. Figure 24 shows the predicted J_s vs. E/N_{HCl} curves for 29:1 Ar:HCl mixtures at two and three atmospheres, using the same source term of $3x10^{21}/cm^3$-sec. Again the predicted J_s values are too large and show a marked decrease with increasing E/N_{HCl} that is not reflected in the experimental data.

The most disturbing observation was that the one distinct pattern that emerged from the experimental current measurements bore no relation to the attachment dominated discharge behavior predicted using the PSI results. For E/N_{HCl} values $\gtrsim 6x10^{-16}$ V-cm^2, dissociative attachment to HCl is predicted to be the predominant electron loss mechanism. Consequently, the steady state electron number density for these E/N_{HCl} values is given by

$$n_e = S/k_a[HCl] \quad . \tag{23}$$

The electron number density at a given E/N_{HCl} is a function of $S/[HCl]$ where S is proportional to the total pressure of the mixture in the 0.5-3 atmosphere region of interest. The result is that n_e is a function only of the mole fraction of HCl rather than the HCl partial pressure or the total pressure. Since the drift velocity is also a function only of E/N_{HCl} and the mole fraction of HCl, the J_s predicted for a 9:1 Ar:HCl at a given E/N_{HCl} is independent of pressure.

This behavior is exploited in constructing Figure 25 which illustrates the expected shape of J_s vs E/N_{HCl} curves for 3.3% and 10% HCl mixtures. For example it was expected that both the 75 torr HCl -

2205 torr Ar and 50 torr HCl - 1470 torr Ar current vs E/N_{HCl} plots would lie along the 3.3% curve. However an entirely different correlation emerged. Regardless of the HCl partial pressure the primary determinant of the observed J_s was the Ar diluent pressure and any difference between various HCl partial pressures was minimal. This Ar-diluent-determined behavior is illustrated by the shaded areas in Figure 25.

Particularly difficult to explain is the sharp decrease in J_s with increasing Ar pressure. Even if the discharge were Ar_2^+ dissociative recombination dominated with n_e given by

$$n_e \sim \sqrt{S/\alpha} \quad , \tag{24}$$

an increase in the Ar pressure, and consequently S, should give rise to an increase in the current observed. No satisfactory explanation of this behavior has yet been advanced, although any final explanation clearly must include the role of HCl. As will be discussed in a subsequent section markedly different behavior was observed in pure argon at the same pressure, where although J_s did not increase between 1 and 3 atmospheres with the expected square root of pressure dependence--it nonetheless did increase. Thus the Ar-HCl J_s behavior cannot be attributed to possible processes such as formation of argon ion clusters larger than the dimer with correspondingly greater recombination rate constants[18]. Otherwise this same behavior should have been equally evident in the pure Ar experiments.

b. Cooled Chamber Experiments

The room temperature Ar:HCl J_s measurements indicated that there

were important electron-molecule processes occurring which the kinetic model, constructed in conjunction with PSI, did not include. Consequently any gain predictions made were unreliable. Two other sets of experiments were conducted which yielded important information. The first was a series of shots taken at 240 K to determine if laser action could be produced at reduced temperature. The second was a complete characterization of the discharge behavior of the NRL e-beam sustainer using pure argon and nitrogen.

The discharge chamber was modified to operate at 240 K by installing a cooling apparatus which has been described in a previous report[19]. Liquid nitrogen flowed through the chamber for approximately thirty minutes to pre-cool it. Then liquid argon was metered into the chamber through one set of drilled PVC pipes while HCl entered through another. Liquid argon was used instead of cooled argon gas because of the more effective cooling that could be achieved. By the time the liquid argon reached the discharge region it had completely vaporized as was evidenced by the lack of scattering of a He-Ne alignment laser beam directed through the discharge region. An A.B. Cain 116U Chromel-Alumel thermocouple with a stainless steel housing monitored the gas temperature near the exit port. As in the room temperature experiment a Wallace and Tiernan 62A-4D-0800X 303 stainless steel gauge was used to measure the chamber pressure. Additional cooling was achieved by packing the exterior of the chamber with dry ice. If the salt flat Brewster angle windows had been in direct contact with the 240 K gases inside the discharge chamber condensation on their external surfaces would have rapidly rendered them useless.

To avoid this problem the absorption cells which had previously been used in HCl fluorescence experiments[19] were reinstalled. In this case however they were evacuated to provide thermal insulation for the Brewster windows. Each of these absorption cells was a 40 cm section of 5 cm O.D. polyvinyl chloride plastic pipe. One end threaded into the inner face of the Brewster angle window holder. The other end was sealed with a salt flat. This salt flat was normal to the optical axis of the chamber introducing a loss of 4% per surface. This 32% round trip loss for the salt flat on each of the two thermal insulators increased the cavity round trip loss from the 10% of the room temperature experiments to 42%. Consequently the required threshold gain for the 100 cm active region was 0.2%/cm compared with 0.05%/cm in the room temperature case.

The Ar:HCl ratio was established by first measuring the flow of argon and HCl out the exit port on the way to the vacuum pump. A coil submerged in water was used to bring the exiting gas up to room temperature before it passed through a Fischer and Porter flowmeter with a B6NL25 tube and BSX-624 float of 316 stainless steel and into the vacuum pump. A stainless steel pressure gauge was used to measure the pressure on the outlet side of the flowmeter. The HCl flow was measured on the inlet side of the discharge chamber by using a Matheson flow gauge with a R-6-15B tube and a 316 stainless steel ball. The pressure on the exit side of this flowmeter was also monitored by a stainless steel pressure gauge. The HCl flow measured in this way was subtracted from the Ar and HCl flow measured at the chamber exit port to determine the argon flow. A needle valve on the

HCl inlet line was adjusted to provide the desired Ar:HCl ratio.

A series of experiments were conducted using the same Ar:HCl mixtures that had been investigated at room temperature with the total pressure decreased by 20% to compensate for the cooling to 240 K. The same 6-12x10^{-16} V-cm^2 E/N_{HCl} values were used. Again laser action was not observed.

Unexpectedly, the current measured for a given set of mixture and E/N_{HCl} conditions dropped by approximately a factor of six making the production of stimulated emission unlikely. Suggestions[20] that this might have been due to HCl accumulating in the discharge region were explored. However the flow behavior as monitored by the inlet and exit flowmeters indicated that condensation or accumulation of HCl in the discharge region was not occurring. The J_s values measured for cooled pure argon were higher by up to a factor of four compared to equivalent room temperature measurements, and significantly higher E/N_{Ar} values could be maintained before arcing occurred. For a given pure Ar number density the applied voltage could be more than doubled. At these cold temperatures J_s for pure argon was independent of the pressure from 0.5 to 3 atmospheres. As will be subsequently discussed this was not the case in room temperature measurements and fails to reflect the expected $P^{1/2}$ dependence.

Arcing in the Ar:HCl mixtures was very severe and led to the destruction of the polyvinyl chloride cooling apparatus. The salt flat Brewster angle windows were also damaged when the aluminum window mounts conducted enough heat away from the flats to cause condensation to accumulate rapidly. This problem was avoided with the installation

of nylon window mounts.

A more serious problem was the optical transmission characteristics of the discharge chamber. A He-Ne alignment beam would continually dance about with oscillations up to 0.5 cm. It was not clear if this were due to severe flow inhomogeneities or temperature gradients, but in either case it was more than enough to ensure that laser action would not be achieved. Any motion of the He-Ne beam would have been greatly amplified in the case of HCl emission because of the proximity of the absorption causing the deflections and the emitting wavelength. The cooling chamber design clearly did not serve to minimize harmful flow inhomogeneities and temperature gradients and should be radically revised before any similar experiments are conducted.

4. E-Beam Measurements

After the destruction of the cooling chamber precluded any further Ar:HCl experiments a series of measurements were made to characterize the discharge behavior of the NRL Maxwell e-beam sustainer using pure gases for which extensive transport data is available. As a necessary first step in this procedure the e-beam current passing through the foil was measured as a function of the cathode to foil spacing and the pulse length.

This information was of interest for several reasons. It would provide a useful check on sustainer current density measurements to be made with argon. Using published values of the drift velocity and characteristic energy versus E/N the dissociative recombination rate constant can be calculated and used with J_s to calculate the source term. This in turn can be compared with that calculated using

the measured e-beam current. Another use of such e-beam data would be to determine under which combination of cathode-foil spacing and pulse length the maximum number of primary electrons is delivered to the discharge chamber. Finally, such measurements would verify that the NRL Maxwell device was in fact operating properly, and would yield a definitive source term to be used in interpreting the anomalous discharge data gathered in the Ar:HCl experiments. The e-beam current measurements indicated that the Maxwell device was operating properly hence suggesting that it was the discharge kinetic model rather than the e-beam current that was open to question.

These e-beam current measurements were made using a conical graphite Faraday cup with a 3.1 cm aperture. The output from this device was displayed on a Tektronix Model 555 oscilloscope. The e-beam voltage was maintained at 300 kV. Figure 26 shows both the beam current J_B, where $J_B \equiv$ e-beam current density through the foil, and the beam current times the pulse length as a function of the cathode-foil spacing and the pulse length. The cathode plasma growth velocity of approximately 2.5 cm/μsec establishes the maximum pulse length that can be used at a given cathode-foil distance. Exceeding this pulse length causes a destructive arc to the foil to occur. It is clear from Figure 26 that the maximum number of electrons are delivered to the discharge chamber for a cathode-foil distance of 9 cm and a pulse length of 3 μsec.

A similar set of measurements carried out at 272 kV indicated that Child's law[21] for beam current vs voltage was reliably obeyed. Thus these results can be extrapolated to other voltages of interest

with confidence. In this way the energy deposited in the discharge chamber gas can be varied in a reproducible manner.

5. Sustainer Current Measurements

The sustainer current densities measured in Ar:HCl mixtures were much lower than expected, and the sharp drop observed in J_s as the Ar diluent pressure increased was unexpected. These results made it necessary to determine the sustainer currents obtained in Argon and Nitrogen for which the transport properties are well known.

a. Argon

J_s measurements were made at 0.5, 1, 2, and 3 atmospheres using an E/N of 2.45×10^{-17} V-cm^2, equivalent to an electric field of 600 V/cm in a one atmosphere sample. This E/N was chosen for two reasons. First, some sustainer voltage droop invariably occurs as the capacitor bank discharges. This can lead to problems in data analysis if the transport properties of the gas are an extremely sensitive function of the Townsend parameter in the E/N region corresponding to the sustainer voltage used. In argon, this would occur for E/N values below 6×10^{-20} V-cm^2. At an E/N of 2.45×10^{-17} V-cm^2 the drift velocity and characteristic energy vary very slowly with E/N[22]. Hence the recombination coefficient α also has a weak dependence on E/N. The second reason for choosing this E/N is imposed by the capacitance of the NRL Maxwell e-beam sustainer, 9 microfarads. At sustainer, electric fields much less than 600 V/cm across the 10 cm discharge region the sustainer capacitor bank was significantly depleted by a 3 μsec discharge into one atmosphere of argon. This necessitated operating in the voltage region selected. In addition a 12 microfarad

capacitor was added to the existing bank to increase the effective capacitance.

It was expected that because the discharge would be Ar_2^+ dissociative recombination dominated the observed current would be proportional to the square root of the pressure for a given E/N. This follows from the steady state electron number density equation

$$\frac{dn_e}{dt} = 0 = S - \alpha n_e^2 \quad , \tag{25}$$

and the expected linear dependence of S on the pressure in the 0.5 to 3 atm region. As Figure 27 illustrates, the pressure dependence is not given by $P^{1/2}$ but instead varies from $P^{1/2}$ to P^2 in the 0.5 to 2 atm region. Beyond 2 atm the current remains constant with increasing pressure. The failure of as simple a system as pure argon to behave in a predictable manner indicated that there were important electron-atom or chemical processes occurring that were not being considered. In addition, although the sustainer current density did not increase between two and three atmospheres, it also did not display the precipitous drop off observed for the Ar:HCl mixtures. It was concluded that there was a predominant process for Ar:HCl mixtures that had been neglected.

One partial explanation of the observed J_s vs pressure behavior could be given in terms of an impurity. Taking the measurements at one-half atmosphere and one atmosphere a pressur dependence of $P^{0.9}$ or almost P^1 is observed. This could be explained in terms of an impurity in the chamber which established a constant background

partial pressure for each shot. If this impurity had a large attachment cross section, as is the case for HCl, the electron number density steady state equation would be

$$\frac{dn_e}{dt} = 0 = S - k_a[X] , \qquad (26)$$

where [X] is the constant concentration of the unknown impurity gas.

To determine if this explanation is plausible the observed currents were divided by the drift velocity of 2.7×10^5 cm/sec[22] to calculate the steady state electron number density. Since n_e is equal to the Ar_2^+ concentration, the reciprocal lifetime of the electron dissociative recombination reaction

$$\frac{dn_e}{dt} = -\alpha[Ar_2^+]n_e = -\alpha n_e^2 , \qquad (27)$$

is given by $1/\tau = \alpha n_e$. To determine the minimum HCl concentration needed to explain the observed data a value for α of 2.1×10^{-8} cm^3/sec was used. This value was selected by first taking the ϵ_K corresponding to an E/N = 2.45×10^{-17} V-cm^2, 7 eV[22], and by determining what α would result if the electron energy distribution were Maxwellian using the Mehr and Biondi[15] expression

$$\alpha = 8.8 \times 10^{-7} \cdot \left(\frac{300\ K}{T_e}\right)^{0.67} . \qquad (28)$$

This produces an $\alpha = 2.1 \times 10^{-8}$ cm^3/sec. However as Engelhardt and Phelps illustrate graphically in their discussion of the argon transport coefficients and cross sections[22], the actual electron energy distribution is not at all like that of a Maxwellian distribution in the case of ϵ_K = 8.60 eV. In fact, a Maxwellian distribution with an

electron temperature corresponding to half the characteristic energy was most similar to the actual electron energy distribution. Assuming that this observation would also apply to the case of ε_K = 7 eV, the dissociative recombination rate constant would be 3.3×10^{-8} cm^3/sec. This larger rate constant would require a greater concentration of HCl if dissociative attachment were to predominate. Using the 2.1×10^{-8} cm^3/sec value of α, $1/\tau$ values as listed in Table V were calculated for Eq. 27. Again to minimize the HCl concentration that would be required to compete with the Ar_2^+ recombination reaction, a rate constant of 1.5×10^{-10} cm^3/sec was assumed for the HCl attachment reaction. This was the largest rate constant for this reaction calculated by PSI. The required HCl concentrations are shown in column 5 of Table V. Approximately one torr of HCl would be required in the 0.5-1 atm cases to account for the linear behavior of J_s vs P in this region. Even though a definite odor of HCl was noticeable when the chamber was disassembled, it is unlikely that a 1-5 torr background pressure of HCl could be repeatedly established in the chamber from HCl still adhering to the walls after pump-out cycles.

Not only were the argon J_s values unexpectedly low at lower pressures, they were surprisingly high at higher pressures, even though there was no increase between two and three atmospheres. The dashed lines in Fig. 27 are for the two cases: $\alpha = 2.1 \times 10^{-8}$ cm^3/sec and $\alpha = 3.3 \times 10^{-8}$ cm^3/sec. In both cases $v_d = 2.7 \times 10^5$ cm/sec and $S = 3 \times 10^{21} \cdot P/cm^3$-atm-sec where P is the pressure in atmospheres. These form limits to the expected J_s vs P curves. It should be noted that

any other predicted curve in the dissociative-recombination dominated model would be parallel to these curves rather than just constrained to lie in the region demarcated by them. The observed behavior is clearly not compatible with the model. For example to achieve an adequate fit at the two atmosphere point (ignoring the extremely poor fit that would result at all other points) the S/α ratio would have to be three and a half times greater than it apparently is based on the characteristic energy of electrons in argon at this E/N and the electron beam currents previously measured.

b. Nitrogen

Similarly suprising results were obtained when nitrogen was examined in a series of similar current measurements. As in the case of argon, 99.975% pure nitrogen was used, passing through a trap to remove water vapor before entering the chamber. Four values of E/N were investigated: 0.41×10^{-16}, 0.49×10^{-16}, 0.57×10^{-16}, and 1.10×10^{-16} V-cm^2. The first three E/N values correspond to sustainer electric fields of 1.0, 1.2, and 1.4 kV/cm for one atmosphere of nitrogen. The 1.10×10^{-16} V-cm^2 E/N corresponds to an electric field of 2.7 kV/cm for one atmosphere. This higher E/N was used to avoid the marked change in the N_4^+ recombination coefficient that any voltage droop would produce for the first three E/N values. The N_4^+ recombination rate study of Douglas-Hamilton[23] indicated that this rate is only very weakly dependent on E/N for E/N values greater than 0.8×10^{-16} V-cm^2.

Figure 28 shows that, like argon, nitrogen displayed near linear dependence of J_s on pressure in the 0.5 to 1.0 atmosphere region for the three lower E/N values. For the 1.10×10^{-16} V-cm^2 E/N case J_s is proportional to $P^{1.3}$ between these pressures. In the region above one atmosphere the J_s curves rolled over to near pressure independence, again in a manner similar to that of argon.

In the one to two atmosphere region the J_s curves display $P^{0.58}$, $P^{0.48}$, and $P^{0.37}$ dependence, the first two of which are at least reasonable approximations to the expected $P^{0.5}$ dependence. Moreover, the observed J_s values at one atmosphere are surprisingly close to those predicted from a knowledge of E/N and the electron-beam current. Using the recombination rate constant vs E/N data reported by Douglas-Hamilton[23] and the drift velocity vs E/N curves calculated by Frost and Phelps[3] to fit the Pack and Phelps[24] transport data, sustainer currents at one atmosphere for the N_4^+ recombination dominated model were computed from

$$J_s = n_e \cdot e \cdot v_d = \sqrt{S/\alpha} \cdot e \cdot v_d \quad . \tag{29}$$

The value of S used in this calculation was 1.8×10^{21}/cm^3-sec which corresponds to the argon value of 3×10^{21}/cm^3-sec corrected for the smaller stopping power[25] of nitrogen and its larger effective ionization potential, W = 35 eV[26]. The resulting J_s values are shown in Table VI together with the actual J_s measurements.

This close agreement between predicted and observed sustainer currents at one atmosphere illustrates the danger of testing such a model at one pressure and assuming that success validates its application

at other nearby pressures. The agreement for nitrogen at one atmosphere may be significant or may be fortuitous, but the model does not accurately predict the currents observed at 0.5 or 3 atmospheres.

This behavior was also observed in a series of careful measurements conducted using the same e-beam source but a considerably smaller sustainer chamber. In the fall of 1974, in connection with the use of the Maxwell device as a CO_2 laser amplifier, a study was made of sustainer currents in nitrogen using a 1.8 cm by 20 cm anode spaced 1.1 cm from the e-gun foil in a small Lucite chamber. This chamber was capable of being readily evacuated to sub-micron pressures to eliminate problems due to gaseous impurities adhering to the anode and inner walls of the chamber. The small anode area prevented any significant sustainer voltage droop. This reduced anode area also minimized any errors introduced by variations in J_s across the height or length of the anode. This could be a significant factor, particularly at pressures greater than an atmosphere for the large 10 cm x 100 cm anode used in the HCl experiments as well as the previously discussed argon and nitrogen J_s measurements. These improved conditions were further aided by the much smaller 2 cm x 20 cm e-beam entrance window and 1 cm anode-cathode distance. Energy deposition gradients and expansion of the discharge beyond the inter-electrode volume would be minimized under such conditions.

As Fig. 29 indicates, even under these carefully controlled conditions the pressure dependence of J_s was observed to be $P^{1.2}$ between 0.1 and 0.5 atmospheres with the four data points involved fitting this

value closely. This again looks like behavior dominated by attachment to some pressure independent impurity in the chamber. However, that explanation is inadequate for two reasons. First it would only produce a P^1 rather than a $P^{1.2}$ pressure dependence and the data strongly implies a $P^{1.2}$ pressure dependence. In addition, a very high partial pressure of the impurity would be required. If the attachment rate constant were assumed to be as large as 1×10^{-10} cm^3/sec for the unknown impurity, a concentration of between 3 torr in the 0.1 atm case and 2 torr in the 0.3 atm case would be needed to explain the divergence from an extrapolation of the well-behaved J_s line between 0.5 and 5 atm into the 0.1 to 0.5 atm region. Even in the unlikely case where the rate constants were ten times larger the corresponding impurity concentration would be unacceptedly large.

As in the previous measurements in argon and nitrogen, a sharp rolloff of J_s at higher pressures is observed. However, rather than occurring at between two and three atmospheres as it did for the large sustainer chamber with the 1000 cm^2 anode, it began at five atmospheres. This suggests, that either the method by which J_s is measured or the configuration of the sustainer chamber itself has a marked influence on the observed J_s behavior for such high e-beam current devices. The influence is apparently strong enough to interfere with any modelling attempts in the large chamber at higher pressures. This effect could reflect inadequacies inherent in measuring a "J_s" over a large area under conditions where significant current gradients are to be expected as the region of e-beam ionization begins to expand beyond the frontal

area of the anode due to increased multiple scattering. Alternately, it could be due to energy deposition deviations from linear behavior as the mass thickness exceeds the "thin" target limit.

Whatever cause, or combination of causes, is responsible, the small chamber measurements clearly demonstrate that the unexpected current behavior observed for argon and nitrogen in the discharge chamber used for the HCl experiments is not peculiar to that device.

6. HCl Experiment Conclusions

Because even pure argon and nitrogen sustainer current measurements under more carefully controlled conditions produced unexpected results, and since the diagnostics available on the present device made a more detailed inquiry impossible, the project was terminated at this point. Although not successful in yielding laser action, these experiments did lead to several useful conclusions and recommendations. The three conclusions relate to the feasibility of a HCl laser. The recommendations establish guidelines which should be followed in executing any similar program in the future.

The direct electric discharge pumping of HCl, even using an e-beam as a source of ionization, is not likely to result in an efficient 3-4 micron laser operating at room temperature. The sixteen possible combinations of 50, 75, 100, and 125 torr HCl partial pressures and 0.5, 1, 2, and 3 atmospheres total pressure in an argon diluent were investigated over a wide range of E/N_{HCl} values centered about those predicted to give maximum gain. The round trip cavity loss was only 10% while the discharge region was 100 cm long so that gains

greater than 0.05%/cm should have resulted in detectable stimulated emission. Laser action was never observed. Any gain produced in the wide parameter space spanned must have been extremely weak. The possibility of gain outside this parameter space seems remote. At higher HCl partial pressures HCl self-quenching becomes an important energy sink, and any laser produced in this region which can overcome such a drawback will be inefficient because of this loss process. At lower HCl partial pressures the direct pumping mechanism is proportionately decreased. This in turn produces a quadratic decrease in the rate of the anharmonic pumping process responsible for channeling vibrational energy into levels from which stimulated emission can occur. Decreasing the argon partial pressure much below the 0.5 atmosphere minimum used in these experiments while maintaining the same HCl partial pressure and E/N_{HCl} would provide inadequate stopping power for the ~ 300 keV electrons of the e-beam. The discharge currents measured in the previously described Ar:HCl experiments showed a significant decrease in going from a total pressure of one atmosphere to 0.5 atmospheres.

It should follow that increasing the argon diluent pressure to exceed the three atmosphere total pressure investigated would increase the ionization produced by the e-beam and lead to greater discharge currents. However, such a course only serves to radically reduce the discharge current observed and hence is not an attractive alternative. In addition, such a diluent pressure increase would serve to decrease the gain by broadening the linewidth of the transitions involved. The final alternative of going to higher or lower E/N_{HCl} values produces

discharge breakdown due to arcing in the case of higher values, and excessive gas heating in the case of lower values. Hence it would seem that the most favorable parameter space has been thoroughly investigated at room temperature without the observation of stimulated emission.

The low temperature Ar:HCl experiments where stimulated emission was also not observed were not as conclusive as the room temperature study. The erratic beam deflections caused by temperature or concentration gradients could easily have prevented any multi-pass operation of the optical cavity. The cavity itself had a round-trip loss of 42% for the cooled runs so that the required threshold gain was 0.2%/cm or four times larger than in the room temperature case. The discharge currents in the cooled case were unfavorable both because of a marked decrease compared to room temperature and because of the anomalous pressure dependence. The Ar.HCl discharge currents decreased by a factor of six, the Ar currents increased by a factor of four, and were independent of pressure over the range of 0.5 to 3.0 atmospheres. The discharge kinetics had clearly been altered by either the cooling or the cooling apparatus.

The room temperature results lead to a third conclusion that deals not with the absence of laser emission, but with the presence of an important kinetic process involving Ar and HCl which has not yet been incorporated into kinetic models of this system. In the course of this investigation the importance of the reaction $Ar^+ + HCl \longrightarrow ArH^+ + Cl$ was established. But there must also be a reaction mechanism

which accounts for the precipitous drop off in the discharge current measured for a given partial pressure of HCl and E/N_{HCl} as the argon diluent brings the total pressure from one to three atmospheres. An explanation for this behavior must be furnished before any further effort is expended on this system.

7. Future Program Recommendations

The recommendations arising from this project pertain to the design of future e-beam sustainers to be used in investigating related proposed lasers. They also suggest how kinetic models of those proposed systems should be checked against experimental data in the early stages of any such study.

A serious drawback in the discharge chamber used in the Ar:HCl experiments was the lack of a port for viewing side emission. Future chamber designs should incorporate at least one pair of windows providing a viewing axis perpendicular to both the laser output axis and the e-beam current direction. Such a coaxial pair of viewing ports would allow simultaneous monitoring of a particular emitting region with two different filter-detector combinations. It would also enable gain or absorption measurements to be made without disrupting the optical cavity lying along the main chamber axis. Since simultaneous gain/absorption and fluorescence measurements are often invaluable in achieving stimulated emission, the installation of two or more such port pairs is advisable.

To avoid having discharge voltage droop become an important consideration it would also be advisable to reduce the width of the anode

as much as possible. In these experiments 2.5 cm optics were used together with an anode that was 10 cm wide. Both of these dimensions were unnecessarily large. One cm optics with a 2 cm wide anode would certainly have sufficed and would have reduced the drain on the discharge capacitor bank by a factor of five. The cathode-anode distance could similarly be reduced from 10 to 2 cm. This would decrease the problem of an energy deposition gradient occurring between the cathode and anode at high argon diluent pressures. It would also reduce the overall discharge chamber size to more manageable proportions. Such a size reduction would also enable a given pumping system to perform more adequately and diminish the required quantities of often expensive gases used.

The chamber itself should be fabricated from materials that are not corroded by the gases used or by transient species produced in the discharge. The chamber used in the Ar:HCl experiments was made of mild steel since it had been originally designed for use with CO_2 N_2 and He. Consequently corrosion problems were severe, and gas entrapment on the corroded surface led to difficulties in trying to achieve a submicron vacuum.

The high voltage leads into the chamber from the discharge capacitor bank should be designed for high vacuum operation. This was another problem encountered in the Ar:HCl experiments which made it very difficult to thoroughly pump out the chamber for the Faraday cup experiments or prior to the critical pure Ar and N_2 studies.

Adequate diagnostics should be incorporated as an integral part of the chamber design. Of prime importance would be at least one, and preferably more, current button[23] built into the anode to permit a more meaningful measurement of the discharge current density. Under evacuated conditions such a button could serve as a built-in Faraday cup to check for e-beam current strength variations whenever the functioning of the e-gun became questionable. A series of buttons would allow the important questions of e-beam and discharge current uniformity to be unambiguously answered. Provision should also be made for the insertion and removal of probes[23] to determine the local E/N across the discharge.

Any device should incorporate, or at least allow for the addition of, a well-designed flow system. For room temperature systems flowing the gas has the advantage of ensuring gas purity. In cooled systems such an approach is mandatory to establish and maintain a known temperature. The serious beam deflections encountered in the cooled Ar:HCl experiments stress the importance of minimizing the temperature and concentration gradients any such cooling system is prone to introduce. At the minimum a flow device similar to the AVCO sintered metal heat exchanger[27] should be used to ensure a uniformly mixed and cooled flow. Again care must be taken to use only materials which resist corrosion.

Before commencing an investigation of the gas mixture of interest in the newly constructed chamber, a preliminary study of discharge currents observed in argon and nitrogen should be completed for that

chamber. Such a study should include pressures ranging from 0.1 to 10 atmospheres for both gases with measurements at several E/N values for each gas. These data will enable an important check to be made against known drift velocity and recombination rate data. Thus even if the e-beam energy deposition source term S is not well known, the observed variation in J_s as a function of E/N can be compared with the known $v_d/\sqrt{\alpha}$ ratios provided by available data since for a recombination dominated discharge

$$J_s = n_e \cdot e \cdot v_d = \sqrt{S/\alpha} \cdot e \cdot v_d \ . \qquad (30)$$

If the observed J_s behavior follows no simple relationship, attempts to model an electric discharge laser in that particular device will be difficult and any experimental program carried out will be essentially an empirical exercise.

If instead predictable behavior is achieved for argon and nitrogen over a wide pressure range the time and funds required to construct a kinetic model for the system of interest will be well invested. However, before such a model advances beyond the discharge kinetics stage, this initial part of the overall model should be used to predict discharge currents over a wide range of partial pressures and E/N values. Only if good agreement is achieved at this point is the considerable expense of incorporating a chemical kinetics package warranted.

References

1. V. A. Bailey and W. E. Duncanson, Phil. Mag. 10, 145 (1930).

2. W. L. Nighan, Phys. Rev. A, 2, 1989 (1970).

3. L. S. Frost and A. V. Phelps, Phys. Rev., 127, 1621 (1962).

4. K. Rohr and F. Linder, J. Phys. B. Atom. Molec. Phys. 8, L200 (1975); K. Rohr (private communication), July 1975.

5. R. E. Center and H. L. Chen, J. Chem. Phys. 61, 3785 (1974).

6. G. E. Caledonia and R. E. Center, PSI TR-44.

7. J. P. Ziesel, I. Nenner, G. J. Schulz, J. Chem. Phys. 63, 1943 (1975).

8. P. F. Zittel and C. B. Moore, J. Chem. Phys. 59, 6636 (1973).

9. R. G. Macdonald, C. B. Moore, I. W. M. Smith, and F. J. Wodarczyk, J. Chem. Phys. 62, 2934 (1975).

10. D. Arnoldi and J. Wolfrum, Chem. Phys. Lett. 24, 234 (1974).

11. J. A. Shirley, B. R. Bronfin, W. L. Nighan, and T. L. Churchill, "E-Beam HCl Laser," UTRC Report L911340-3, November 1972.

12. Y. Noter, I. Burak, and A. Szoke, J. Chem. Phys. 59, 970 (1973).

13. S. G. Lias (private communication), July 1975.

14. E. W. McDaniel, V. Cermak, A. Dalgarno, E. E. Ferguson, L. Friedman, Ion-Molecule Reactions (Wiley-Interscience, New York, 1970), p. 338.

15. F. J. Mehr and M. A. Biondi, Phys. Rev. 176, 322 (1968).

16. S. R. Leone and C. B. Moore, Chem. Phys. Lett. 19, 340 (1973).

17. J. A. Shirley, R. J. Hall, and B. R. Bronfin, "E-Beam HCl Laser," UTRC Report N911340-13, August 1974.

18. W. F. Liu and D. C. Conway, J. Chem. Phys. 62, 3070 (1975).

19. G. A. Hart and L. F. Champagne, ARPA-NRL Laser Program Semiannual Technical Report to Defense Advanced Research Projects Agency, 1 January 1975 - 30 June 1975.

20. R. E. Center (private communication), November 1975.

21. C. D. Child, Phys. Rev. 32, 492 (1911).

22. A. G. Englehardt and A. V. Phelps, Phys. Rev. 133, A375 (1964).

23. D. H. Douglas-Hamilton, J. Chem. Phys. 58, 4820 (1973).

24. J. L. Pack and A. V. Phelps, Phys. Rev. 121, 798 (1961).

25. M. J. Berger and S. M. Seltzer, in Studies in Penetration of Charged Particles in Matter, Nuclear Science Series Report No. 10, NAS-NRC Pub.1133 (National Academy of Sciences, Washington, 1964).

26. G. N. Whyte, Radiat. Res. 18, 255 (1963).

27. M. J. W. Boness and R. E. Center, "CO Laser Semiannual Technical Report," DARPA-AVCO Contract No. N00014-72-C-0030, September 1975.

TABLE I

COMPARISON OF HCl EXPERIMENTAL

AND PREDICTED DRIFT VELOCITIES

E/N (10^{-16} V-cm^2)	v_d DATA[a] (10^6 cm/sec)	v_d PREDICTION[b] (10^6 cm/sec)
3	2.5	2.5
4.5	4.4	3.7
6	4.5	4.5
7	---	5.1
9	5.0	5.7
10	---	5.8
12	6.0	6.1
15	---	6.4

[a]Obtained from transport data of V. A. Bailey and W. E. Duncanson, Phil. Mag. 10, 145 (1930).

[b]Calculated using the Physical Sciences Incorporated electron-molecule cross section set for HCl.

TABLE II

COMPARISON OF HCl EXPERIMENTAL AND

PREDICTED ELECTRON CHARACTERISTIC ENERGIES

E/N (10^{-16} V-cm^2)	ε_K DATA[a] (eV)	ε_K PREDICTION[b] (eV)
3	0.084-0.093	0.08
4.5	0.145	0.12
6	0.162-0.175	0.165
7	------	0.20
9	0.294-0.32	0.33
10	------	0.43
12	0.54-0.56	0.73
15	------	1.31

[a]Obtained from transport data of V. A. Bailey and W. E. Duncanson, Phil. Mag. 10, 145 (1930).

[b]Calculated using the Physical Sciences Incorporated electron-molecule cross section set for HCl.

TABLE III

PREDICTED STEADY STATE ELECTRON NUMBER DENSITY AND SUSTAINER CURRENT DENSITY VS E/N_{HCl} FOR 1 ATMOSPHERE 300 K 9:1 Ar:HCl MIXTURE

E/N_{HCl} (10^{-16} V-cm^2)	k_a[a] (cm^3/sec)	ε_K[b] (eV)	α[c] (cm^3sec)	n_e[d] (cm^{-3})	v_d[e] (10^6cm/sec)
4	1.40×10^{-12}	0.112	3.29×10^{-7}	7.30×10^{13}	3.18
6	1.80×10^{-11}	0.163	2.56×10^{-7}	3.73×10^{13}	4.36
8	6.00×10^{-11}	0.231	2.03×10^{-7}	1.34×10^{13}	5.18
10	1.11×10^{-10}	0.332	1.59×10^{-7}	7.32×10^{12}	5.57
12	1.37×10^{-10}	0.482	1.24×10^{-7}	5.95×10^{12}	5.50
14	1.50×10^{-10}	0.685	9.79×10^{-8}	5.43×10^{12}	5.19
16	1.44×10^{-10}	0.920	8.04×10^{-8}	5.66×10^{12}	4.87
18	1.36×10^{-10}	1.180	6.80×10^{-8}	6.00×10^{12}	4.67

[a] HCl dissociative attachment rate constant calculated using Physical Sciences Incorporated (PSI) electron-molecule cross section set and resulting electron energy distribution vs E/N_{HCl}.

[b] Characteristic electron energy calculated using PSI electron-molecule cross section set for HCl.

[c] Ar_2^+ dissociative recombination rate constant calculated using relation $\alpha = 8.8\times10^{-7}\ (300^oK/T_e)^{0.67}$ cm^3/sec observed by F. J. Mehr and M. A. Bondi, Phys. Rev. 176, 322 (1968). For this calculation a Maxwellian distribution was assumed so that $T_e = \varepsilon_K \cdot 11605^oK/eV$.

[d] Predicted electron number density = $(-k_a [HCl] + \sqrt{k_a^2[HCl]^2 + 4S\alpha})/2\alpha$. Electron-beam S = $2\times10^{21}/cm^3$-sec.

[e] Electron drift velocity calculated using PSI electron-molecule cross section set for HCl

[f] Predicted sustainer current density = $n_e \cdot v_d \cdot e$

[g] Energy density product of sustainer current density J_s, voltage V, and pulse length τ = 3 μsec.

TABLE IV

PREDICTED FRACTIONAL POWER TRANSFER INTO HCl (v=1,2)
AND GAS HEATING FOR 1 ATMOSPHERE 300 K 9:1 Ar:HCl MIXTURE

E/N_{HCl} (10^{16}V-cm^2)	$k_{v=1}$[a] (10^{-8}cm^3/sec)	$k_{v=2}$[b] (cm^3/sec)	v_d[c] (10^6cm/sec)	$f_{v=1}$[d]	$f_{v=2}$[e]	$J_s \cdot V \cdot \tau$[f] (mJ/cm^3)	$E_{v=1}$[g] (mJ/cm^3)	$E_{v=1,2}$[h] (mJ/cm^3)	ΔT[i] (K)
4	0.16	6.12×10^{-12}	3.18×10^6	0.437	0.003	109	47.7	48.0	113
6	0.48	7.50×10^{-11}	4.36×10^6	0.658	0.020	115	75.4	77.7	68
8	0.85	3.35×10^{-10}	5.18×10^6	0.735	0.057	65	48.0	51.7	25
10	1.14	8.40×10^{-10}	5.57×10^6	0.734	0.106	48	35.1	40.1	14
12	1.30	1.34×10^{-9}	5.50×10^6	0.706	0.143	46	32.4	38.9	12
14	1.40	1.78×10^{-9}	5.19×10^6	0.690	0.173	46	32.0	40.0	8
16	1.38	2.03×10^{-9}	4.87×10^6	0.634	0.184	52	32.8	42.3	9
18	1.32	2.24×10^{-9}	4.67×10^6	0.563	0.188	59	33.5	44.7	10

[a] Rate constant for electron impact excitation of HCl into v=1 calculated using Physical Sciences Inc. (PSI) electron-molecule cross section set and resulting electron energy distribution vs E/N_{HCl}.

[b] Rate constant for electron impact excitation of HCl into v=2 calculated using PSI electron-molecule cross section set and resulting electron energy distribution vs E/N_{HCl}.

[c] Electron drift velocity calculated using PSI electron-molecule cross ection set for HCl.

[d] Fraction of power transferred to excitation of HCl into v=1. Calculated from $k_{v=1} \cdot hc\tilde{\nu}/(v_d \cdot E/N_{HCl} \cdot e)$.

[e] Fraction of power transferred to excitation of HCl into v=2. Calculated from $k_{v=2} \cdot hc\tilde{\nu}/(v_d \cdot E/N_{HCl} \cdot e)$.

[f] Energy density product of sustainer current density J_s, voltage V, and pulse length τ=3 μsec, taken from Table III.

[g] Energy/cm^3 resulting from multiplying fractional power transfer coefficient for HCl(v=1) excitatinon by $J_s \cdot V \cdot \tau$ product.

[h] Energy/cm^3 resulting from multiplying fraction power transfer coefficient for HCl(v=1) and (v=2) excitation by $J_s \cdot V \cdot \tau$ product.

[i] Rotation-Translational temperature rise calculated using 1.6R as the gas constant for the mixture. Energy not transferred into vibrational excitation assumed to go into gas heating. Correction to this assumption is applied for four highest E/N_{HCl} values where 1.5,4,9, and 16% of $J_s \cdot V \cdot \tau$ product is channeled into electronic excitation.

TABLE V

MINIMUM GAS IMPURITY PARTIAL PRESSURE REQUIRED TO PRODUCE OBSERVED SUSTAINER CURRENT DENSITY IN ARGON

P (atm)	J_s[a] (A/cm^2)	n_e[b] ($10^{14}/cm^3$)	$\alpha \cdot Ar_2^+$[c] (sec^{-1})	X[d] (torr)	$J_{s,min}$[e] (A/cm^2)	$J_{s,max}$[f] (A/cm^2)
0.5	7.45	1.72	3.61×10^6	0.75	9.21	11.55
1.0	13.75	3.18	6.68×10^6	1.38	13.03	16.33
2.0	42.20	9.77	2.05×10^7	4.29	18.42	23.09
3.0	42.20	9.77	2.05×10^7	4.29	22.56	28.28

[a] Observed sustainer current density at $E/N = 2.45 \times 10^{-17}$ V-cm^2 and $T = 300^\circ K$.

[b] Electron number density calculated from J_s using drift velocity 2.7×10^5 cm/sec reported for $E/N = 2.45 \times 10^{-17}$ V-cm^2 by A. G. Englehardt and A. V. Phelps, J. Chem. Phys. 133, A375 (1964).

[c] Electron number density reciprocal lifetime established by Ar_2^+ dissociative recombination reaction. Ar_2^+ concentration assumed equal to n_e. $\alpha = 2.1 \times 10^{-8}$ cm^3/sec calculated using Englehardt and Phelps characteristic electron energy, $\varepsilon_K = 7$ eV, and the relation $\alpha = 8.8 \times 10^{-7} (300^\circ K/T_e)^{0.67}$ observed by F. J. Mehr and M. A. Biondi, Phys. Rev. 176, 322 (1968). For this calculation a Maxwellian distribution was assumed so that $T_e = \varepsilon_K \cdot 11605$ K/eV. This produces a lower bound estimate of α.

[d] Impurity concentration required to have electron number density reciprocal lifetime established by dissociative attachment to X equal that due to dissociative recombination with Ar_2^+. k_a was assumed equal to largest value predicted using Physical Sciences Incorporated electron-molecule cross section set for HCl, 1.5×10^{-10} cm^3/sec.

[e] Predicted sustainer current density = $v_d \cdot \sqrt{S/\alpha} \cdot e$ using $v_d = 2.7 \times 10^5$ cm/sec, $S = 3 \times 10^{21}/cm^3$-sec, and $\alpha = 3.3 \times 10^{-8}$ cm^3/sec. This α was calculated using $\varepsilon_K = 3.5$ eV since electron energy distribution computed by Englehardt and Phelps for $\varepsilon_K = 8.60$ eV was most closely fit by Maxwellian distribution with $\varepsilon_K = 4.30$ eV. This increased α produces lower estimate of J_s.

[f] Predicted sustainer current density = $v_d \cdot \sqrt{S/\alpha} \cdot e$ using $v_d = 2.7 \times 10^{15}$ cm^3/sec, $S = 3 \times 10^{21}/cm^3$-sec, and $\alpha = 2.1 \times 10^{-8}$ cm^3/sec corresponding to the Englehardt and Phelps $\varepsilon_K = 7$ eV.

TABLE VI

PREDICTED AND OBSERVED SUSTAINER CURRENT DENSITY VS E/N FOR NITROGEN AT ONE ATMOSPHERE, 300°K

E/N (10^{-16} V-cm^2)	α[a] (10^{-7} cm^3/sec)	v_d[b] (10^6 cm/sec)	$J_{s,pred}$[c] (A/cm^2)	$J_{s,obs}$ (A/cm^2)
0.40	1.50	0.98	17.2	17.0
0.49	1.03	1.14	24.1	21.5
0.57	0.90	1.20	27.2	26.4
1.10	0.84	2.00	46.8	47.1

[a] N_4^+ dissociative recombination rate constants reported by D. H. Douglas-Hamilton, J. Chem. Phys. 58, 4820 (1973).

[b] Electron drift velocities calculated by L. S. Frost and A. V. Phelps, Phys. Rev. 127, 1621 (1962) to fit transport data of J. L. Pack and A. V. Phelps, Phys. Rev. 121, 798 (1961).

[c] Predicted sustainer current density = $v_d \cdot \sqrt{S/\alpha} \cdot e$. $S = 1.8 \times 10^2$/cm^3-sec was calculated from the known e-beam current density of 5A/cm^2.

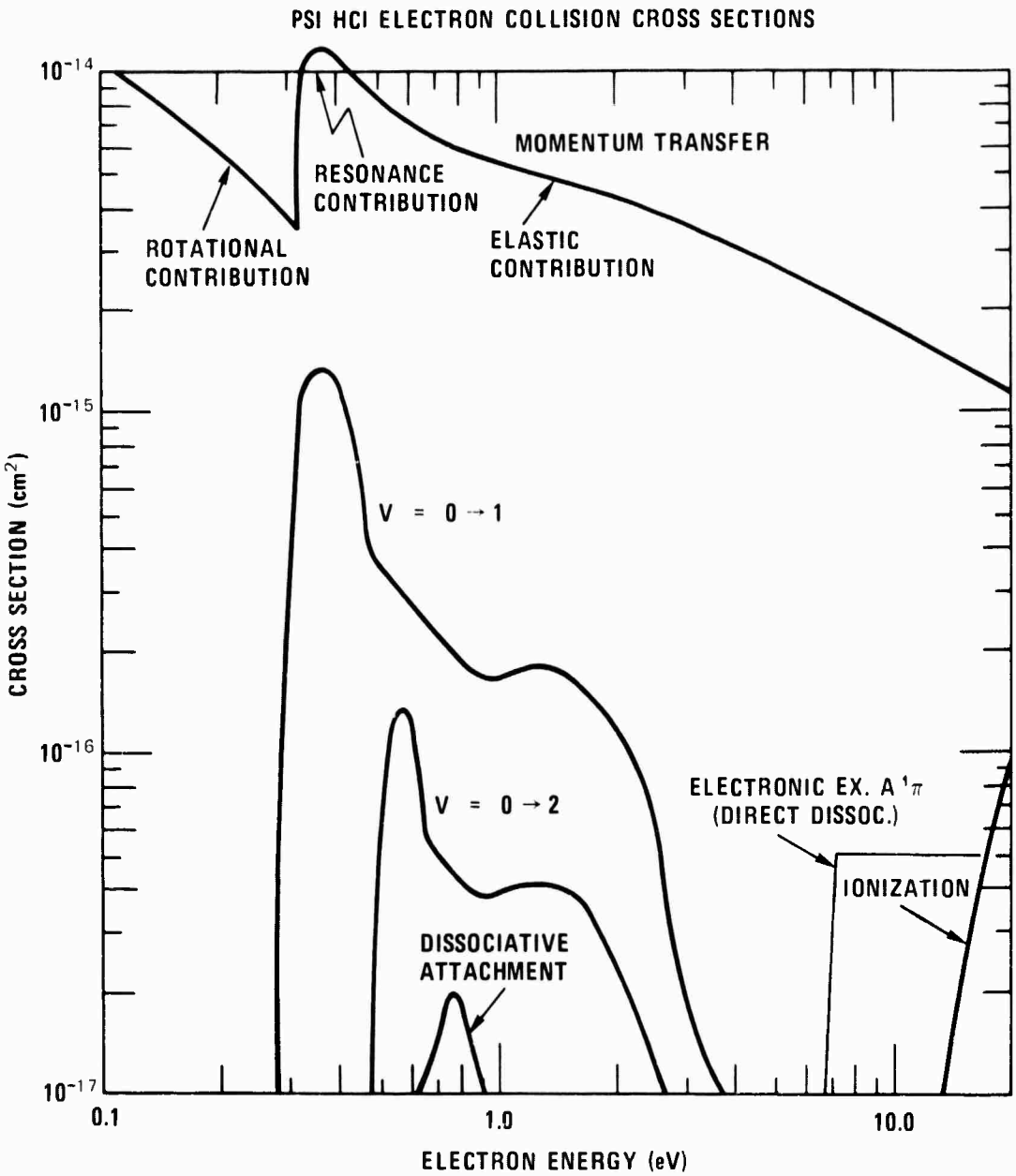

Figure 10 – Physical Sciences Incorporated electron-HCl cross section set. Vibrational cross section shapes are from Rohr and Linder (Ref. 4).

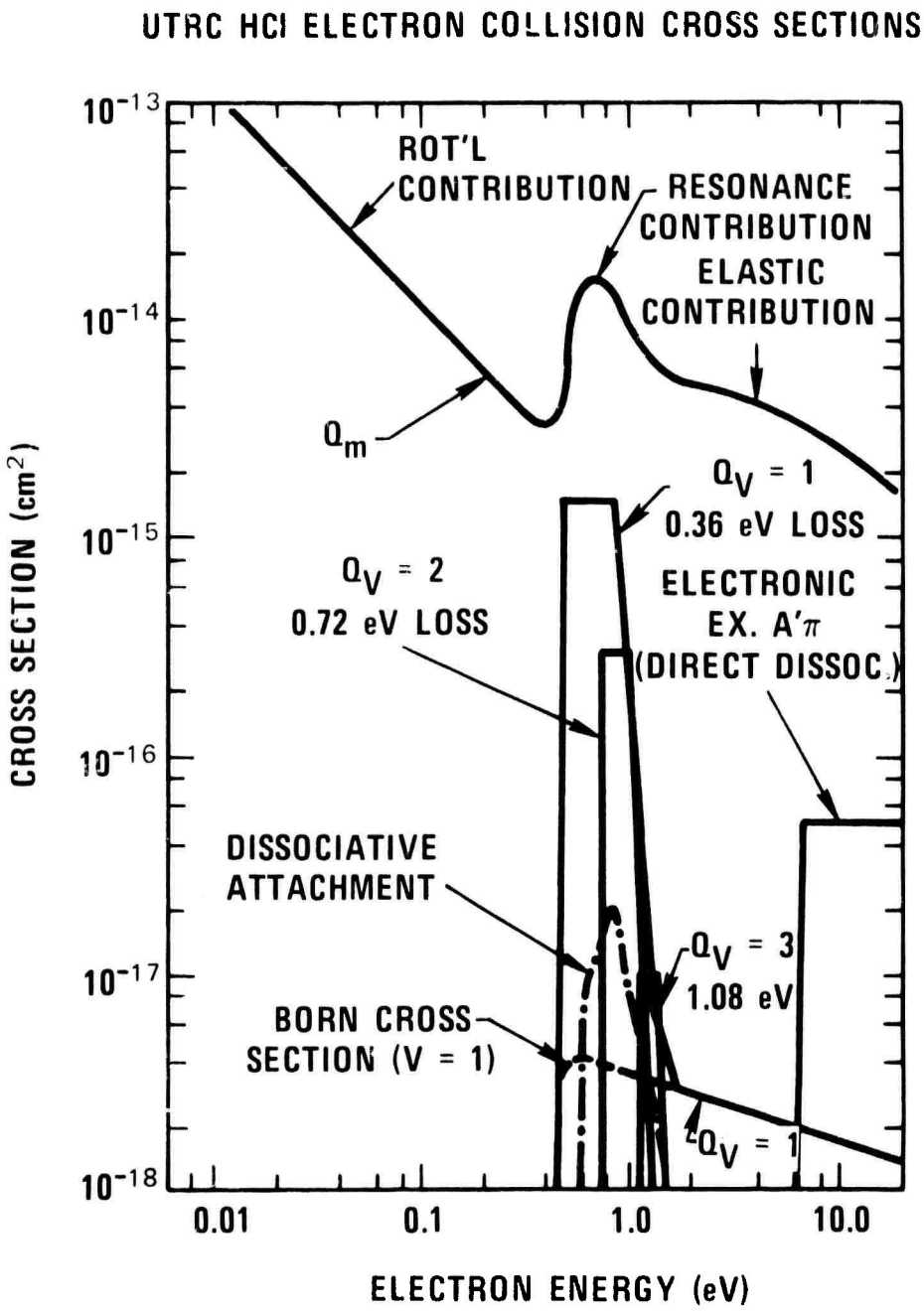

Figure 11 – United Technology Research Center electron-HCl cross section set. Figure taken from Ref. 17.

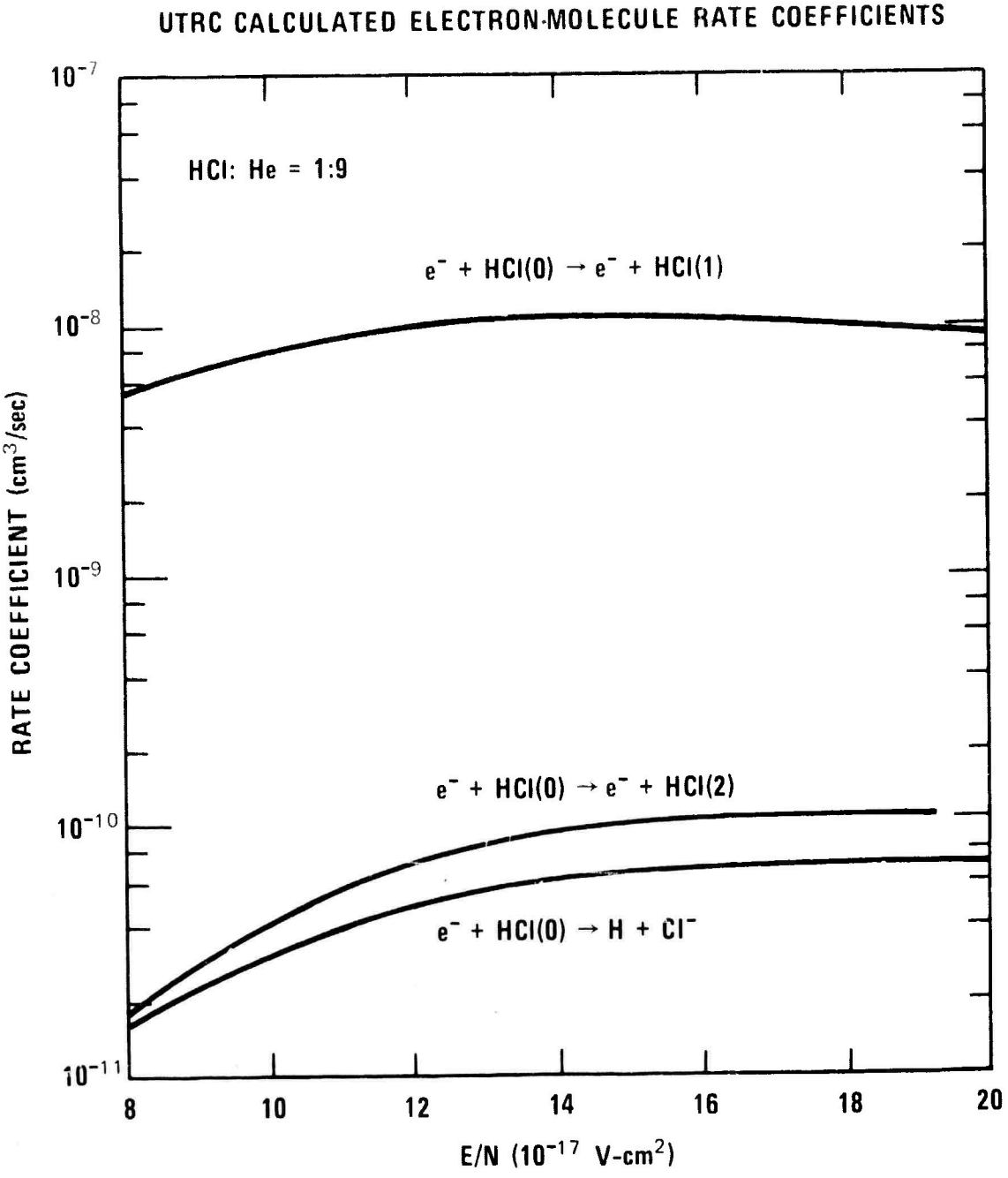

Figure 12 – HCl electron-molecule rate coefficients calculated for 1:9 HCl:He mixture using United Technology Research Center HCl cross section set and resulting electron energy distribution vs E/N. Figure taken from Ref. 17.

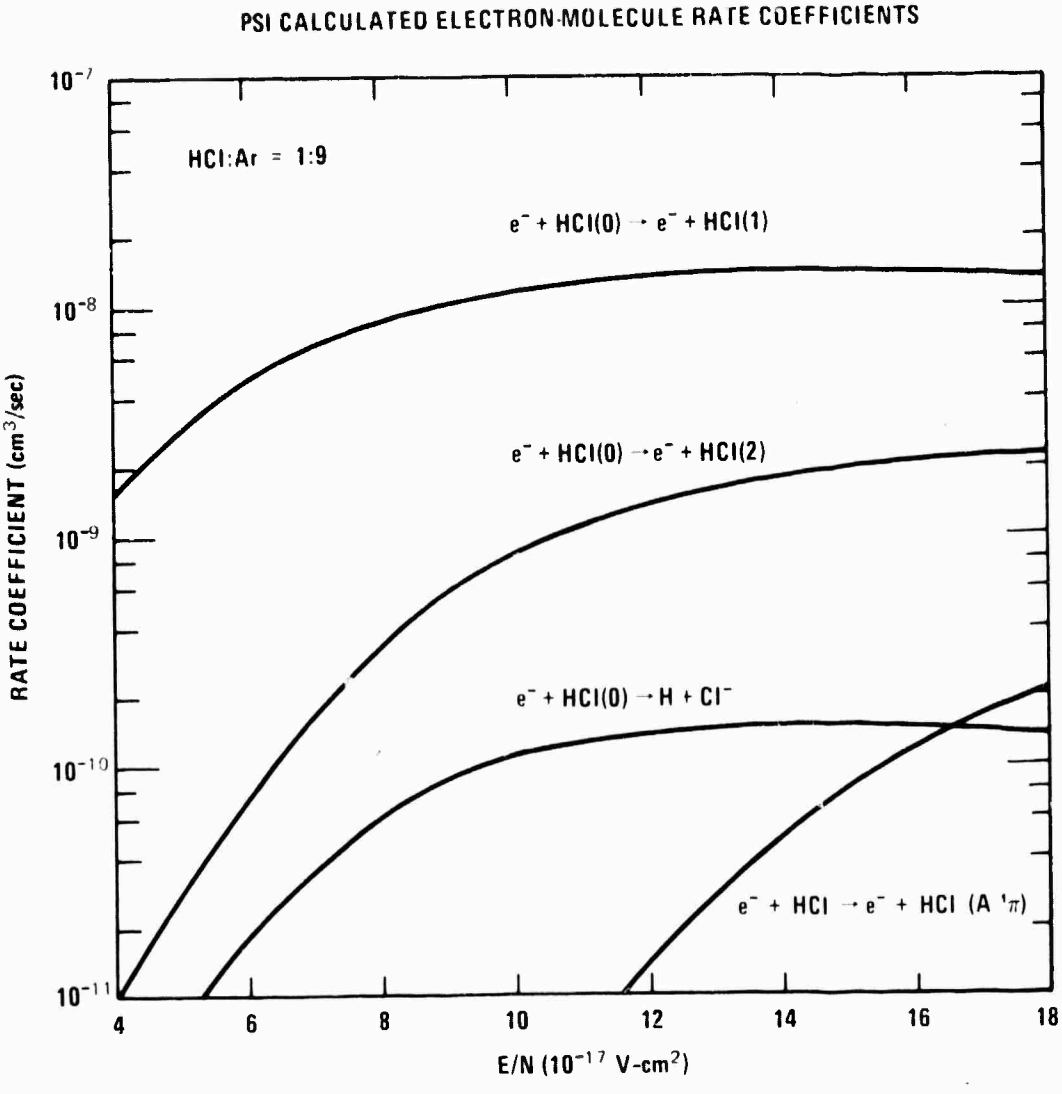

Figure 13 – HCl electron-molecule rate coefficients calculated for 1:9 HCl:Ar mixture using Physical Sciences Incorporated HCl cross section set and resulting electron energy distribution vs E/N.

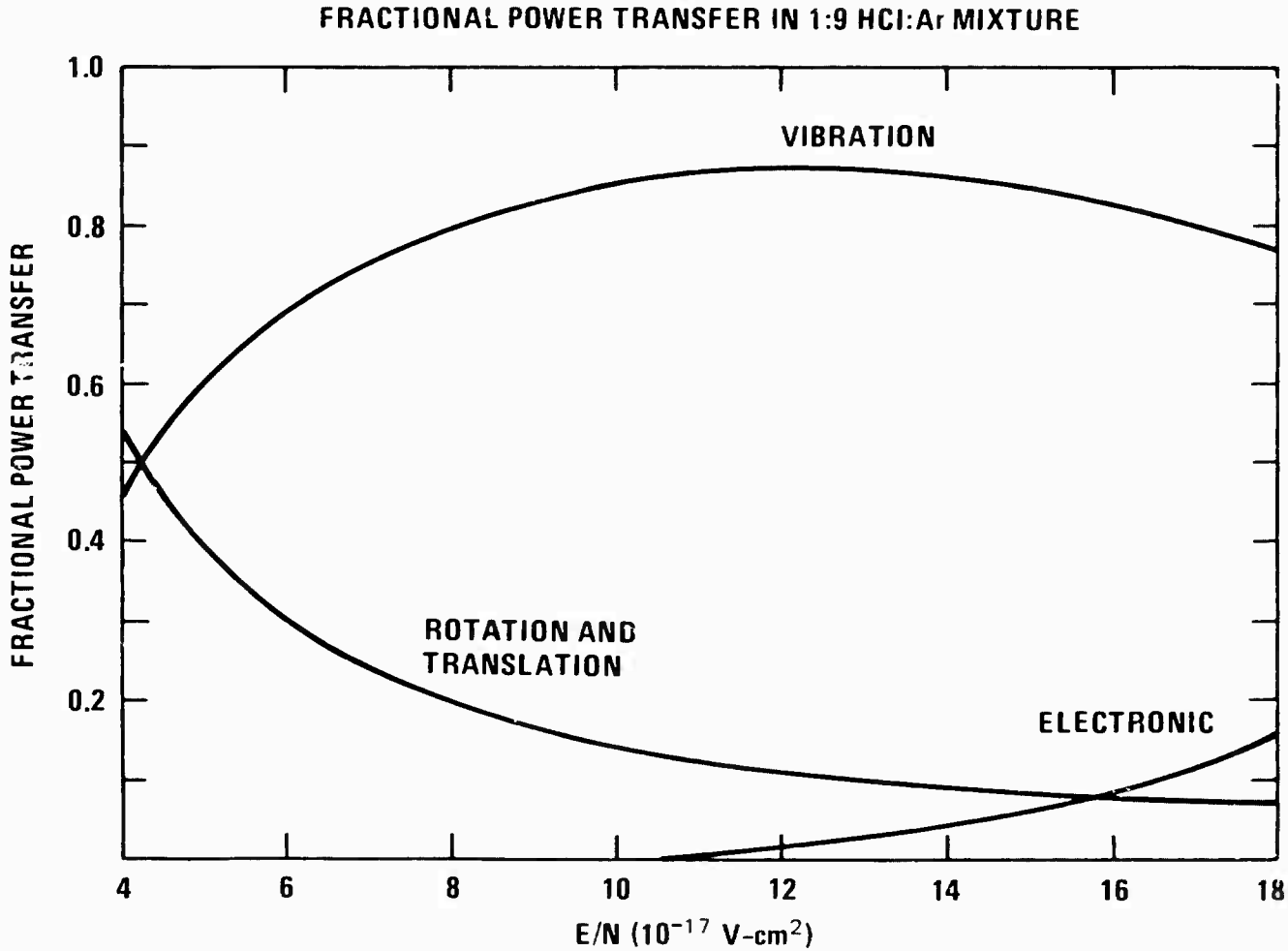

Figure 14 — Fractional power transfer in 1:9 HCl:Ar mixture calculated using Physical Sciences Incorporated HCl cross section set and resulting electron energy distribution vs E/N.

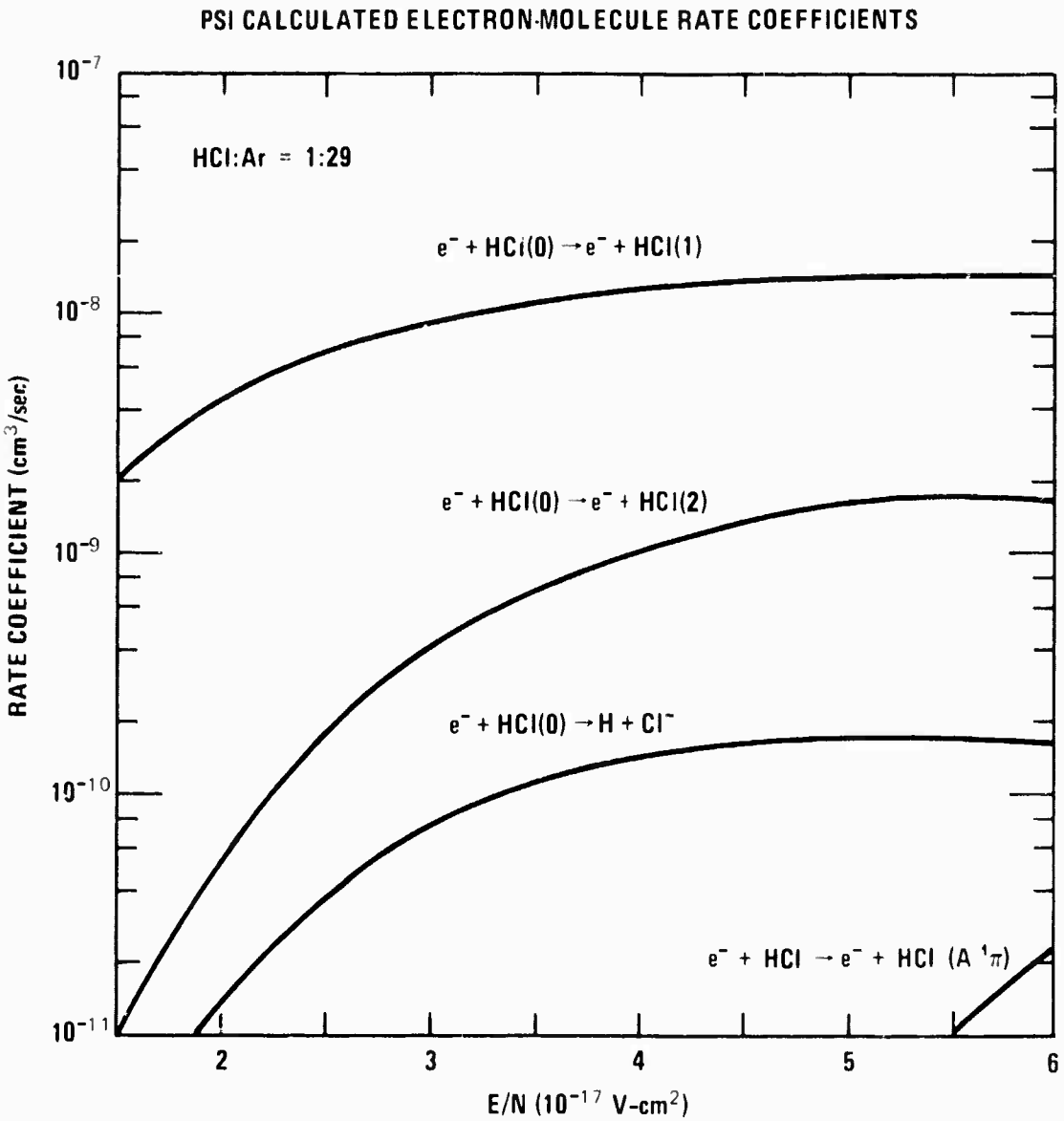

Figure 15 – HCl electron-molecule rate coefficients calculated for 1:29 HCl:Ar mixture using Physical Sciences Incorporated HCl cross section set and resulting electron energy distribution vs E/N.

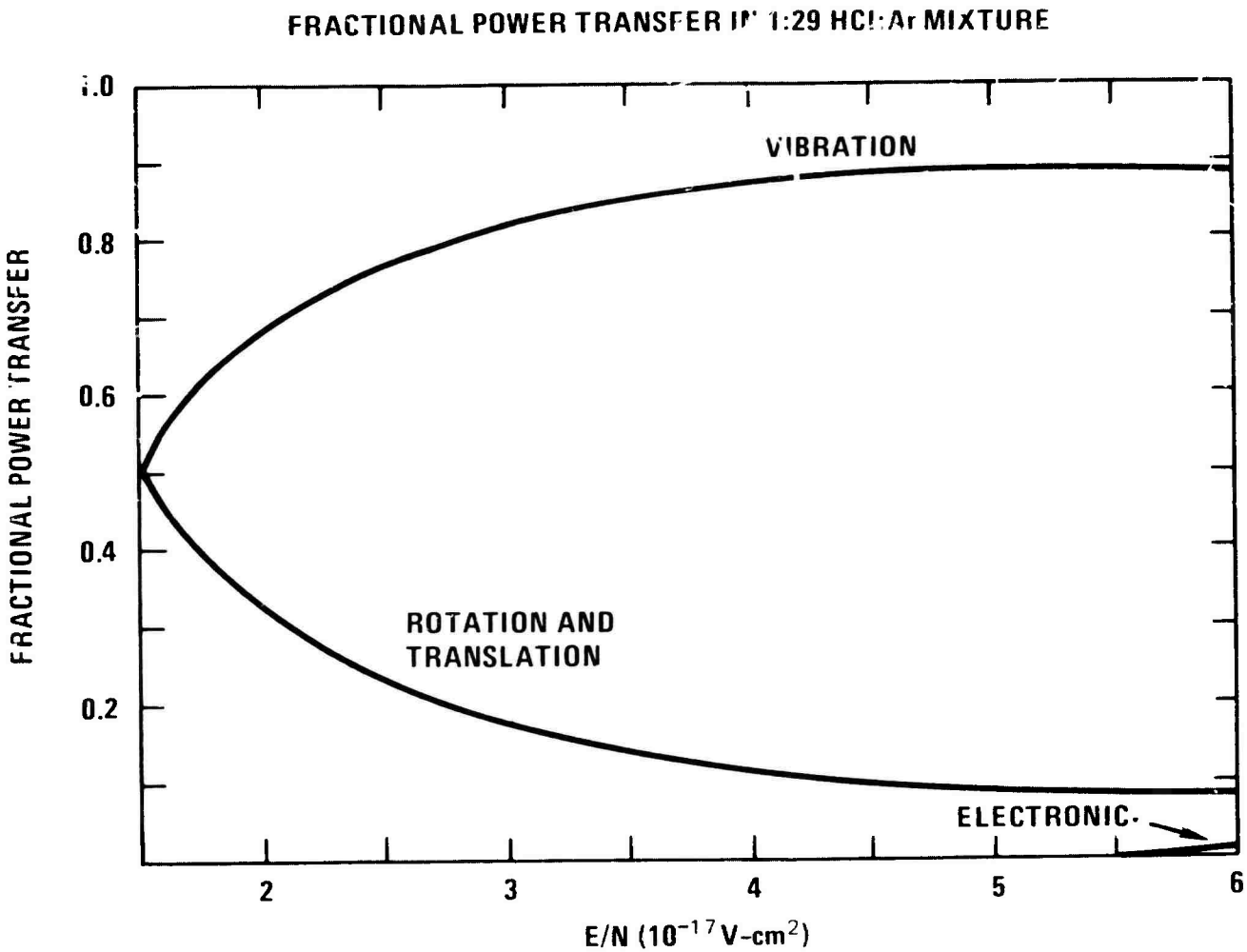

Figure 16 — Fractional power transfer in 1:29 HCl:Ar mixture calculated using Physical Sciences Incorporated HCl cross section set and resulting electron energy distribution vs E/N.

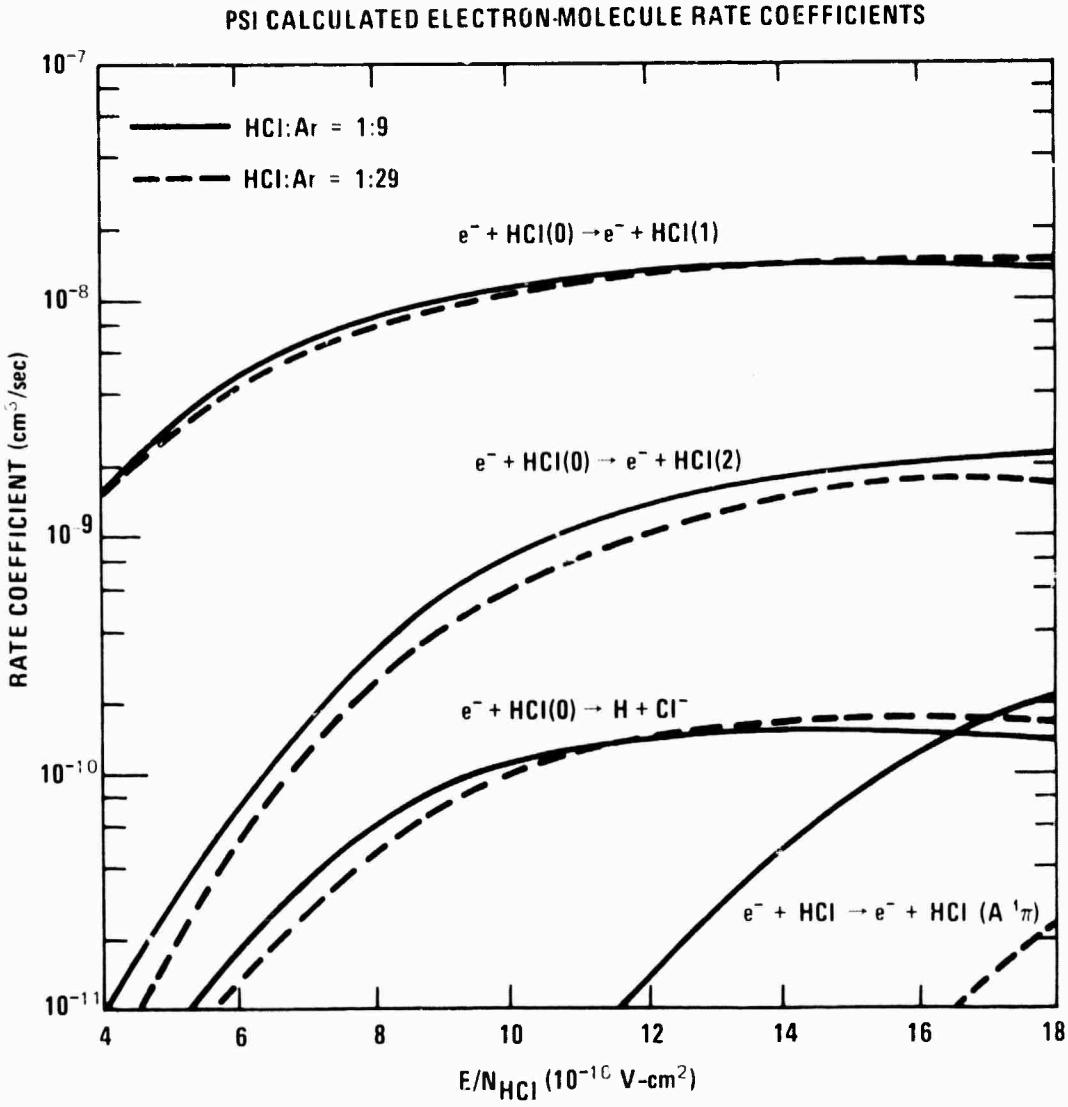

Figure 17 -- Comparison of HCl electron-molecule rate coefficients for 1:9 HCl:Ar (——) and 1:29 HCl:Ar(– – –) mixtures as a function of E/N_{HCl} indicating that this parameter predominantly determines the discharge kinetics. Rate coefficients were calculated using Physical Sciences Incorporated HCl cross section set and resulting electron energy distributions vs E/N.

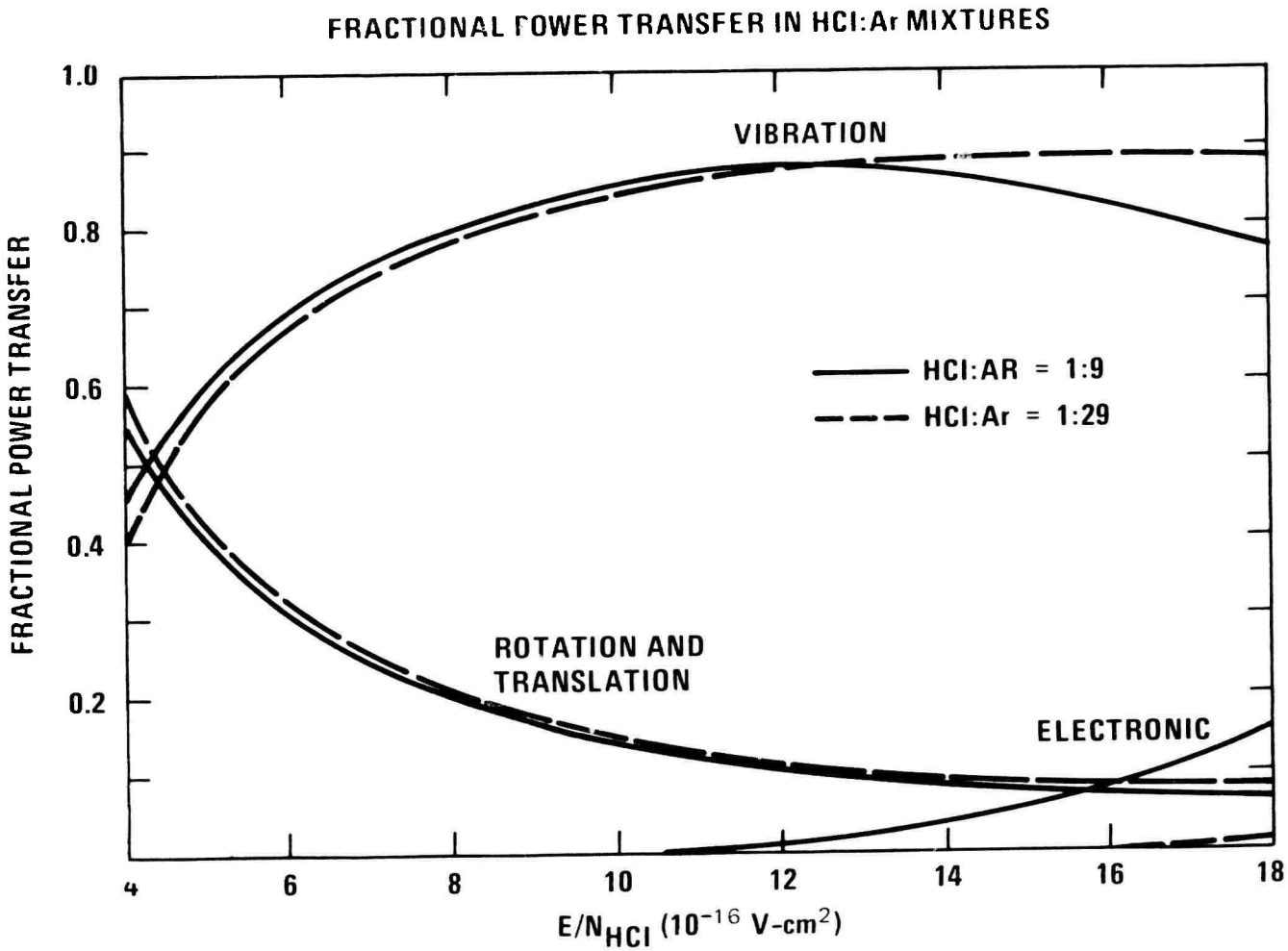

Figure 18 – Comparison of fractional power transfer in 1:9 HCl:Ar(——) and 1:29 HCl:Ar (– – –) mixtures as a function of E/N_{HCl} indicating that this parameter predominantly determines the discharge energy allocation. Fractions were calculated using Physical Sciences Incorporated HCl cross section set and resulting electron energy distributions vs E/N.

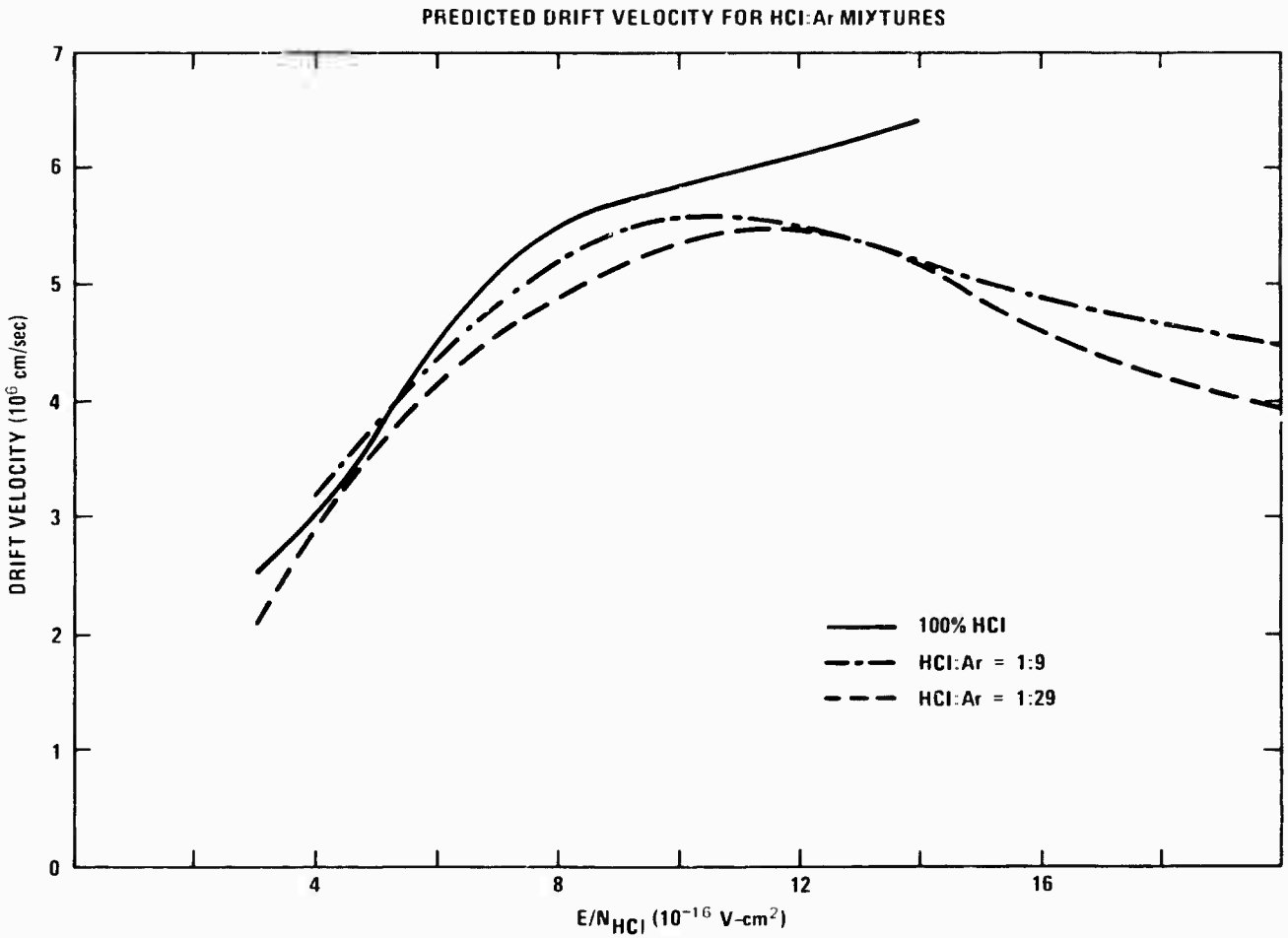

Figure 19 — Drift velocity predicted for 100% HCl(——), 1:9 HCl:Ar(— · —), and 1:29 HCl:Ar (— — —) mixtures using Physical Sciences Incorporated HCl cross section set and resulting electron energy distribution vs E/N.

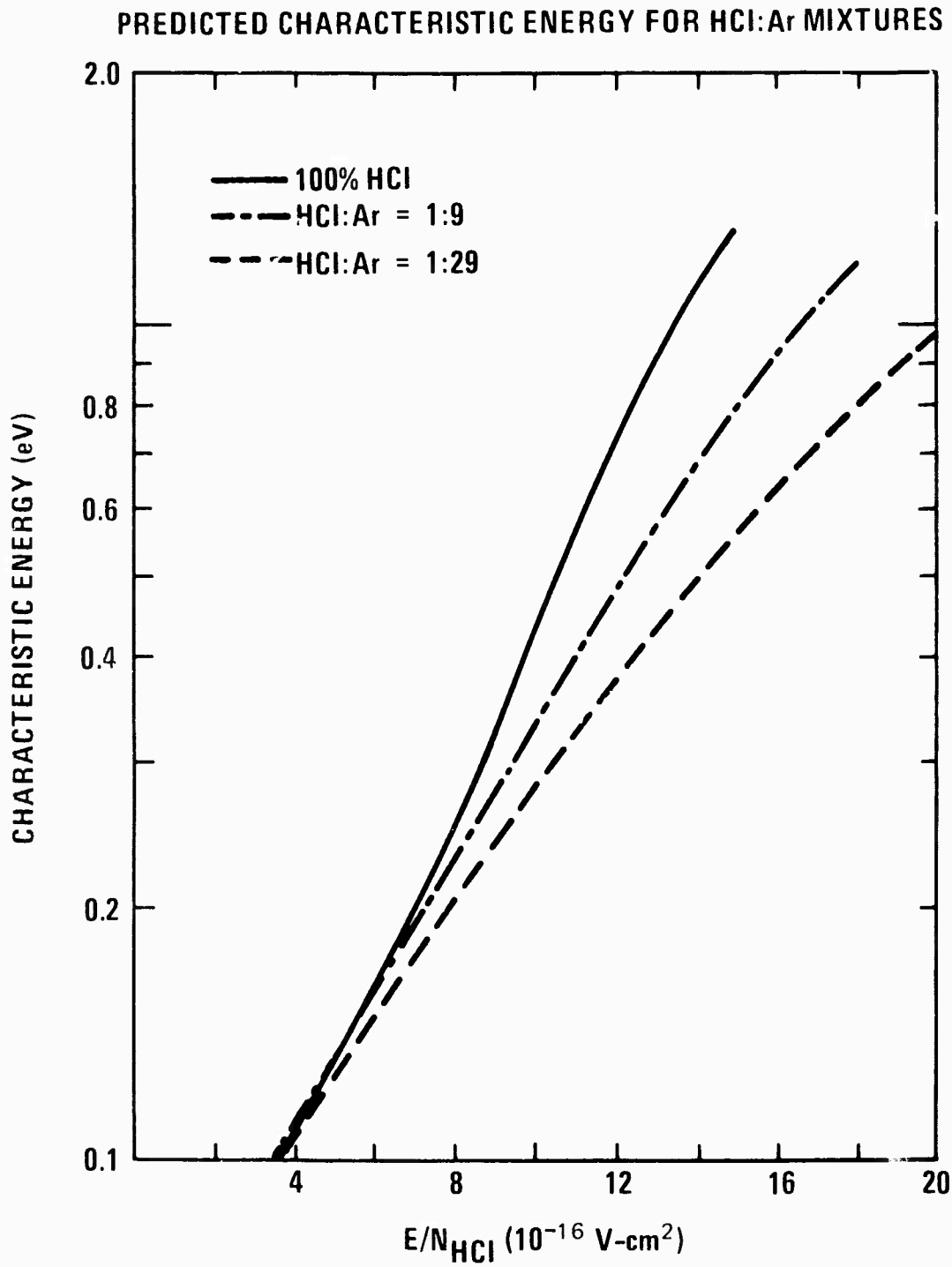

Figure 20 – Characteristic energy predicted for 100% HCl(——), 1:9 HCl:Ar (– · –), and 1:29 HCl:Ar(– – –) mixtures using Physical Sciences Incorporated HCl cross section set and resulting electron energy distribution vs E/N.

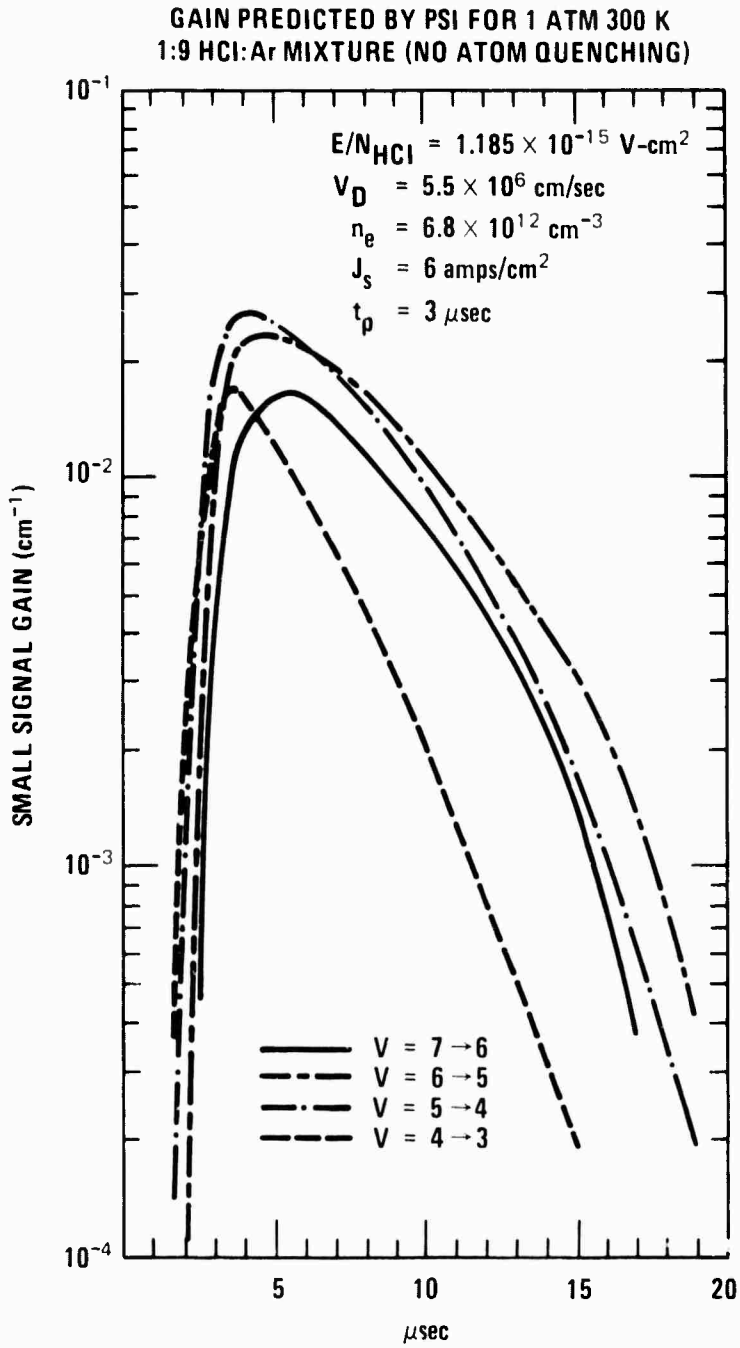

Figure 21 – Gain predicted by Physical Sciences Incorporated for one atmosphere 300°K 1:9 HCl:Ar mixture with a 3 μsec 6 amps/cm² sustainer current pulse at an $E/N_{HCl} = 1.185 \times 10^{-15}$ V-cm². The four lines with the highest peak gain are shown. Quenching due to H, Cl, and Cl^- was not included in these calculations.

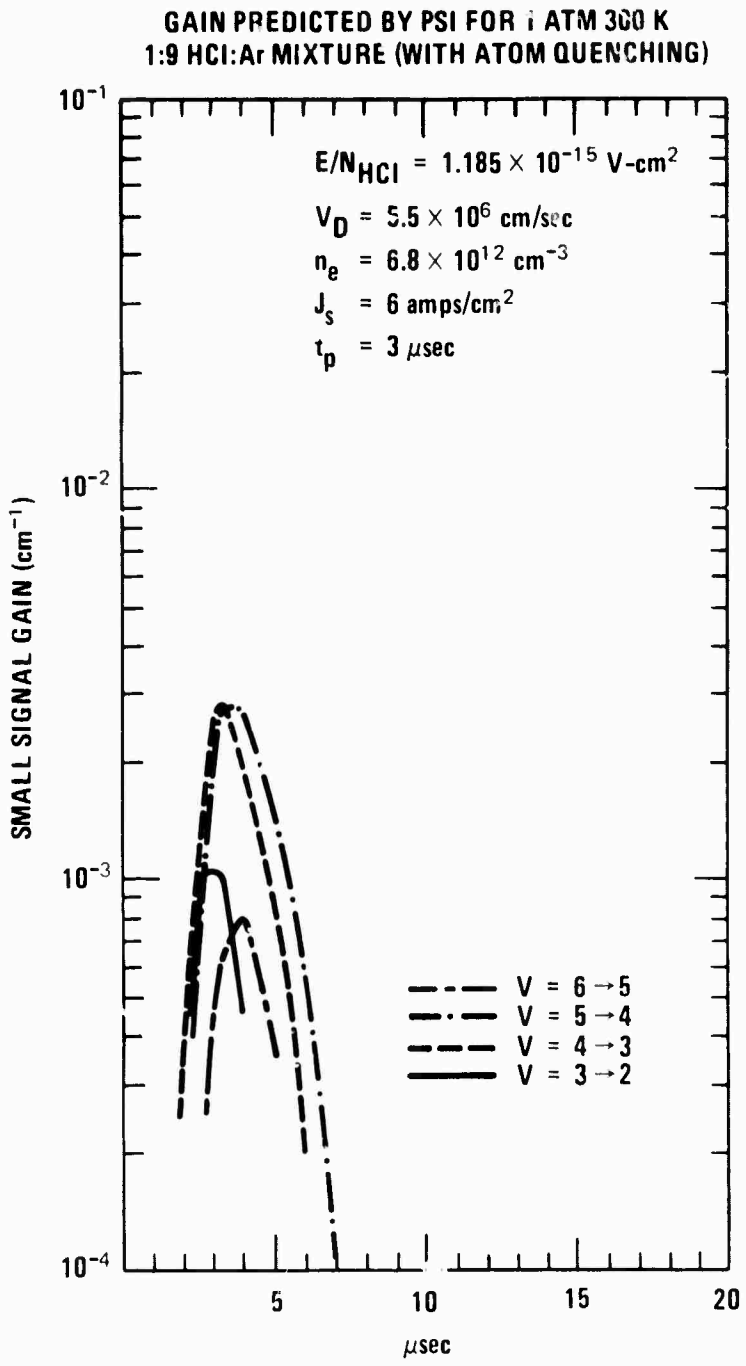

Figure 22 – Gain predicted by Physical Sciences Incorporated for one atmosphere 300°K 1:9 HCl:Ar mixture with a 3 μsec 6 amps/cm² sustainer current pulse at an $E/N_{HCl} = 1.185 \times 10^{-15}$ V-cm². The four lines with the highest peak gain are shown. Quenching due to H, Cl, and Cl^- was included by increasing the HCl self-deactivation rate by a factor of three.

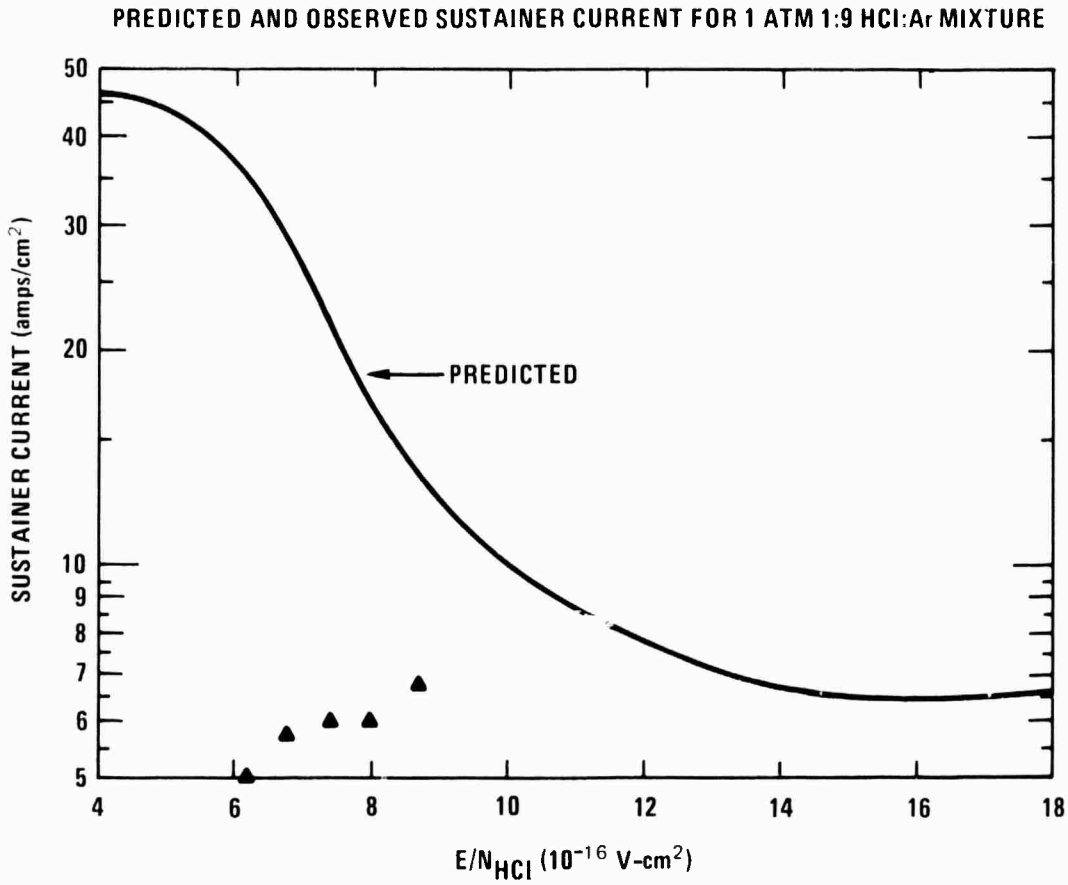

Figure 23 – Predicted (——) and observed (▲) sustainer current for 1 atm 1:9 HCl:Ar mixture. Predictions were made using the drift velocity, characteristic energy and rate constant for dissociative attachment calculated using the Physical Sciences Incorporated HCl cross section set and resulting electron energy distribution vs E/N. Dissociative recombination rate constant for Ar_2^+ was computed using the characteristic energy in the Mehr and Biondi (Ref. 15) expression for α. E-beam ionization source term $S = 3 \times 10^{21}/cm^3\text{-sec}$ was used.

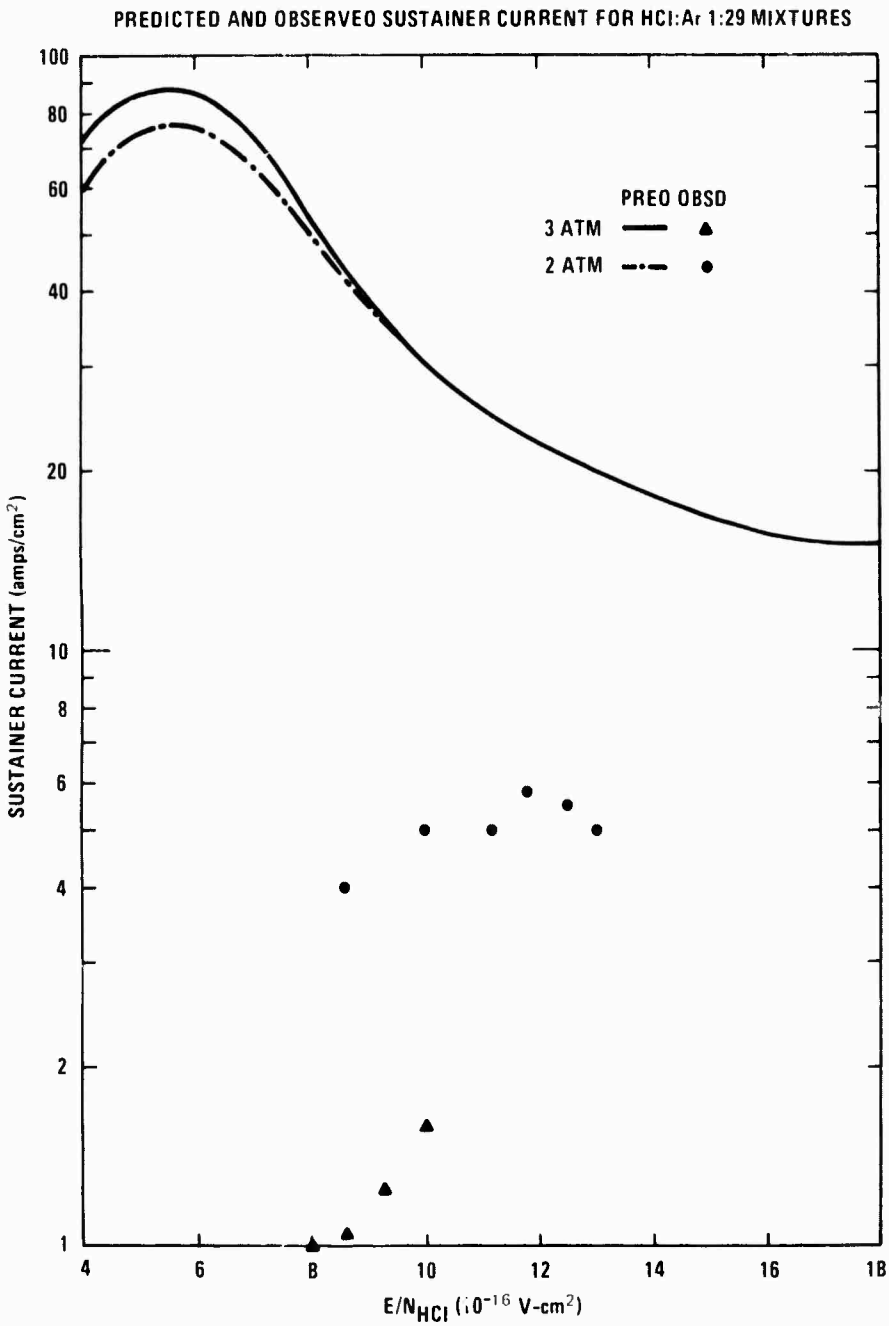

Figure 24 – Sustainer current for 1:29 HCl:Ar mixtures at 2 atm (– · – predicted; ● observed) and 3 atm (—— predicted; ▲ observed) total pressure. Predictions were made using the drift velocity, characteristic energy and rate constant for dissociative attachment calculated using the Physical Sciences Incorporated HCl cross section set and resulting electron energy distribution vs E/N. Dissociative recombination rate constant for Ar_2^+ was computed using the characteristic energy in the Mehr and Biondi (Ref. 15) expression for α. E-beam ionization source term $S = 3 \times 10^{21}/cm^3\text{-sec}$ was used.

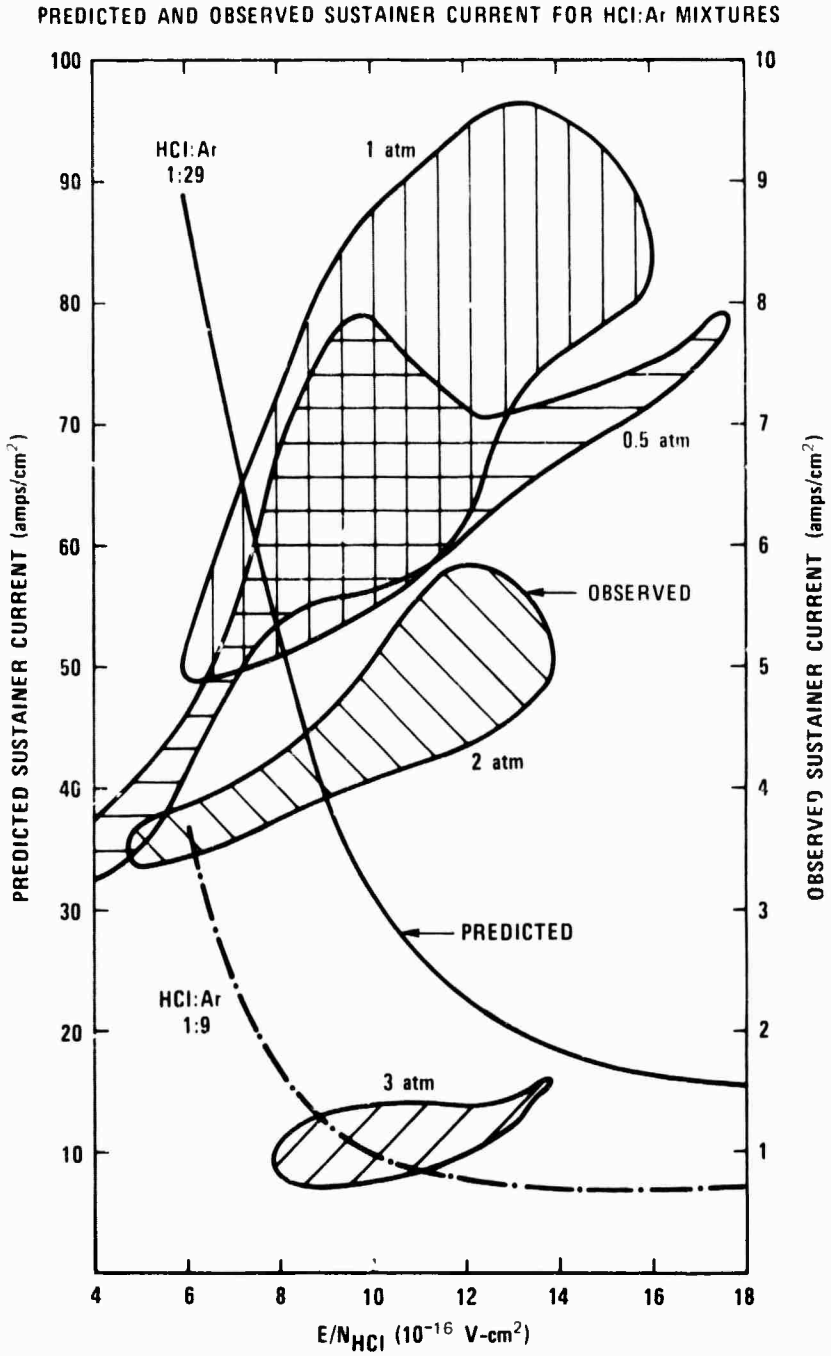

Figure 25 – Predicted and observed sustainer current for HCl:Ar mixtures. Shaded areas indicate range of sustainer currents observed for a given argon diluent pressure and E/N_{HCl}. Any difference between various HCl partial pressures was minimal. Predictions were made using the drift velocity, characteristic energy and rate constant for dissociative attachment calculated using the Physical Sciences Incorporated HCl cross section set and resulting electron energy distribution vs E/N.

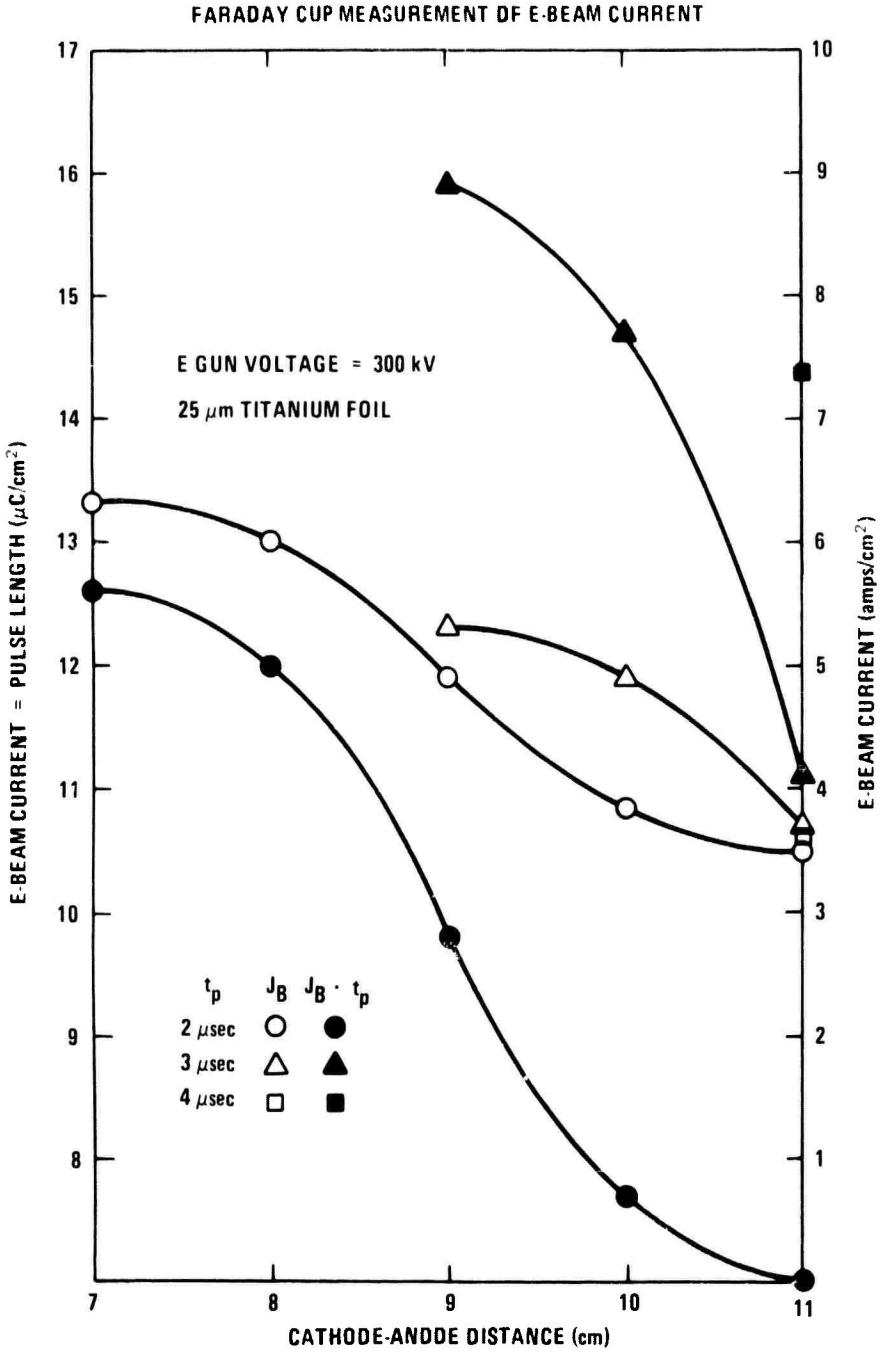

Figure 26 – Faraday cup measurements of the e-beam current passing through a 25 μm titanium foil for 2μsec (○), 3 μsec (△) and 4 μsec (□) pulses and an e-gun voltage of 300 kV. Also shown is the product of the e-beam current and the pulse length.

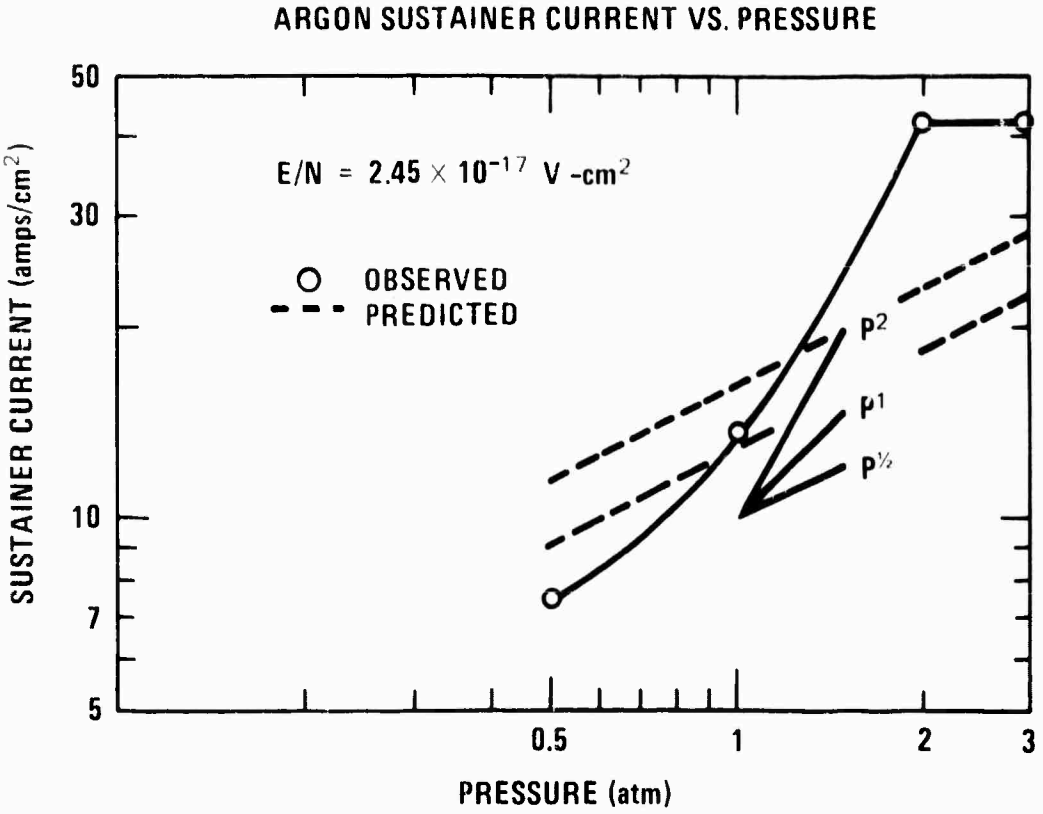

Figure 27 – Observed sustainer current in pure argon vs pressure for an E/N = 2.45×10^{-17} V-cm^2. Slopes corresponding to P^2, P^1, and $P^{1/2}$ pressure dependence are also shown. The dashed lines show the sustainer currents predicted for a drift velocity of 2.7×10^5 cm/sec, an e-beam ionization source term S = 3×10^{21}/cm^3-sec-atm, and Ar_2^+ dissociative recombination rate constants, α, of 2.1×10^{-8} cm^3/sec (– – –) and 3.3×10^{-8} cm^3/sec (——).

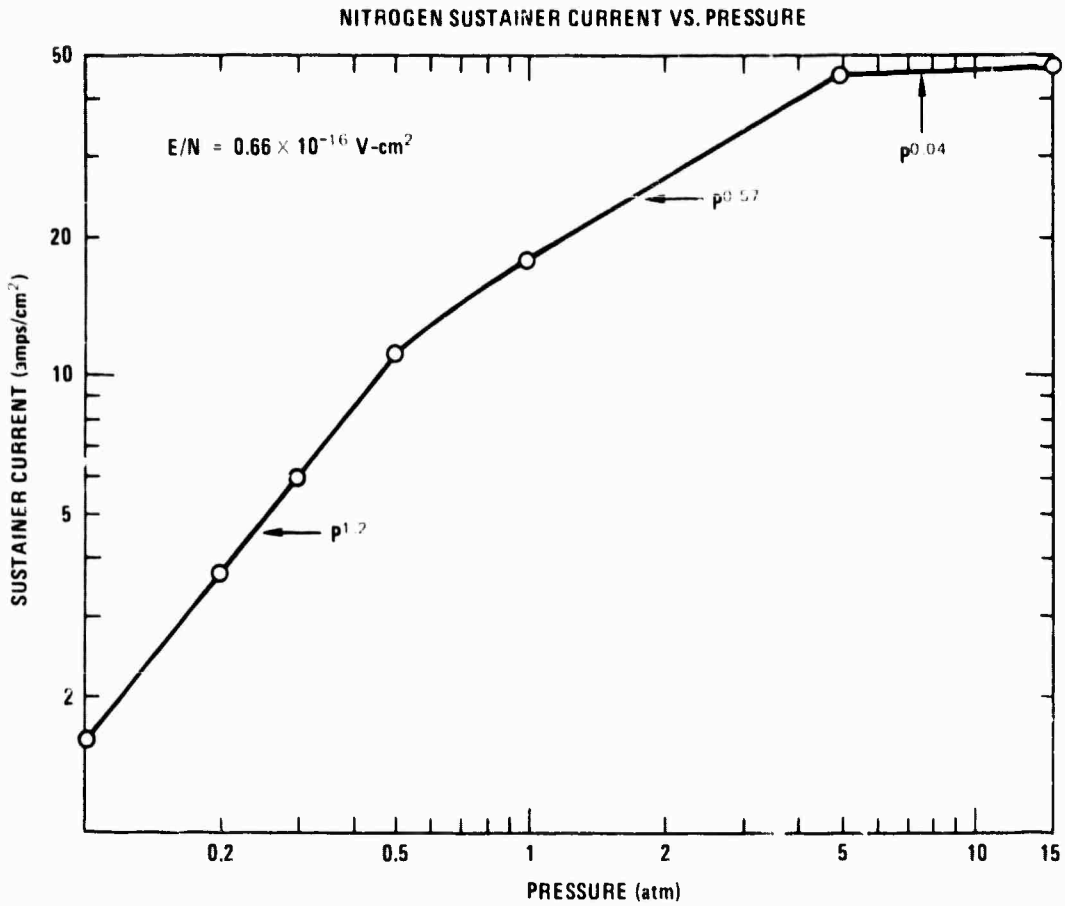

Figure 28 – Observed sustainer current in pure nitrogen vs pressure for E/N values of 1.10×10^{-18}V-cm² (◇), 0.57×10^{-16}V-cm² (□), 0.49×10^{-16}V-cm² (△), and 0.41×10^{-16}V-cm² (○). Slopes corresponding to P^2, P^1, and $P^{1/2}$ pressure dependence are also shown.

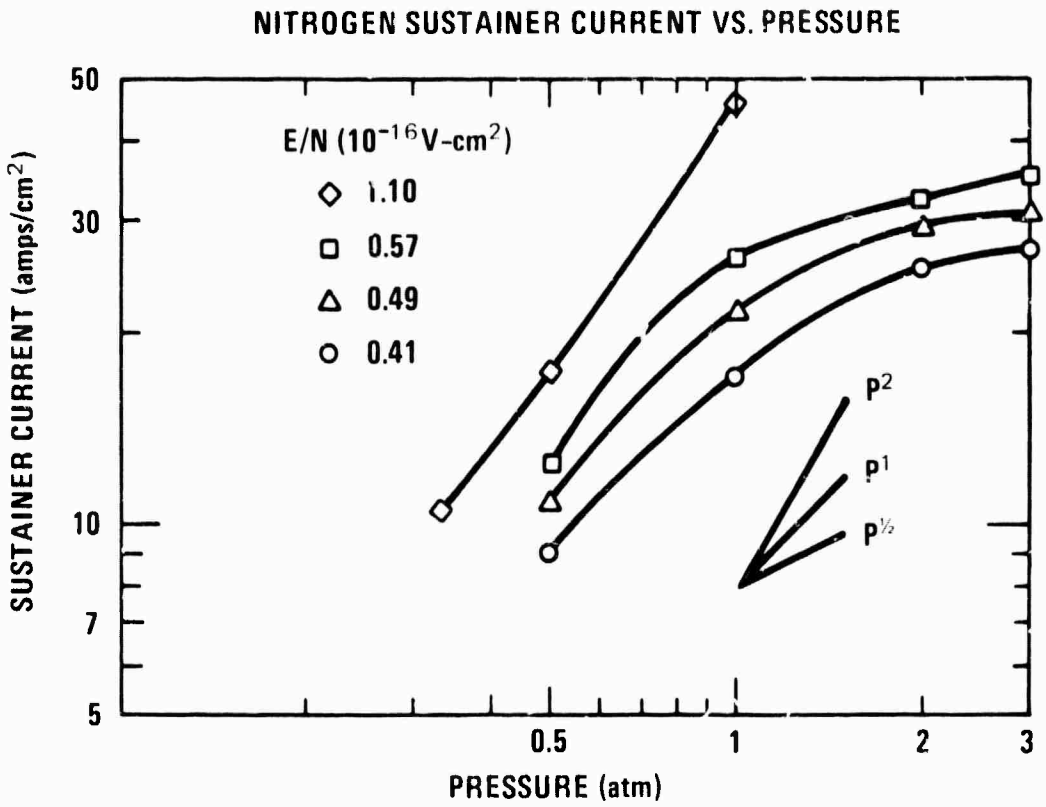

Figure 29 – Observed sustainer current in pure nitrogen vs pressure for an E/N = 0.66×10^{-16} V-cm². Measurements were made in a small discharge chamber with a 1.8×20 cm anode.

ELECTRONIC STATE LASERS

1. Electron Beam Initiated Visible/UV Transition Lasers

Under previous DARPA sponsorship the first rare gas halide laser, XeBr, was discovered at NRL.[1] In conjunction, kinetic modelling techniques were utilized to establish an elementary reaction mechanism for the production and loss of transient species relevant to the laser operation.[2] During the current reporting period, the NRL e-beam facility was used to obtain further information about the XeBr laser and about the excitation and decay processes related to the KrF laser system. The KrF kinetics were investigated by the fluorescence pulse shape analysis technique.

The operating conditions of the XeBr laser including laser power and fluorescence intensity were monitored as a function of the partial pressures of Xe and Br_2. Laser emission was found to occur over a limited range of conditions and was sensitive to small fluctuations in the e-beam pumping current. These observations indicate the near threshold nature of the laser. Consequently, it is believed that the peak laser output of ~ 200 W could be substantially increased but that it is unlikely to be competitive with the KrF laser. Experimental details are given in Appendix 3.

Emission resulting from reactions (1) and (2)

(1) $Xe^* + BrCN \rightarrow XeBr^* + CN$

(2) $Xe^* + BrCN \rightarrow Xe + Br + CN(B)$

was examined next. It was felt that e-beam excited Xe-BrCN mixtures might generate more powerful laser emission than Xe-Br_2 mixtures since deactivation by Br_2 would be avoided. BrCN was chosen as a Br donor because it is diatomic and a pseudo halogen molecule.

The experimental approach was to determine the yield of XeBr* from step (1) relative to the yield of XeBr* from a similar reaction with Br_2. A mixture of 1% BrCN in Xe gave the brightest fluorescence, however, the inte..... at 1 atm was lower by an order of magnitude than that from Br_2. Although this fact alone virtually precludes any possibility of efficient laser emission, some additional experiments were undertaken. Figures 30 and 31 show spectra at total pressures of 33 and 370 torr respectively. At the higher pressure XeBr* emission at 282 nm is dominant whereas CN(B) emission is seen exclusively at 33 torr. Apparently the CN(B) emission is more readily quenched than XeBr* and it appears that step (1) is a minor reaction pathway. The spectrum of XeBr* differs from previously observed spectra, in that the broad band at 330 nm is absent. This strongly suggests that the two bands originate from different excited electronic states of XeBr. The number of states involved has been a matter of controversy.[3]

Finally, a search was made for emission from XeCN*. While this species has never been observed, the similarity between CN and the halogens suggests its existence. The region from 250-650 nm was monitored on Polaroid type 57 film and a solar blind and an S-5 ITT

photodiode were used to cover the 170-600 nm region photoelectrically. Emission from the proposed XeCN* was not observed.

These tasks completed the investigation of the XeBr laser. Subsequently, the fluorescence pulse shape analysis technique was used to obtain mechanistic information on e-beam excited Kr-SF_6 and Kr-F_2 mixtures at low pressure. The objective was to measure the radiative lifetime of KrF* which is needed for laser modelling calculations. At present the value has been estimated to be 50 ns but has not been measured and it was felt that at NRL we were in a unique position to make the measurement because the required computer pulse synthesizer program was available from our XeBr* research program. Furthermore, the lifetime cannot be measured by the more direct laser fluorescence technique because the lower level is unbound.

The approach to the problem is as follows. Time resolved fluorescence measurements are taken from excited rare gas-halide mixtures at low pressure which is essential to simplify the reaction mechanism so that a minimum number of unknown rate constants are involved. At sufficiently low pressure, quenching reactions become negligible and the pathway beginning with rare gas ion formation and ending with rare gas halide creation can be ignored. The ion route simply occurs over a much longer time interval than the direct rate listed in steps (3-5) which are the only important reactions at low pressure.

(3) $\vec{e} + Kr \longrightarrow Kr^* + \vec{e}$

(4) $Kr^* + F_2 \xrightarrow{k_4} KrF^* + F$

(5) $KrF^* \xrightarrow{k_5} Kr + F + h\nu$

In the low pressure limit, step (4) becomes almost completely rate determining and emission measurements under these conditions lead to k_4. As the pressure is raised reaction (5) begins to affect the fluorescence pulse shape but a correction must be made for quenching.

Experimentally, emission intensities are measured over the appropriate pressure ranges. These data are digitized and compared to computer generated traces arising from a matrix of k_4 and k_5 values and a best fit is selected. The procedure must be free of complications because under no conditions does rate (5) become the rate-controlling step.

An initial series of experiments were performed with Kr-SF_6 mixtures. Fluorescence traces resulting from KrF* emission were recorded over a wide range of partial pressures and surprisingly the pulse-widths (FWHM) were always much shorter than expected. For example, at the lowest pressure, 3.1 torr of Kr with .0625% SF_6, the FWHM was 1.2 μsec. The direct mechanism indicates that the FWHM should not be less than approximately 40 μsec if a gas kinetic rate constant for Kr* reaction with SF_6 and a sub-microsecond rate constant for emission are assumed. These data, along with the knowledge that the e-beam initially makes about three times as many rare gas ions as metastable species suggests that some much faster ion-electron reaction is dominating the fluorescence spectrum. Because charge recombination occurs after a three-body dimerization step the ion chemistry route to RX* is so slow that it can be ignored[2,3] at low pressure. However, in Kr-SF_6 mixtures the narrow pulse widths observed forces a reconsideration

of this assumption. We believe that the following fast reactions account for the short fluorescence pulse,

(6) $\vec{e} + Kr \rightarrow Kr^+ + e + \vec{e}$

(7) $e + SF_6 \rightarrow SF_5^- + F$

(8) $Kr^+ + SF_5^- \rightarrow KrF^* + SF_4$

The dissociation attachment step (7) is expected to be fast because of its large cross section, and reaction (8) is also expected to be fast because this type of process typically has a rate constant on the order of 10^{-7} cm^3/sec.

In further experiments fluorine was used as the halogen donor but the fluorine was available to us only as a He/2% F_2 mixture. Helium is essentially transparent to the electron beam and does not complicate the reaction kinetics as a result of energy transfer from electronically excited helium species to Kr or F_2 except at the highest pressures reported here. Multiple e-beam shots of a single gas fill were found to seriously degrade the exciplex emission intensity, hence the stainless steel cell was evacuated and refilled after each shot.

Fluorine is a better reactant than SF_6 because the recombination step (9) is much slower than reaction 8 at low pressure. The pulse-

(9) $Kr^+ + F^- + M \rightarrow KrF^* + M$

widths for the KrF fluorescence were, as a result, in agreement with the original predictions. The next effort was to verify that steps (3)-(5) were sufficient to explain the observations for Kr/F_2 mixtures.

Other possible areas of importance are the quenching reactions, steps (10) and (11)

(10) $KrF^* + F_2 \longrightarrow Kr + F + F_2$

(11) $KrF^* + Kr \longrightarrow Kr + Kr + F$

Step 8 can be ignored at low pressure because the maximum rate of reaction is less than the radiative rate. However, even at the lowest pressures investigated, step (11) can be significant and its importance can be seen by the effect of the Kr pressure on the fluorescence pulse-width. The effect according to steps (3)-(5) would be a linear increase in the fluorescence amplitude with increasing Kr pressure. The results of this experiment are plotted in Fig. 32. It is seen that doubling the Kr pressure from 25 to 50 torr decreases the FWHM by 60%. Therefore, clearly a step such as reaction (11) is needed to explain this observation.

The effect of krypton pressure was not expected because a similar effect was not observed for the $Xe-Br_2$ system.[2] A similar set of experiments were done to investigate the role of helium as a KrF^* quencher. The results presented in Fig. 33 demonstrate that the addition of small amounts of helium substantially increases the emission intensely.

There is no simple explanation for the surprising behavior of the fluorescence output for these gas mixtures. It is known that the addition of small amounts of helium to the heavier rare gases can drastically affect the electron temperature through momentum transfer. It is probable that step (13) will be a fast process

(12) $e_{(1\text{-}2\ ev)} + He \longrightarrow He + e$

(13) $e_{(1\text{-}2\ ev)} + KrF^* \longrightarrow Kr + F^-$

and therefore it was hypothesized that the He effect on the fluorescence amplitude is caused indirectly through moderation of the electron energy distribution. This implies that at low electron densities reaction (13) will become unimportant and the He effect will diminish. Figure 34 reveals that the effect is still evident at substantially lower electron densities even when the electron density was reduced, by decreasing the e-beam current to a point where the fluorescence was diminished by an order of magnitude. However it can be seen that the FWHM of the emission does depend on the e-beam current. An effect of this type can only be caused by a reaction such as step (13) in which two transient species react with each other. A series of bimolecular reactions involving only one transient species per reaction is not a possible explanation since such a mechanism will generate fluorescence whose temporal dependence is invariant with pumping intensity.

Reaction (13) remains a candidate to explain the observed phenomena. It was anticipated that it might reduce the electron density sufficiently to eliminate step (12). The dependence of the FWHM on electron density shows that this was not accomplished. Hence, the effect of helium under weak excitation conditions is not entirely clear. If, indeed, the role of helium is to moderate the electron energy distribution additional steps must still be proposed to fully explain the data.

Any explanation for the observed decrease in the FWHM with added Helium must include a step leading to the formation or destruction of

KrF* which is accelerated by the presence of the helium. The destruction of KrF* has already been discussed. A faster formation rate could occur if two electronically excited states of Kr were involved. Steps (14)-(16)

(14) $Kr^{**} + F_2 \xrightarrow{slow} KrF^* + F$

(15) $Kr^* + F_2 \longrightarrow KrF^* + F$

(16) $He + Kr^{**} \longrightarrow Kr^* + He$

outline a possible mechanism to explain the data. It is known that a number of electronically excited states of Kr are created by the electron beam and collisions with helium likely will alter the initial distribution of excited states. Until now, Kr* has been used to represent a composite of all the neutral excited states which are present in the plasma. For the first time the data cannot be explained unless the composite is divided into two groups labelled Kr* and Kr** as in steps (12)-(14). Kr** reacts more slowly and has a low yield of KrF* while Kr* reacts more quickly and has a higher yield of KrF*. This proposal accounts for both the increased fluorescence intensity and decreased FWHM as a function of He concentration.

In summary, the fluorescence from e-beam excited $Kr:He:F_2$ mixtures cannot be simply explained. A similar study is being made of XeF* emission from $Xe:He:F_2$ mixtures in order to evaluate the operative mechanisms in this laser system.

References

1. S. K. Searles and G. A. Hart, Appl. Phys. Lett. 27, 243 (1975).

2. G. A. Hart and S. K. Searles, J. Appl. Phys., May (1976).

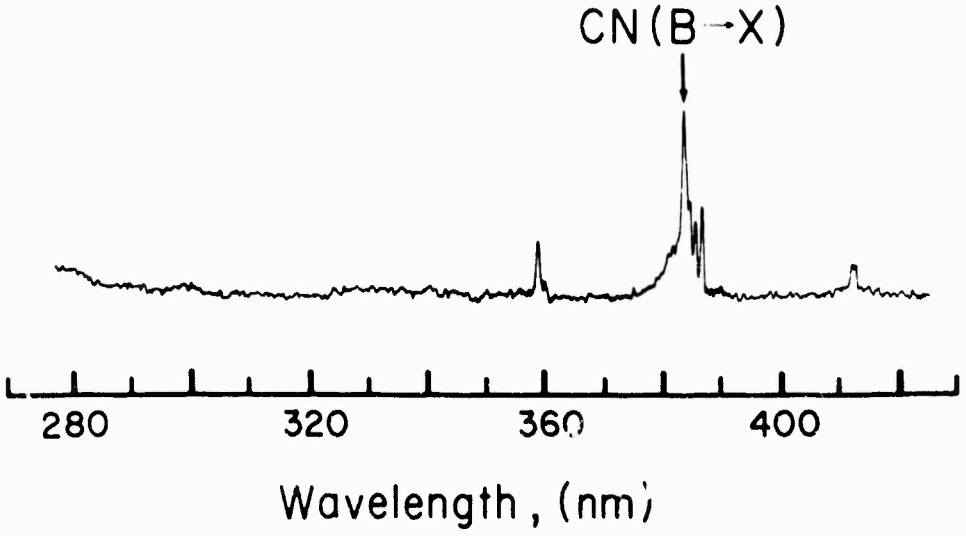

Fig. 30 — Emission spectrum from Xe:BrCN(13:1) mixture at 33 torr total pressure. The microdensitometer trace was taken from a negative made from the type 57 Polaroid original.

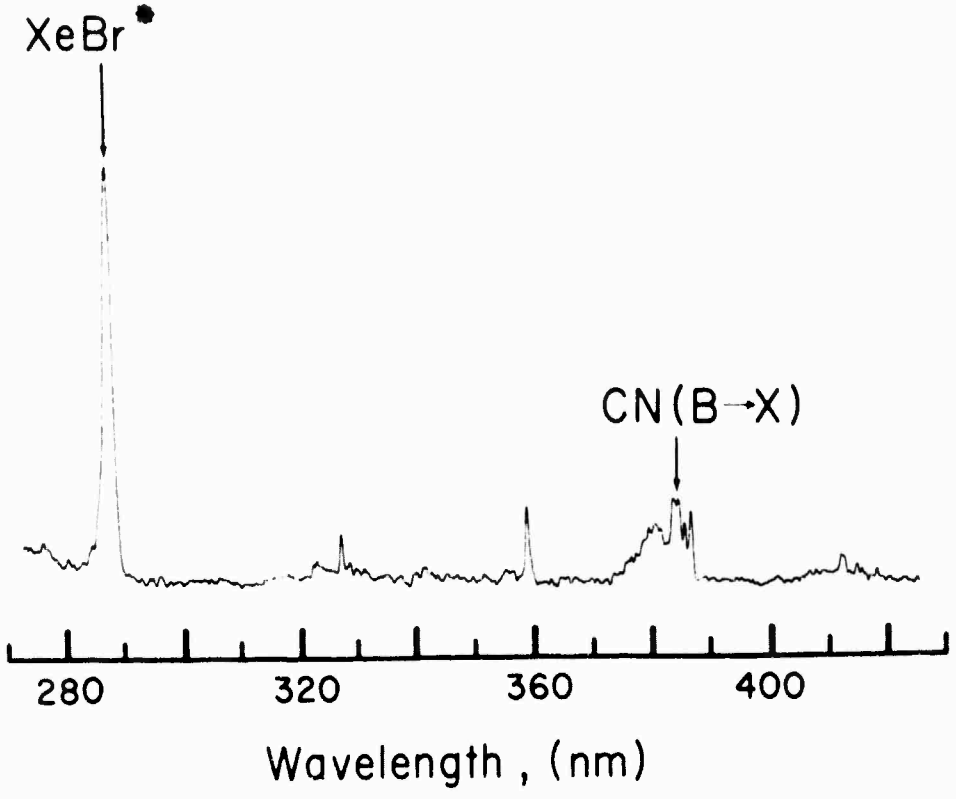

Fig. 31 — Same as Fig. 30 but total pressure 370 torr

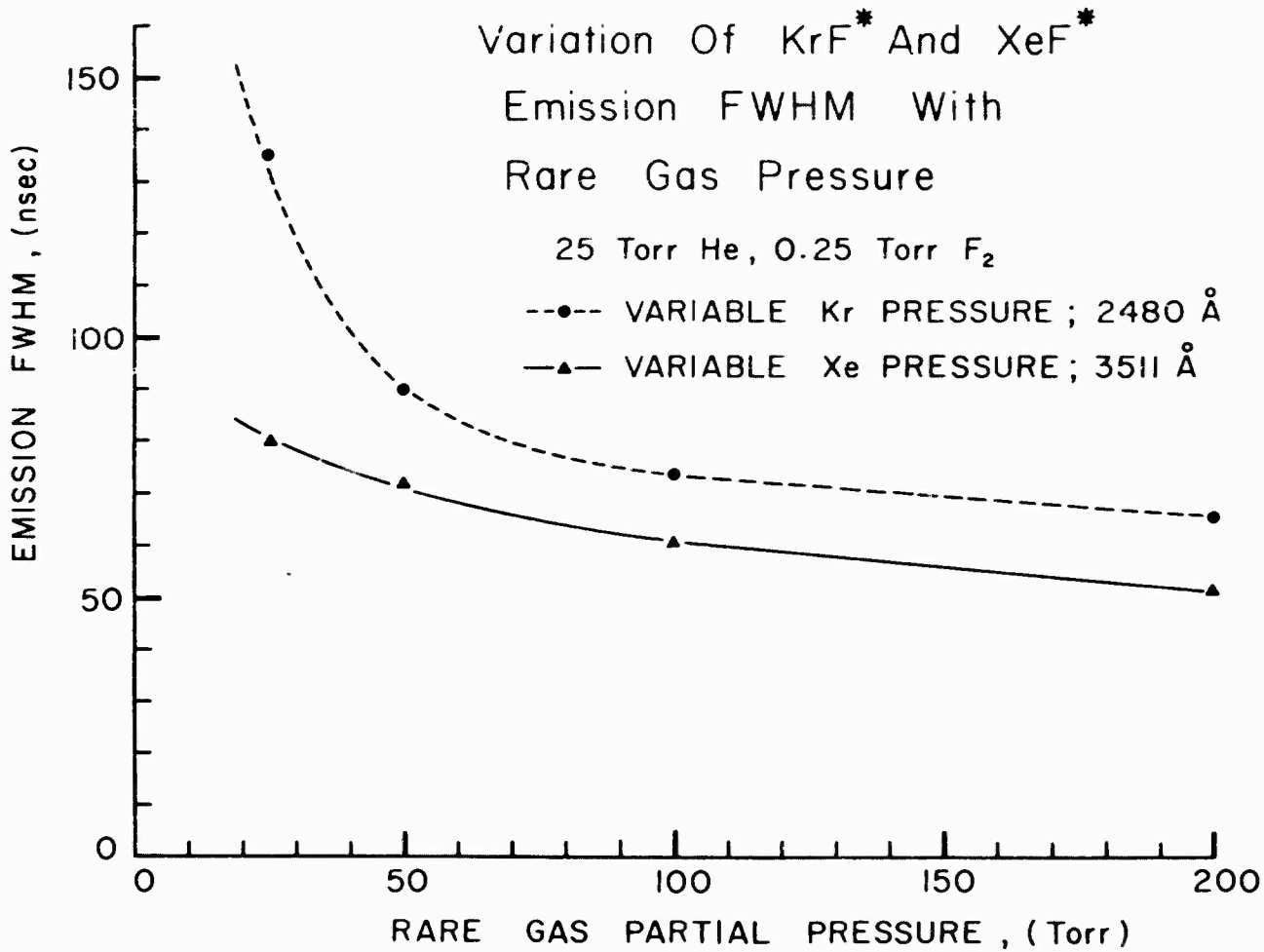

Fig. 32 — Effect of rare gas pressure on emission FWHM for He = 25 torr and P_{F_2} = 0.25 torr. Top curve: quenching of KrF* by Kr; bottom curve: quenching of XeF* by Xe.

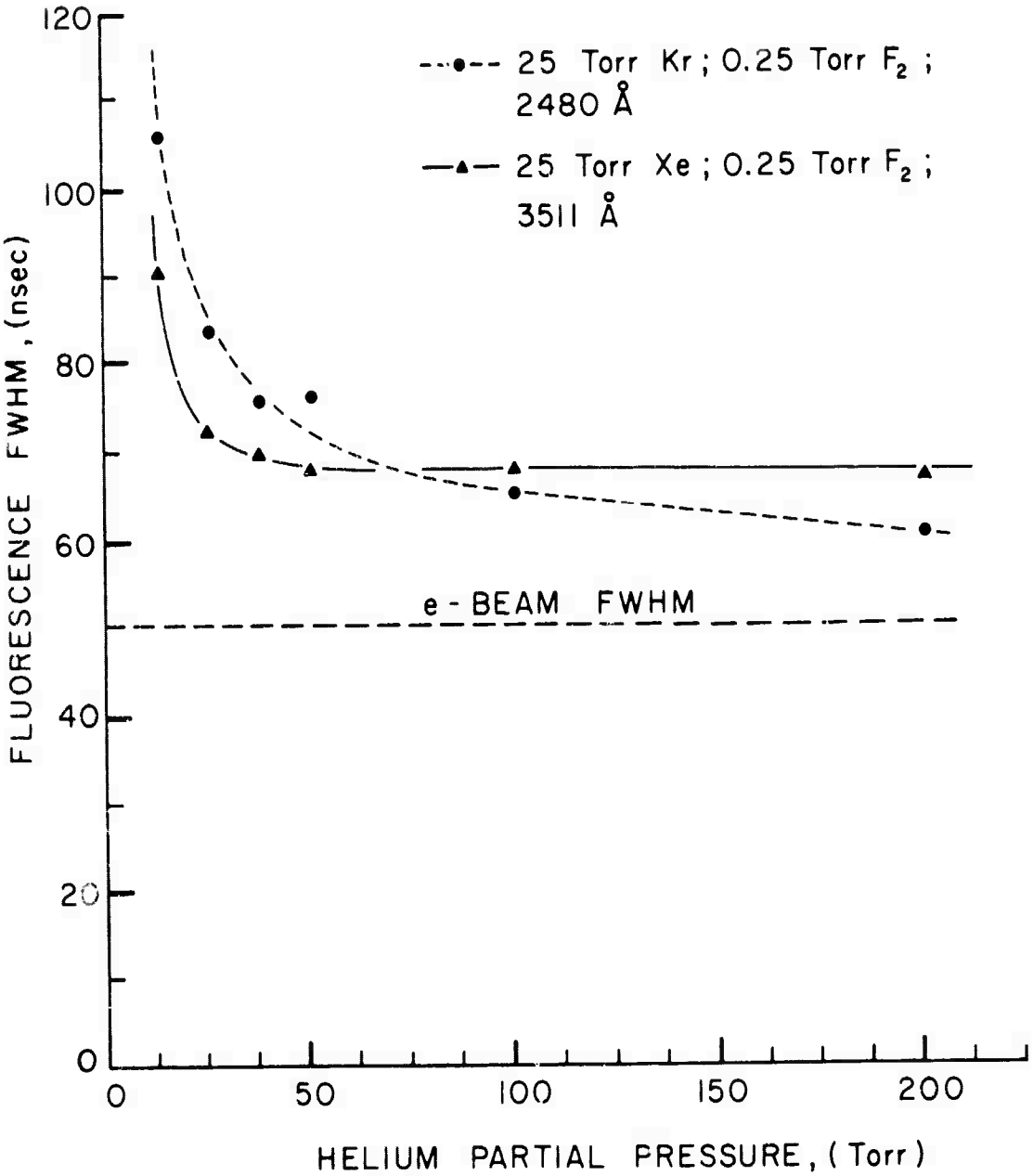

Fig. 33 — Enhancement of XeF* (dashed curve) and KrF* (solid curve) fluorescence with increasing He pressure

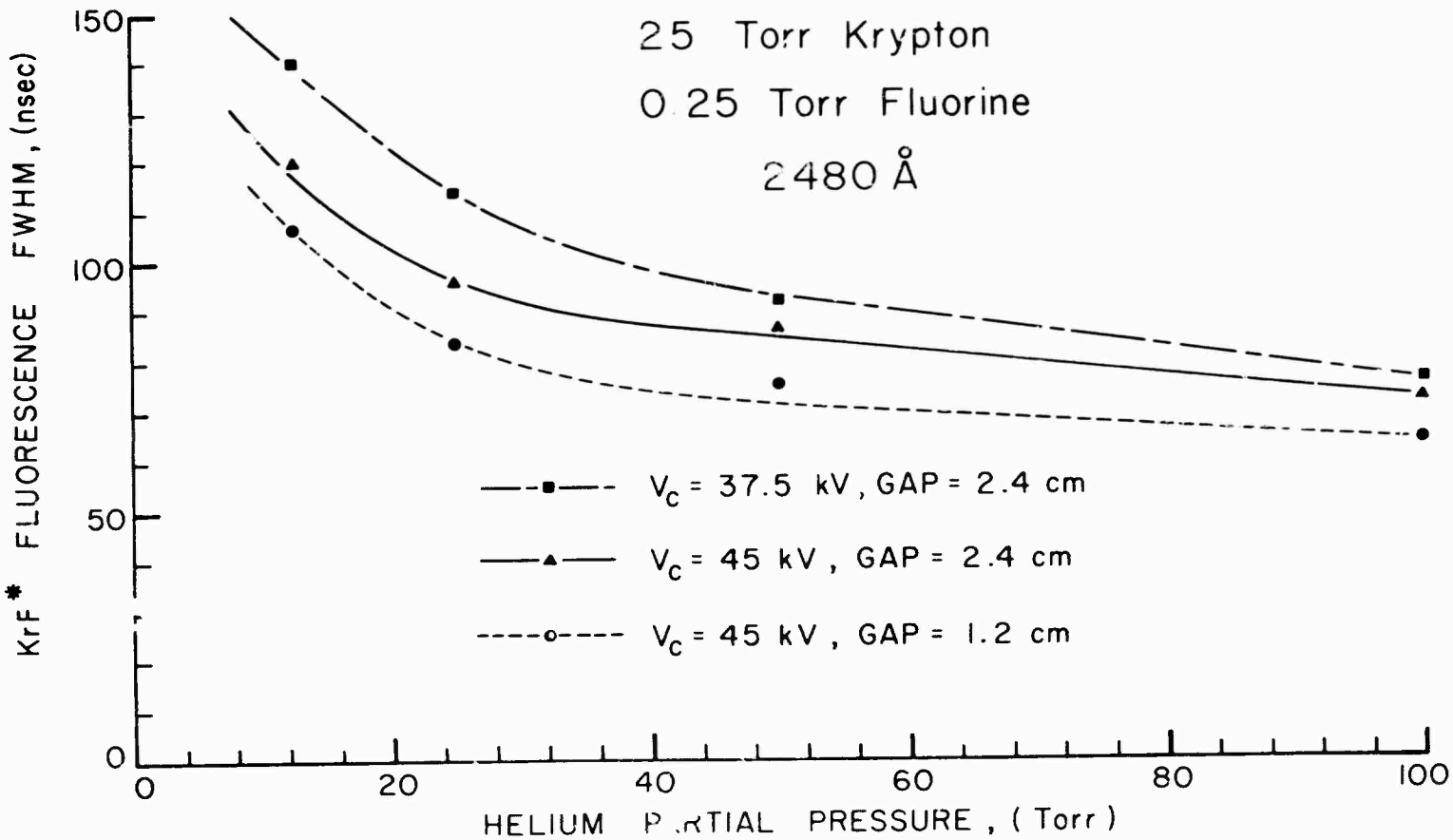

Fig. 34 — Emission FWHM of KrF* as a function of He pressure and e-beam pumping intensity. The plasma diode was gapped and the charging voltage V_c was reduced such that the integrated fluorescence intensity had the relative values: (●) 1.0, (▲) 0.1, and (■) 0.05.

3. J. Tellinghuisen, J. M. Hoffman, G. C. Tisone, and A. K. Hays, J. Chem. Phys., to be published.

2. Discharge XeF and KrF Lasers

Toward the end of the last reporting period, the first rare gas halide laser (in the form of XeBr) was discovered under this contract. Shortly afterwards, many other rare gas halide lasers were discovered in laboratories elsewhere. Among them, the KrF and XeF lasers were found to be particularly powerful and efficient. All those initial laser experiments were performed in high energy electron-beam devices.

At NRL, the first successful operation of the rare gas halide laser (in the form of XeF) with electric discharge excitation was demonstrated (see Appendix 4). The initial observation of discharge pumped XeF laser action was made in a capacitive transfer device commonly used for the N_2 laser. Since then, greatly improved performance of the XeF laser in a Blumlein-type apparatus has been obtained. In the latter case, we have also succeeded in achieving laser action in KrF. At present, the energy output and overall efficiency in XeF and KrF in the Blumlein device are 80 mJ at 0.8% and 30 mJ at 0.3% respectively. Compared with the best overall efficiencies obtained in e-beam experiments, the XeF result is about 25 times better and the KrF result about a factor of 3 lower. We are at present limited in operating pressure to a maximum of 1 atm if severe arcing is to be avoided. The incorporation of some preionization scheme should allow much higher pressure operation with accompanying higher energy output and efficiency. It would also make possible scaling to larger volumes.

It is apparent that direct discharge excitation is an attractive mode of operation from high repetition rate considerations. Large volume discharge excitation of high pressure CO_2 lasers (with preionization) is a well developed technology. We believe that a similar device can be effective for pumping the rare gas halide systems, and will actively explore that possibility.

3. Chemical Ba Laser

An experimental evaluation of the chemical Ba laser concept was initiated during this reporting period. The idea for this laser scheme came from the realization that by transferring excitation from reaction product molecules to some atomic species, one could achieve orders of magnitude increase in state densities. The higher state densities in turn means a greater likelihood that useful gains can be achieved in a reasonable-sized device. The basic steps involved in the chemical Ba laser scheme are the following.

(1) $Ba + N_2O \rightarrow BaO^* + N_2$

(2) $BaO^* + Ba(^1S) \rightarrow Ba(^1P) + BaO$

(3) $Ba(^1P) \rightarrow Ba(^1D) + h\nu\ (1.5\ \mu)$

(4) $Ba(^1D) + M \rightarrow Ba(^1S, ^3D) + M$

These are indicated schematically in Fig. 35. Past studies have shown that collisional quenching of BaO* by Ba proceeds at near gas kinetic rate. It, therefore, appears that an efficient transfer to the atom can be effected in this case.

As we believed that proper gain diagnostics is an essential part in the discovery of new lasers, the initial phase in this program

centered on the development of a suitable probe source. It was felt that one might be able to make a cw optically pumped Ba laser at 1.5 μ by using a 5535 Å cw dye laser output to excite the Ba ($^1S \longrightarrow {}^1P$) transition. One could then use steps 3 and 4 above to complete the laser process. This idea was tested experimentally and was found to work well. At first, N_2 was used as a quenching gas in the optically pumped 1.5 μ Ba laser. But, subsequently, it was found that the laser worked even in pure Ba. This optically pumped laser has since served as the backbone for the diagnostic work on the chemically pumped Ba system.

The reactor itself consists of a resistively heated oven-nozzle combination with the nozzle situated in the middle of a 5" x 0.5" flow cross section. The gas flow rate in the region of the nozzle is estimated to be near sonic. In typical runs, Ba vapor at ~ 1 torr is picked up by He and transported through the nozzle, to be mixed with the N_2O stream which flows around it. At the operating pressure of ~ 1 torr, the extremely bright flame which results stretches downstream for about 0.5". Brewster's windows with 0.5" aperture at the two ends of the nozzle permit either intracavity probing or direct laser oscillation attempts.

In the intracavity probing experiments, the Ba oven (for the optically pumped laser) and the reactor are placed on the same optical axis inside a laser cavity. The 5535 Å pump beam enters the cavity from the end nearer to the Ba oven and is totally absorbed in the latter. The intensity of the 5535 Å beam is adjusted to get the

optically pumped 1.5 μ laser just above threshold, The power of the 1.5 μ laser beam emerging from the opposite end is monitored as conditions in the reactor are varied. When the Ba flow in the reactor is turned on, a decrease in the 1.5 μ laser output is observed due to the presence of a thermal population of Ba in the ^1D state. This decrease can be made smaller when N_2O is introduced into the reactor and the flame initiated. But, thus far, we have not yet observed net gain in the form of a power increase over the original level when there is no Ba in the reactor.

To assess to what extent the partial recovery in laser power is due to the production of Ba(^1P) from the Ba + N_2O reaction, a separate experiment was performed. The Ba oven was removed from the cavity, and the 5535 Å beam allowed to pump the Ba vapor in the reactor in the absence of N_2O. The 1.5 μ laser was made in that manner, and the pump beam adjusted to give near threshold oscillation. Then the exit mirror was removed, and the 1.5 μ spontaneous emission from the reactor was measured with a detector on the optical axis. This spontaneous emission signal was compared to that produced by the Ba + N_2O flame, with the 5535 Å beam now blocked. The two signals were found to have almost equal intensity. This experiment shows that there is sufficient density of the Ba(^1P) level in the Ba + N_2O flame for laser action, and the failure to obtain net gain must be due to an insufficiency in the quenching of the Ba(^1D) level.

We are encouraged by the results of the studies so far and still believe the Ba transfer system to be a good candidate for an electronic

state chemical laser. The intracavity probe experiments will be continued, but we think it will be particularly useful to commence a program to identify those gases which would selectively and efficiently quench the Ba(^{1}D) state.

4. Collisional Quenching of Electronic States

The possibility of using collisional quenching of the lower laser level in an electronic transition laser was just demonstrated at NRL in the optically pumped atomic Hg system. Unfortunately, for many potential electronic state lasers, there is not sufficient data on the quenching of the relevant states to allow an assessment of their lasing potential. The dual goals of the NRL program are to measure those quenching cross sections essential for an evaluation of specific laser schemes and to advance the overall understanding of electronic state quenching.

Since we are particularly interested in the possibility of three-level lasers where the upper laser level is optically connected to both the ground state and the lower laser level, we have chosen to prepare the lower laser level by dye laser excitation of the upper state followed by cascade. The decay of the lower state density is then monitored via the time resolved absorption of another transition which terminates it.

The Tl(^{2}S$\rightarrow$^{2}P$_{3/2}$) transition at 5350 Å is a very intense line in most discharges and has been made to lase in a pulsed device. Since the laser has been operated in the self-terminating mode, its efficiency has been low. A search is therefore being made to uncover

compatible elements which would efficiently quench the Tl ($^2P_{3/2}$) state. Quartz cells filled with Tl and various quenching elements were heated to 600-1000°C. A dye laser tuned to the Tl ($^2P_{1/2} \rightarrow {}^2S$) transition at 3776 Å was used to excite the mixtures, and a collimated probe beam at 3529 Å from a low pressure Tl lamp used to monitor the Tl($^2P_{3/2}$) population. Preliminary experiments with Xe, Hg, Cd, and Tl as quenching gas have yielded rates of 5×10^{-15}, 10^{-14}, 10^{-14}, and 10^{-10} cm^3 sec^{-1} respectively. At present, more careful measurements on Tl self-quenching are underway.

5. Pulsed Metal Vapor Laser

During this reporting period research has continued using the transverse discharge system, detailed in previous reports[1,2] and in Appendix 5 , operated as a copper laser using Cu Cl as the parent molecule. Previously the inverse pressure dependence of the laser power was discussed, and the hypothesis was made that this behavior was due to "tracking" of the discharge along the walls of the tube at high buffer gas pressure, with subsequent loss of energy deposited in the gas. These results were presented at the 2nd Summer Colloquium on Electronic State Lasers in September, 1975, and are summarized in Appendix 5.

To improve operation of the laser at high pressure, the tube was modified to reduce the possibility of tracking. The cylindrical cathode rod was replaced with a bar of triangular cross-section. The apex of the triangle opposite the anode bar was serrated to insure breakdown there rather than at the other edges, and to improve the

the linear homogeneity of the discharge. The cathode-anode spacing also was reduced so that the teeth of the cathode were ~ 1.5 cm from the anode. Testing of the discharge at room temperature confirmed that the previously observed tracking of the discharge along the walls had been eliminated for neon pressures up to 1 atmosphere.

The modified tube was initially operated with the same circuitry as had been used previously. With the delay between dissociating and pumping discharges set at 50 μs, lasing was observed to occur in two pressure regimes. From 5 to 80 torr the laser power decreased monotonically as the pressure increased, and no lasing was observed at 100 torr. At 200 torr, lasing was again observed and the power increased as the neon pressure was raised further. The peak power in this pressure regime was ~ 5 kW at 400-600 torr, and decreased slightly in the range 600-800 torr. The data were quite erratic in the high pressure regime, which may have been due to certain effects associated with the large amount of energy dissipated in the gas by the first discharge pulse.

The energy made available for the first pulse was 9 joules, in order to insure complete dissociation of the CuCl. Recent evidence by other investigators[3] indicated that increased first pulse energies were necessary for higher optimum buffer gas pressures, and that the dissociation energy necessary at near atmospheric pressures would be even higher than that used. However, increasing the energy of the first pulse by increasing its associated capacitor resulted in a decrease in laser performance.

The value of Cs_1, the storage capacitor for the first pulse, had been .1 μf, and because of the current limitation of the thyratron switch, an inductor had been placed in the circuit to limit the current rise. As a result, when the gas breakdown occurred, only the relatively small energy stored in the "dumping capacitors" was immediately available to the discharge. This energy ionized the gas, lowering its impedance, so that the much larger charge remaining in Cs_1 passed through the gas in a long pulse at low voltage. This low voltage discharge would be inefficient at dissociating the CuCl, but effective in locally heating the gas and hence perturbing it as a result of the associated density changes propagating through the medium. Therefore, Cs_1 was halved and the circuit impedance lowered so that all of the stored energy could be discharged in the initial breakdown pulse. At high pressures the width of the second current pulse had been observed to increase, and hence to better match this pulsewidth to the laser pulse the values of the storage capacitor for the second pulse, Cs_2, and the "dumping" capacitors C_D, were also reduced.

These changes had a significant effect on the operation of the laser. Output was observed continuously from 8 to 750 torr, with above atmospheric pressure operation forbidden only by the vacuum seal design. A graph of laser power vs. neon pressure is shown in Fig. 36. These data were taken with an ITT 4018 photodiode and neutral density filters. The manufacturer's calibration values were used. The conditions under which the data were taken are summarized in Table 1.

Table 1

V_1	14 kV
V_2	25 kV
Cs_1	48 nf
Cs_2	5.7 nf
C_D	5.7 nf
τ_D	15 μsec
T	390 C
Output mirror	10 M radius of curvature, uncoated quartz
Back mirror	2 M radius of curvature, high reflectivity

The laser pulse at 400 torr had a FWHM of ~ 8 nsec, typical of the emission under these conditions. The energy of this pulse as measured with a Gen-Tec joulemeter was 220 μJ. Observation of the discharge area and of the laser emission indicated that the active region of the laser was $\leq$ 3 mm wide. Since the discharge region is only 20 cm long and 1.5 cm high, the active volume is estimated at 9 cm^3. Using this value, the specific energy of the laser is conservatively estimated at 24 $\mu J/cm^3$, comparable to the best results of other investigators. The specific power of 2.7 kW/cm^3 is higher than any known for a copper halide laser.

The time delay in Table 1 was the optimum delay at 480 torr. At lower pressures the optimum delay increased. At 50 torr, for instance, laser emission was not observed with the 15 μs delay, and

was optimum with a 60 μs delay. The variation in optimum delay with pressure in the range 400-750 torr seems small, but the tendency is for optimum delay to decrease as the pressure is increased, It would appear that either the fraction of copper metastables atoms produced by the dissociation pulse decreases as the neon pressure is raised, or that some process dependent on the neon density is deactivating the metastable atoms. The 15 μs optimum delay at high pressure is unexpectedly short for a tube of these dimensions. These results imply that high repetition rates will be possible for tubes of larger dimensions when operated at high pressure.

The data were taken with the laser run at the optimum temperature observed for the earlier, low pressure experiments. The maximum available copper atom density at this temperature is 9×10^{14} cm^{-3}. The specific energy of 24 $\mu J/cm^3$ corresponds to an upper state population of 1.2×10^{14} cm^{-3}, i.e., approximately 13% of the ground state population. The numbers assume 100% dissociation of the copper chloride trimer, and that all of the observed output is at 510.6 nm. While it might be possible to increase the fractional excitation, significant improvement would not be expected in the specific energy of the laser unless the optimum temperature can be increased. The temperature dependence of this device is yet to be investigated at high pressure, but some improvement in laser output can be expected with increased temperature. At 450°C the available Cu atom density is 7×10^{15} cm^{-3}.

The efficiency of the device is low, .012% of the energy in the pumping capacitor Cs_2. Because of the breakdown of the gas at

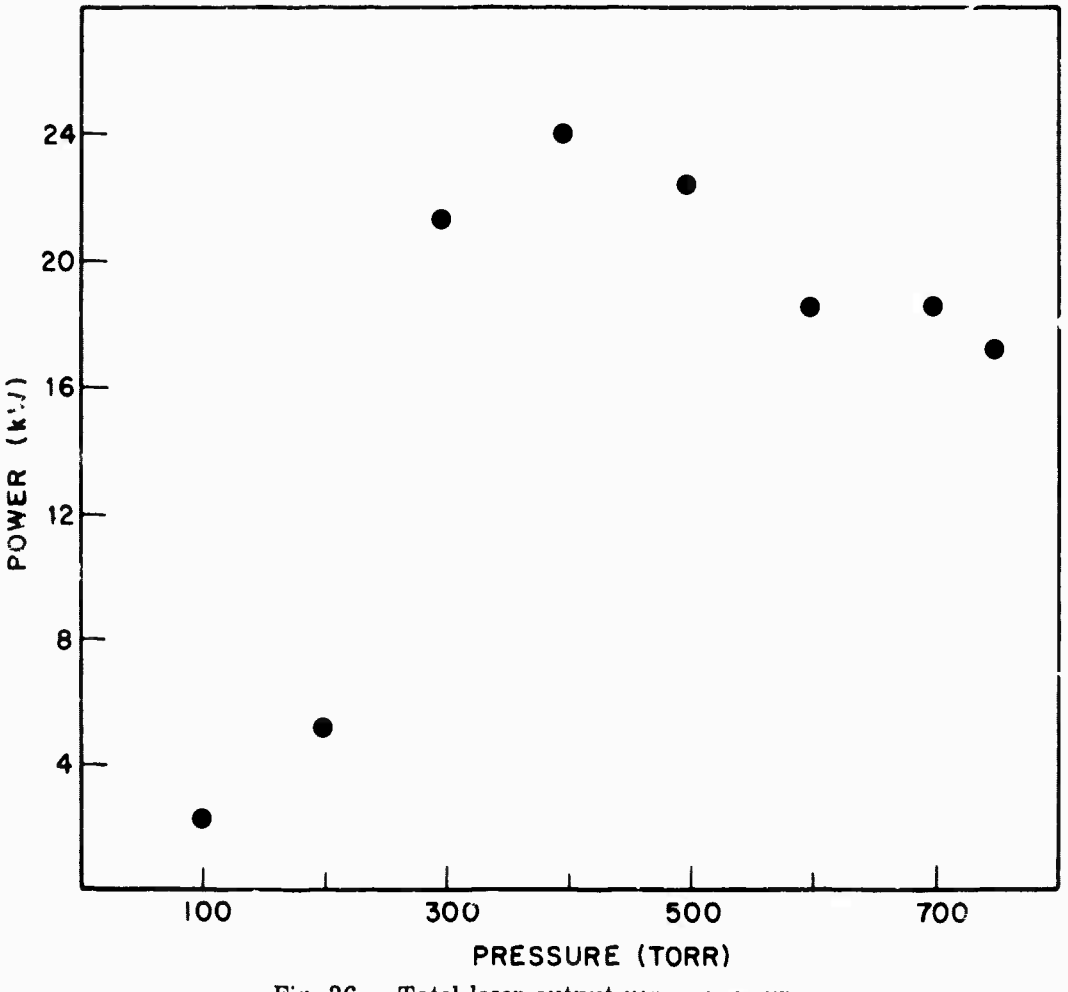

Fig. 36 — Total laser output versus pressure

relatively low voltage when the neon pressure is high, the discharge circuitry is very inefficient and only a small fraction of the energy in the storage capacitor is expended by the end of the lasing pulse. Modifications of the double pulse circuitry would be expected to improve the overall electrical efficiency.

In summary, recent experiments with the double-pulse transverse discharge apparatus have resulted in high specific energy and power operation at buffer gas pressures up to 1 atmosphere. This result and the very short optimum delay times observed demonstrate the utility of the system and the feasibility of larger scale devices.

References

1. NRL-DARPA Laser Program, Semiannual Technical Report, 1 July - 31 December 1974, NRL Memorandum Report 3084.

2. NRL-DARPA Laser Program, Semiannual Technical Report, 1 January - 31 June 1975, NRL Memorandum Report 3217.

3. N. M. Nerheim and C. J. Chen, "Visible Wavelength Laser Development," Final Report Phase I. Prepared for DARPA Order Number 2756 by Jet Propulsion Laboratory, August, 1976.

6. Boron Atom Reactions

Boron monoxide (BO) and boron mono-halides have comparatively strong bonds, e.g., ΔH_f^o (BO) = -187 kcal. Therefore, it should be relatively easy to produce electronically excited BO radicals via chemical reactions. The BO radical has several low-lying electronic states as shown in Fig. 37. Since the $A^2\pi$ state is doubly degenerate, the B → A transition, which occurs in the range of 455-590 nm, is particularly attractive for possible population inversion.

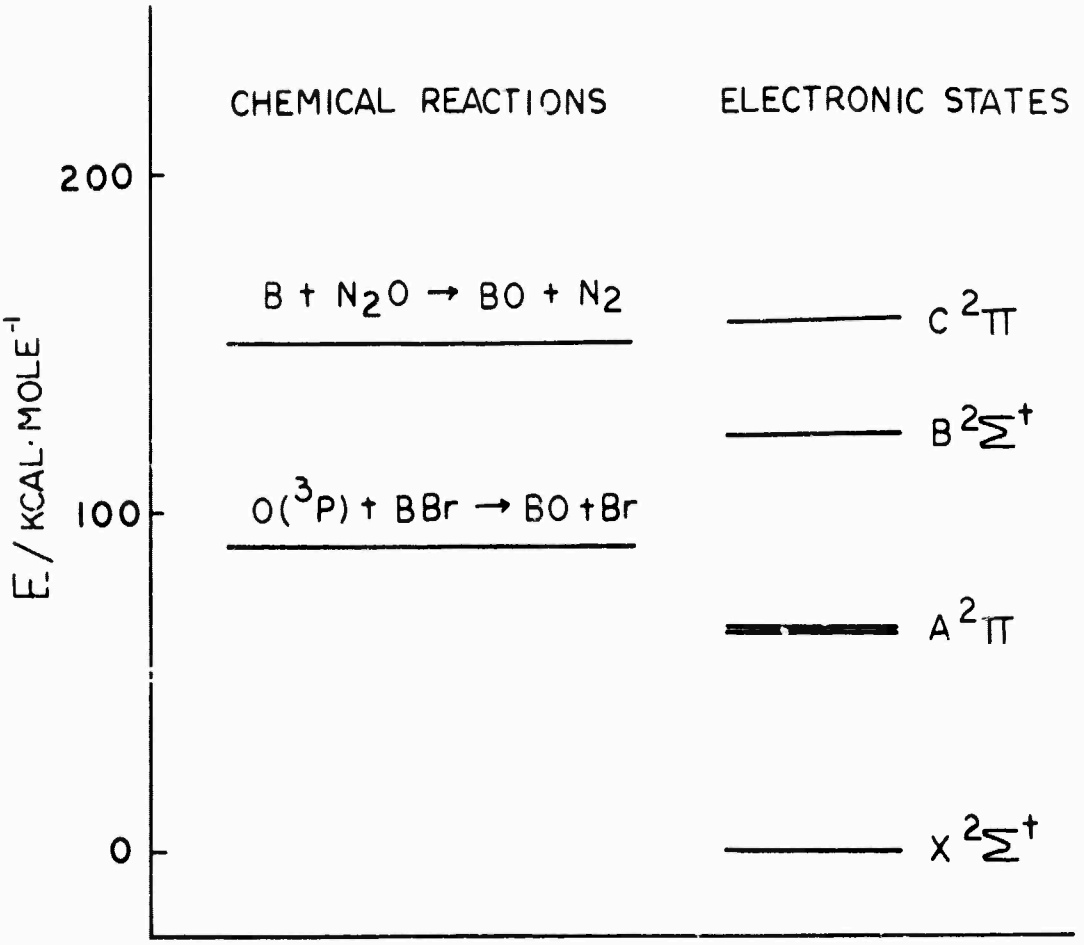

Fig. 37 — Energy diagram of the BO system

In this work, the possibility of generating an electronic transition BO laser based on B + N_2O and/or BBr + O reactions was examined (see Fig. 37). BBr_3 was employed to provide B atoms via successive photodissociation reactions in the vacuum uv region,[1]

$$BBr_3 + h\nu\ (\lambda \gtrsim 105\ nm) \longrightarrow BBr_2 + Br \xrightarrow{h\nu'}$$

$$BBr + 2Br \xrightarrow{h\nu''} B + 3Br$$

When 10-20 torr of 1:2:5/BBr_3:N_2O:He was flash-photolyzed in a previously constructed LiF-window laser system, a weak emission pulse was detected at 3 μsec after flash initiation as shown in Fig. 38a. The optical cavity was formed by a pair of dielectric coated high-reflectivity mirrors (450-530 nm); one of them has 1-2% transmission. A similar pulse was also noted in experiments with a 1:5:4/BBr_3:N_2O:He mixture (Fig. 38b). In both mixtures, the peak disappeared when the laser tube was evacuated (see the bottom traces of both Fig. 38a and 38b) or when the cavity was detuned (see Fig. 38c). These tests indicated that the observed pulse could not arise from electrical interferences or artifact. Most unfortunately, the emission could not be reproduced for careful spectral analysis before LiF windows and both internal mirrors were seriously coated by BBr_3 (which is very hygroscopic) and its reaction products. Further experiments with other B-atom sources such as BH_3CO are planned.

The reactions shown in Fig. 37could energetically account for emission at 500 nm. The $O(^3P)$ + BBr reaction, which is exothermic by about 87 kcal/mole, is sufficient to pump the $A^2\pi \rightarrow X^2\Sigma^+$ transition

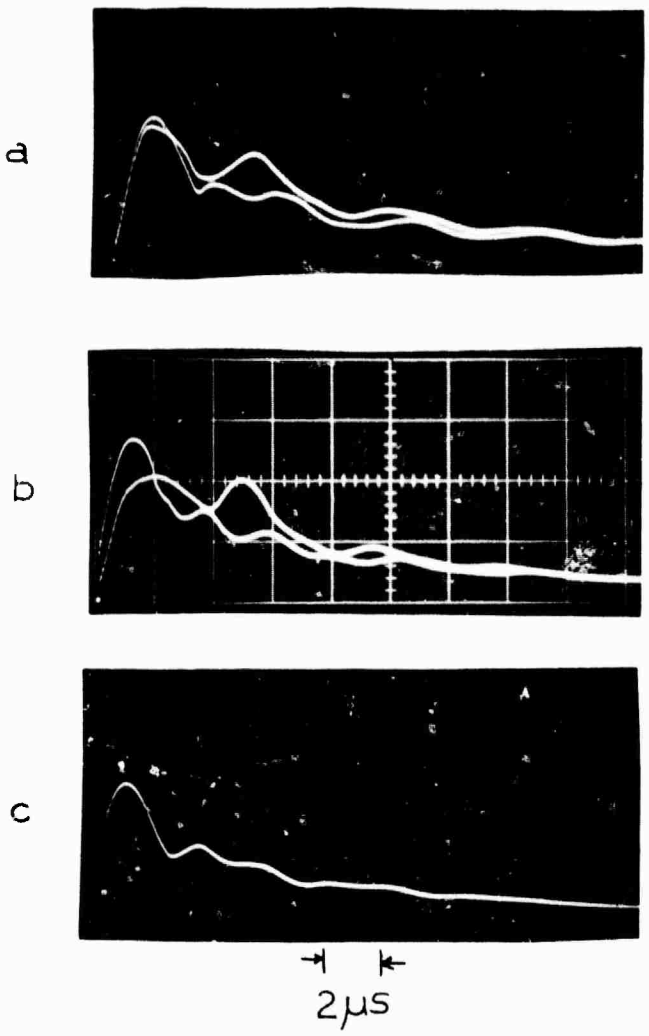

a. Upper trace: 20 torr 1:2:5/BBr_3:N_2O:He flashed at 2.5 KJ.
   Lower trace: flashed without sample.
b. Upper trace: 10 torr 1:5:4/BBr_3:N_2O:He flashed at 2.5 KJ.
   Lower trace: flashed without sample.
c. Conditions similar to "a" upper trace, but the laser cavity was detuned.

Fig. 38 — Emission signals detected by a photodiode

(310-850 nm). In addition, the photodissociation of N_2O in this spectral region $\lambda \gtrsim 105$ nm readily generates $O(^1S)$ and $O(^1D)$ atoms. Their participation in reactions with BBr would increase the exothermicity by 100 and 45 kcal/mole, respectively, either being sufficient to excite BO to the $B^2\Sigma^+$ state. The B + N_2O reaction can release as much as 150 kcal/mole of energy, but its rate and photon yield under our experimental conditions are still not known.

7. E → V I* + CO Energy Transfer Study

The electronically excited ^3P Hg atom has been shown to transfer its 112 kcal/mole electronic energy very effectively to CO giving rise to a complete vibrational population inversion.[2] We have examined the possibility of a similar effective E → V energy transfer process involving the 6s $^2P_{3/2}$ I atom lying approximately 160 kcal/mole above the $5p^5\ ^2P_{3/2}$ ground electronic state. If the I* + CO quenching reaction proceeded via a strong chemical interaction similar to the $O(^1D)$ + CO reaction,[3] one would expect the product CO molecule to carry as high as 35 kcal/mole vibrational energy.

The $I(6s\ ^2P_{3/2})$ atom was produced by optical pumping of the $I(5p^5\ ^2P_{1/2})$ atom formed in the photodissociation of CF_3I above 200 nm, viz.,

$$CF_3I + h\nu \longrightarrow CF_3 + I\ (5p^5\ ^2P_{1/2})$$

$$I(5p^5\ ^2P_{1/2}) + h\nu\ (206.3\ nm) \longrightarrow I\ (6s\ ^2P_{3/2}).$$

The absorption occurring at 206 nm is known to be very strong and has been employed by many to monitor the concentration of the $I(^2P_{1/2})$ atom.

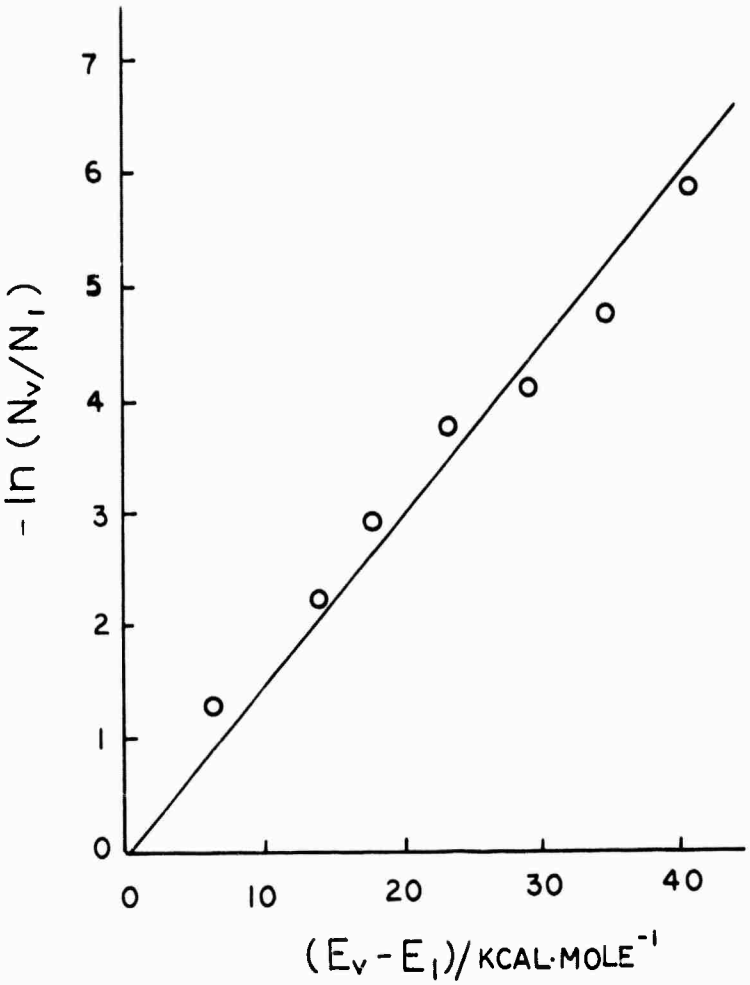

Fig. 39 — The vibrational population of CO formed in the $I(6S\ ^2P_{3/2})$ + CO reaction

The extent of CO vibrational excitation from the I(6s $^2P_{3/2}$) + CO reaction was determined by a small signal gain (or absorption) measurement employing a cw CO laser. The result obtained from the photolysis of 5 torr 1:2:37/CF_3I:CO:He mixture is shown in Fig. 39. These data indicate that the CO formed in this E → V transfer reaction, unlike Hg* + CO[2] and O* + CO,[3] has a relatively low partial inversion, with a vibrational temperature of only 4000°K. Only a few percent of the 160 kcal/mole electronic energy of the I(6s $^2P_{3/2}$) atom was converted into CO vibrational excitation. The detailed dynamics of this reaction is being studied to investigate the principles underlying E → V and V → E energy transfer.

References

1. M. C. Lin, Int. J. Chem. Kin. 5, 173 (1973). It has been demonstrated that the weak C-Br bonds of bromomethanes can be successively detached by photons generating high yields of CH and CH_2 radicals from $CHBr_3$ and CH_2Br_2, respectively.

2. Y. Fushiki and S. Tsuchiya, Chem. Phys. Lett. 22,47 (1973).

3. M. C. Lin and R. G. Shortridge, Chem. Phys. Lett. 29, 42 (1974), J. Chem. Phys. (in press).

8. Laser Diagnostics via Coherent Anti-Stokes Raman Spectroscopy

Coherent Anti-Stokes Raman Spectroscopy (CARS) is a new and potentially powerful method of probing gas lasers and other similar systems.[1-4] The technique utilizes two high power lasers, one fixed in frequency at ω_ℓ, the other tunable which we call the Stokes beam, ω_s. When ω_s is adjusted such that $\omega_\ell - \omega_s$ matches a vibrational (Raman)

resonance, ω_R, in the medium, a coherent beam of light at the anti-Stokes frequency, $2\omega_\ell - \omega_s = \omega_{as}$, is generated at high conversion efficiency. The high conversion efficiency (as much as 1% in favorable cases), the coherency and anti-Stokes character of the emission make CARS a sensitive analytical tool for gas laser diagnostics, free from laser induced fluorescence interference or luminescent background.

CARS is basically a Raman process and hence, all molecules can be detected by the technique. For example, D_2, H_2 or other homonuclear diatomic molecules which cannot be observed in the infrared, are readily detected by Raman techniques. However, CARS is many orders of magnitude more efficient than normal Raman spectroscopy, which is not sufficiently sensitive for low pressure gas-phase applications such as detecting vibrationally excited states in gas laser systems. Hence, the method is currently under development to monitor the temperature and the number density of D_2 (v = n) (and HCl (v = n)) in the D_2-HCl transfer laser.

Vibrational temperatures can be determined from CARS spectra by analyzing the data in terms of the following equation (see reference (5)):

$$\frac{P'}{P} = \frac{4\Gamma^2}{\Gamma'^2} \exp\left\{\frac{-2hc}{kT_v}\left[\omega_e - 2\omega_e x_e - \alpha_e J(J+1)\right]\right\} \qquad (1)$$

where P and P' are the anti-Stokes power for a particular Q-branch of ground state and vibrationally excited state D_2, Γ and Γ' are the corresponding line widths; h,c,k are the usual physical constants, ω_e is the vibrational frequency, x_e is the anharmonicity, α_e is the vibration-rotation interaction constant, v and J are the vibrational and rotational quantum numbers, respectively.

The rotational/tranlational temperature is calculated by measuring relative intensities of the Q-branches within a particular vibrational manifold, i.e.:

$$\frac{P'}{P} = \left(\frac{\Gamma}{\Gamma'}\right)^2 \left(\frac{2J'+1}{2J+1}\right)^2 \exp\left\{-\frac{2hcB}{kT_r}\left[J(J+1)-J'(J+1)\right]\right\} \qquad (2)$$

where all constants and parameters are identical to those in equation (1). T_r is the rotational temperature and B is the rotational constant.

Apparatus

The apparatus developed for carrying out CARS diagnostics is illustrated in Fig. 40 and consists of a high power (~ 5 MW at 532 nm) Q-switched Nd:YAG laser operating single mode on its second harmonic. The laser has a line width of ~ 0.03 cm^{-1}, a pulse width of ~ 20 ns, and a maximum repetition rate of 10 pps. A portion of the YAG laser (~ 0.8 MW) is used to pump a dye laser which is angle tuned with a grating and an "inch worm" driver. Another portion of the YAG laser (~ 1.5 MW) pumps a dye laser amplifier (not shown in the figure). The resulting dye laser beam (0.4 MW) and remainder of the YAG (~ 2.0 MW) are combined and focused (f = 10 cm) in a sample gas cell. CARS signals generated in the sample cell are separated by a beam splitter which reflects the CARS beam but transmits the two exciting laser beams, which may then be used to create anti-Stokes signals in a reference gas. The reference signal may be ratioed against the sample signal to minimize the jitter in the CARS signal. Additional filters are used to further reduce stray light. With regard to low level detection, in some early experiments signals from D_2 below 100 mtorr total pressure were

detected (without reference cell and with rather broad laser line widths - 0.3 cm^{-1}). With refinements, the lower limit of detection for species like D_2 should be on the order of 1 mtorr.

Results

As preliminary laboratory experiments, the apparatus described in Fig. 40 has been used to probe a volume element of D_2 at the center of an electrical discharge. Figure 41 illustrates the resulting spectra taken without dividing out the reference signal. Although the initial pressure of the D_2 was 48 torr, the actual D_2 pressure was ~ 10-20 torr because the gas absorbs readily on the electrodes during the discharge. The ground state (v = 1) are clearly visible in Fig. 41. The partial pressure of vibrationally excited D_2 is well below 1 torr and the signals are quite strong even without extensive signal averaging and use of the reference cell to reduce the jitter in the CARS signal. From these preliminary scans, the vibrational temperature is estimated to be approximately 1050^{o}K with a rotational temperature near ambient (~ 400 K). In other words, within the plasma region the gas is vibrationally hot but rotationally cool. The accuracy of this technique now reeds to be explored, since the results obtained are strongly dependent on molecular line widths and calibration. After these experiments have been completed and the system is proven to provide consistent, accurate and reliable data, the apparatus will be moved to the EDGDL facility for temperature and species profile measurements.

References

1. P. R. Regnier and J.-P. E. Taran, Appl. Phys. Lett. 23, 240 (1973).

2. J. J. Barrett and R. F. Begley, Appl. Phys. Lett. 27, 129 (1975),

3. R. F. Begley, A. B. Harvey, and R. L. Byer, Appl. Phys. Lett. 25, 387 (1974).

4. A. B. Harvey, J. R. McDonald, and W. M. Tolles, in "Progress in Analytical Chemistry," Plenum Press, in press.

5. F. Moya, S.A.J. Druet, and J.-P. E. Taran, Optics Comm. 13, 169 (1975).

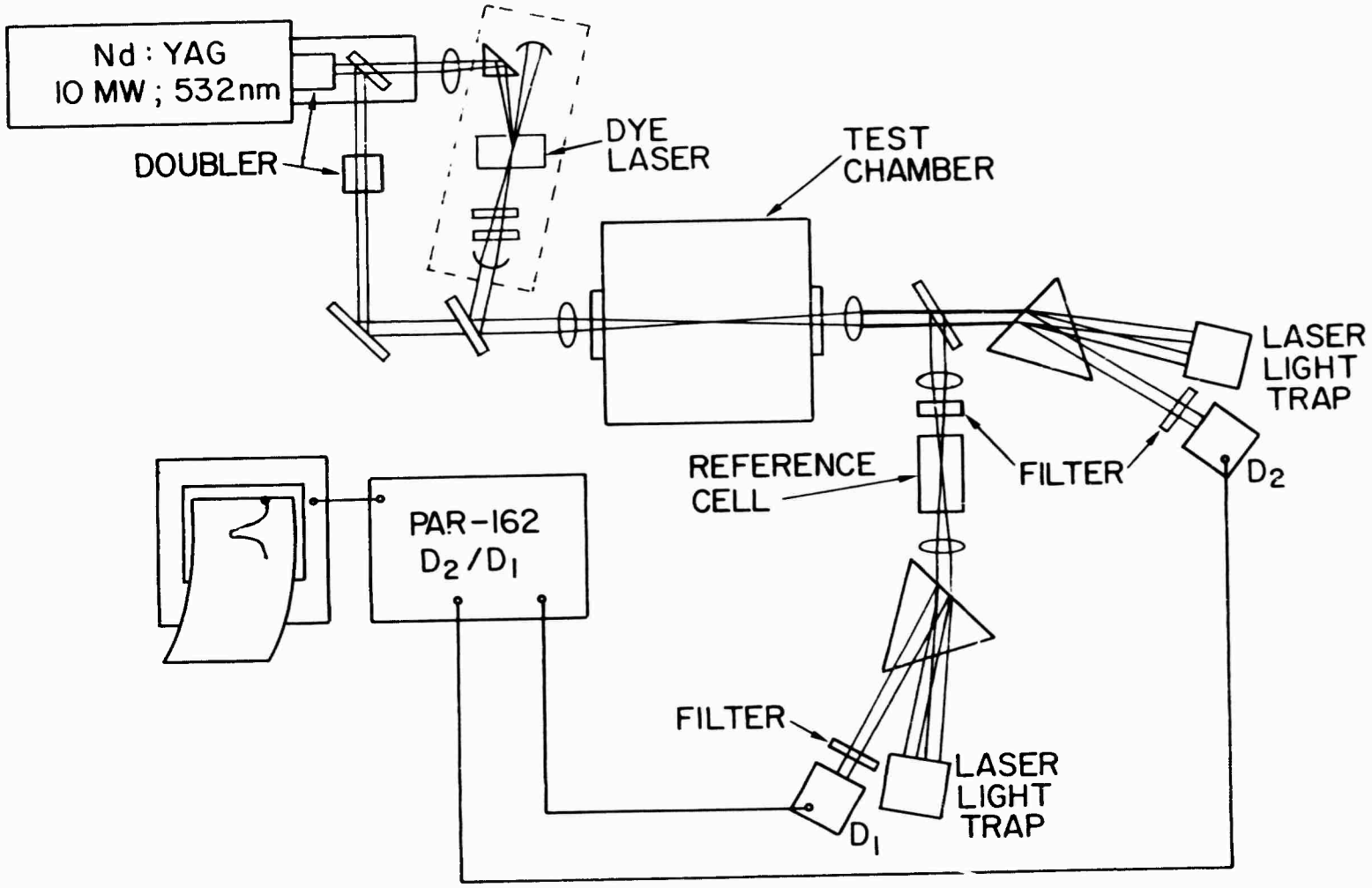

Fig. 40 — CARS apparatus for measuring temperatures and number densities in gases

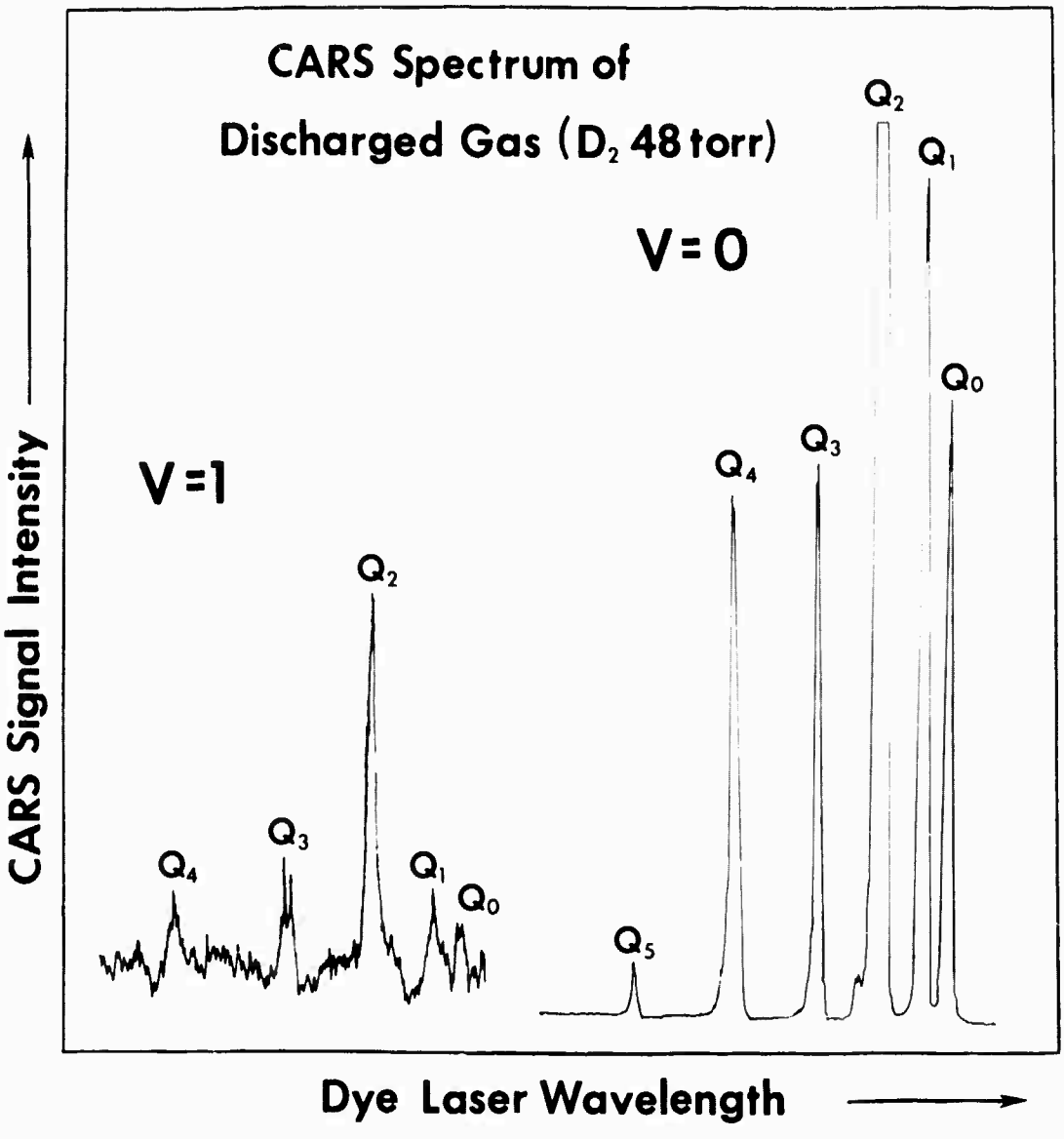

Fig. 41 — CARS spectra of D_2 gas in a dc discharge region

APPENDIX 1

D_2-CO_2 AND D_2-N_2O ELECTRIC DISCHARGE GASDYNAMIC LASERS*

J. A. Stregack, B. L. Wexler, and G. A. Hart†

Abstract

CW CO_2 and N_2O lasing has been obtained in a new electric discharge gasdynamic laser device. The device consists of a subsonic plenum discharge region where vibrational excitation occurs, a supersonic nozzle array where the laser species is injected, and a supersonic cavity where mixing, energy transfer, and lasing occur. In the present experiments both CO_2 and N_2O are pumped by energy transfer from D_2 excited in the discharge. Comparisons are made for CO_2 pumped by both N_2 and D_2, and N_2O and CO_2 pumped by D_2.

---

*Work partially supported under DARPA Order No. 2062.

†NRC-NRL Postdoctoral Research Associate (1973-1975).

Previous electrically excited cw molecular lasers have been limited to molecules that could have their vibrational degrees of freedom excited either directly by electron impact or could be pumped by energy transfer from electrically excited N_2. On the basis of measured rates[1,2] it appeared probable that a CO_2 laser could be produced by energy transfer from D_2 which is vibrationally excited in a glow discharge. A cw D_2-CO_2 energy transfer laser was produced in the NRL electric discharge gasdynamic laser (EDGDL) facility which under the conditions of these experiments is comparable in performance to a N_2-CO_2 energy transfer laser.[3]

The EDGDL is shown schematically in Fig. 1. Subsonic plenum excitation of a D_2-diluent (Ar or He) mixture by a dc, or rf-augmented dc, discharge significantly populates the lower vibrational levels of D_2. The dc discharge occurs between a series of individually ballasted (100 kΩ) pins and the rear of each nozzle blade. The rf augmentation was capacitively coupled into the plenum through the top and bottom walls. From an energy balance calculation it is estimated that with dc excitation, approximately 65% of the electrical energy deposited in the gas goes into vibrational energy. The excited plenum gas is then accelerated through an array of supersonic nozzles where the CO_2 is injected approximately 4 mm downstream of the throat. Mixing, energy transfer, and lasing occur in the supersonic cavity region which extends 30.5 cm downstream from the nozzle exit plane. The supersonic cavity region terminated in a diffuser and the entire system was pumped by a steam ejector. Two different chambers were used. The first was constructed entirely of G-10 Fiberglas while the second

consisted of Pyrex plates bonded together to form the plenum to which separate nozzle and cavity regions formed from anodized aluminum were attached. The nozzle array consisted of 34 uncontoured wedge-shaped nozzle elements with the end ones having no secondary injection of the laser species. Instead argon is injected through these end elements to provide a window curtain. The nozzle throats were 1.2 mm and the geometric area ratio of the expansion was 6. Two sets of rectangular Brewster windows enable the laser cavity and diagnostic apparatus to be positioned up to 27 cm downstream from the nozzle exit plane. The optics are mounted on a motor-driven translation table which enables continuous scans of the region downstream of the nozzle exit plane to be easily made.

By removing the laser species from the discharge region, it is possible to maximize the channeling of electrical energy into vibrational excitation without encountering possible limitations imposed by the laser species. While other workers have injected the laser species under subsonic or sonic flow conditions,[4-8] in the above device the laser species is injected into the cold supersonic flow region. This can have several advantages for different potential laser systems--promote anharmonic pumping of diatomic molecules, depopulate lower laser levels near the ground state in polyatomic molecules, improve mixing at lower pressures, decrease vibrational deactivation in the low-pressure supersonic flow, increase the gain by decreasing temperature, etc. The net effect is to produce an electrical analog to the GDL mixing lasers originally proposed by Bronfin[9] and refined by Taran et al.[10]

The best results have been obtained with D_2-He plenum mixtures (stable flow discharges in the D_2-Ar mixtures have been hard to maintain) which necessitated a forced mixing configuration for the heavier secondary CO_2. This configuration has two distinct sets of operating conditions, one where the laser cavity remains supersonic and therefore maintains a low translational temperature, and the second where too much secondary flow causes a sharp increase in cavity pressure and increased translational temperature. This effect is caused by some shock phenomenon "choking" the flow due to too much secondary mass addition.

In order to confirm this description of the two operating regimes produced by varying the secondary flow, gain measurements were performed as a function of J at several cavity locations. From these gain measurements, vibrational and rotational temperatures were extracted. Figure 2 shows the vibrational temperature of the D_2-CO_2 system for the two cases at the four positions for which data were taken. The temperatures measured at the position 12.1 cm downstream from the nozzle exit plane appear to be high. If these points are lowered, the general shape of the variation of T_v is similar to scans of fluorescence vs. distance downstream. In the first case, the vibrational temperature increases through the cavity region and maximizes near the end of the cavity while in the "choked" case it peaks halfway through the cavity and then decreases. The latter effect is probably due to a longer flow time through the cavity caused by the decelerated flow after the shock wave.

Table I summarizes the conditions in the experiment which produce maximum power in the D_2-CO_2 laser to date and Table II compares D_2-CO_2 and N_2-CO_2 laser performance under similar conditions in the EDGDL. Maximum output has been achieved to date under "choked" conditions, since for the CO_2 laser the temperature effect is not critical and "choking" the flow maximizes the energy transfer and mixing processes for the cavity lengths of this experiment.

The EDGDL facility was also used to produce a D_2-N_2O energy transfer laser operating on the N_2O 10.7-μm transition. A comparison of the performance of the D_2-CO_2 and D_2-N_2O lasers reflects the importance of available near-resonant vibrational levels for such energy transfer lasers. It was found that for identical He and D_2 flow rates and discharge conditions, roughly 3-5 times as much power could be extracted for a given injection rate of CO_2 than could be achieved from N_2O. This correlated well with a plausible description of the major energy transfer pathways in these two systems. D_2 with a v = 1 to v = 0 vibrational spacing of 2994 cm^{-1} is in very close resonance with the CO_2 (01^11) level at approximately 3000 cm^{-1}. Rapid quenching of the CO_2 bending mode yields CO_2 in its 00^01 state which subsequently undergoes stimulated emission to the 10^00 level. This proposed mechanism also applies to N_2O which has a manifold of vibrational states similar to those of CO_2. However, there is one significant difference. The N_2O (01^11) state at 2798 cm^{-1} lies 200 cm^{-1} below D_2 (v = 1). Consequently, the favorable resonance between D_2 and CO_2 is not found in the case of D_2 and N_2O.

The successful use of electrically excited D_2 to pump a CO_2 laser through vibrational energy transfer, and the subsequent application of this technique to N_2O, indicated that this procedure can be used with many diatomic and polyatomic molecules whose vibrational spacing precludes efficient energy transfer from N_2. Among the many candidates of interest with vibrational levels which satisfy the criteria of near resonance with those of D_2 are HCl and HBr. In addition, the cooling effect may make possible improved cw lasing from CS_2 as well as producing a cw C_2H_2 laser, both of which have lower laser levels nearer the ground state than CO_2.

The authors wish to thank T. McClelland and C. Kyle for their technical assistance.

References

1. C. B. Moore, R. E. Wood, B. L. Hu, and J. T. Yardley, J. Chem. Phys. 46, 4222 (1967).

2. J. C. Stephenson and C. B. Moore, J. Chem. Phys. 56, 1295 (1972).

3. J. A. Stregack and B. L. Wexler, IEEE J. Quantum Electron. QE-11, 705 (1975).

4. C. K. N. Patel, Phys. Rev. Lett. 13, 617 (1964).

5. C. K. N. Patel, Appl. Phys. Lett. 6, 12 (1965).

6. T. A. Cool and J. A. Shirley, Appl. Phys. Lett. 14, 70 (1969).

7. C. O. Brown, Appl. Phys. Lett. 17, 388 (1970).

8. H. Brunet and M. Mabru, Appl. Phys. Lett. 21, 432 (1972).

9. B. R. Bronfin, L. R. Boedecker, and J. P. Cheyu, Appl. Phys. Lett. 16, 214 (1970).

10. J. P. E. Taran, M. Charpenil, and R. Borghi, AIAA 6th Fluid and Plasma Dynamics Conference AIAA Paper No. 72-622, Palm Springs, California, 1973.

TABLE I

FLOW CHARACTERISTICS OF D_2-CO_2 LASER

Mach number	2
Plenum pressure	53 Torr
Cavity pressure	11 Torr
dc Discharge:	
Voltage	3 kV
Current	0.8 A
Power output	60 W
Peak small-signal gain	0.016/cm

TABLE II

COMPARISON OF D_2-CO_2 AND N_2-CO_2 LASER PERFORMANCE IN EDGDL

	N_2-CO_2	D_2-CO_2
Total flow rate (moles/sec)	1.11	1.29
Fractional molar composition:		
X_{He}	0.74	0.64
X_{CO}	0.05	0.06
X_{D_2}	....	0.32
X_{N_2}	0.21	....
Electrical efficiency	3%	2.5%
E/N ($V\text{-}cm^2$)	1.7×10^{-16}	1.0×10^{-16}

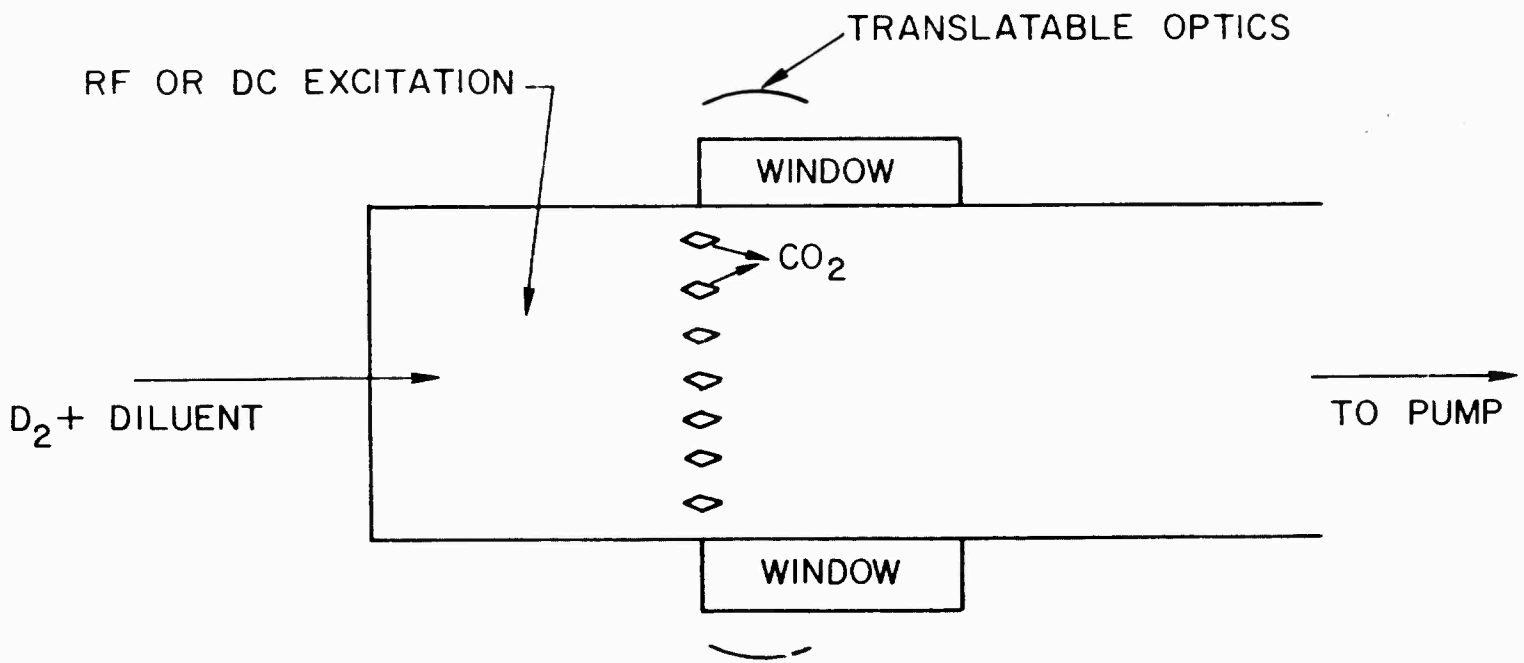

Fig. A1-1 — D_2-CO_2 electric discharge gas dynamic laser

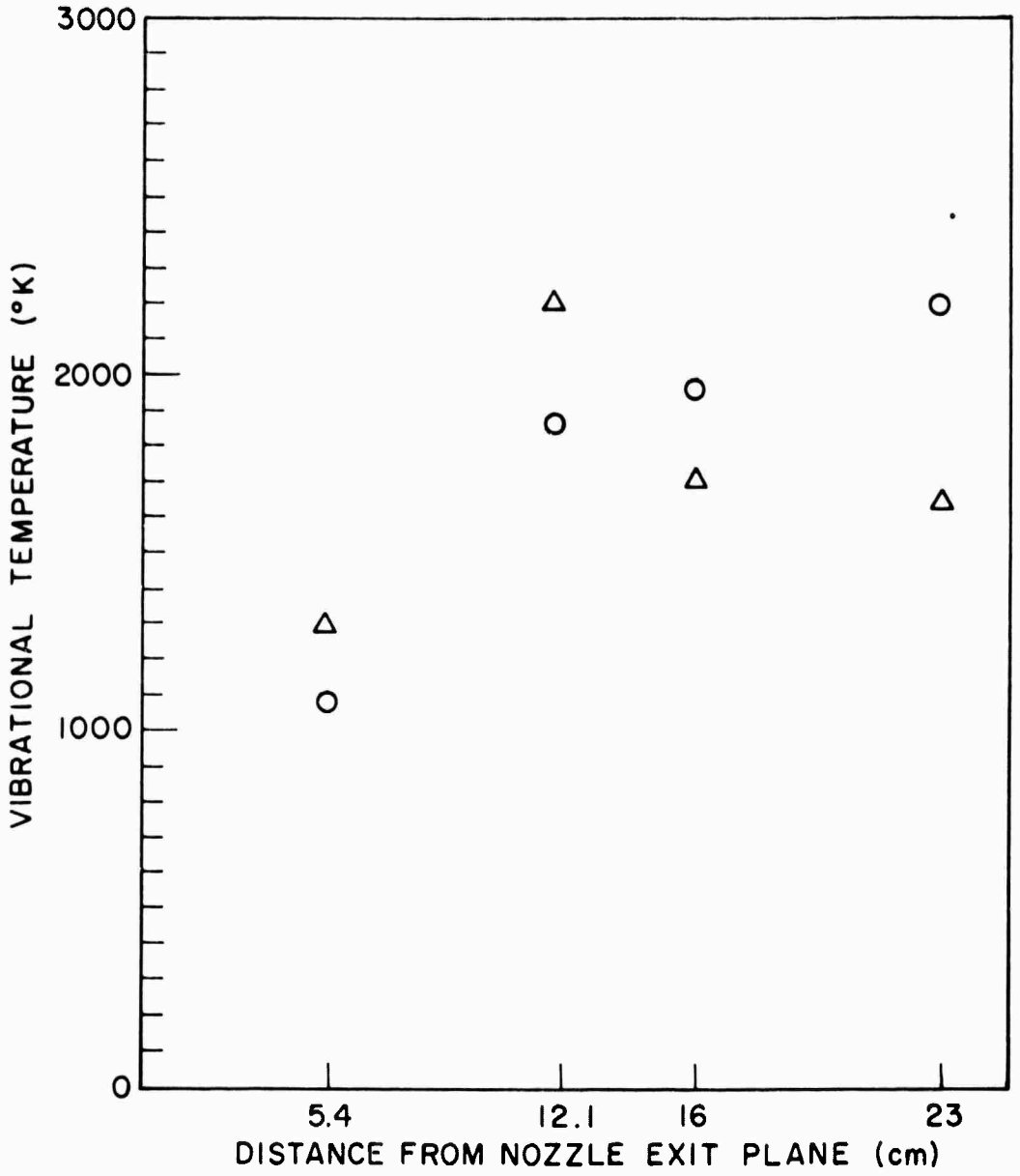

Fig. A1-2 — CO_2 (00°1) vibrational temperature vs. distance from the nozzle exit plane for both choked (Δ) and unchoked (0) cases

APPENDIX 2

CW $CO-CS_2$, $CO-C_2H_2$, AND $CO-N_2O$ ENERGY-TRANSFER LASERS*

J. A. Stregack, B. L. Wexler, and G. A. Hart†

Abstract

CW laser emission has been observed from CS_2 (11.5 μ), C_2H_2 (8 μ), and N_2O (10.6 μ) transitions pumped by energy transfer from vibrationally excited CO in an electric discharge gasdynamic laser device. Proposed energy-transfer pathways for these three lasers are described. Supersonic expansion cooling plays a critical role in depopulating the lower laser levels in the $CO-CS_2$ and $CO-C_2H_2$ systems. Maximum output powers measured for each of these systems are presented. The dependence of output power on the flow rate of the injected laser species is discussed.

---

*Work partially supported under DARPA Order No. 2062.

†NRC-NRL Postdoctoral Research Associate (1973-1975).

Several new electrically excited cw molecular lasers have been demonstrated in the NRL electric discharge gasdynamic laser (EDGDL) facility. The laser species are CS_2, C_2H_2, and N_2O which are excited via energy transfer from vibrationally excited CO produced by a glow discharge. All have been demonstrated previously as pulsed lasers using energy transfer from vibrationally excited CO which has been optically pumped by a frequency-doubled CO_2 laser.[1] N_2O has also been pumped by vibrationally excited CO produced by the reaction: $O + CS \rightarrow CO^{\dagger} + S$,[2] while CS_2[3,4] and C_2H_2[5] have been pumped by CO excited in an e-beam-sustained discharge. Based on the measured fast transfer rates from CO to CS_2, C_2H_2, and N_2O,[6] it appeared feasible to make cw lasers from these energy-transfer schemes as long as the populations of the lower laser levels could be reduced by fast vibration-transition (v-t) relaxation in a cold supersonic flow.

The operation of the EDGDL has been described in detail previously.[7] In the present experiments CO is premixed with He and is excited by a glow discharge in a subsonic plenum. This mixture is accelerated through an array of supersonic nozzles where the laser species is injected. Mixing, energy transfer, and lasing occur in the supersonic cavity region. Removing the laser species from the discharge region makes it possible to maximize the channeling of electrical energy into the long-lived vibrational mode of CO without encountering possible limitations imposed by the laser species (i.e., electron attachment, dissociation, etc.).

Figure 1 is a diagram of the relevant energy levels for the laser transitions as well as the energy for the first eight vibrational transitions in CO. Both CS_2 and C_2H_2 have a lower laser level energy of approximately 700 cm^{-1} and therefore have a thermal population which is 3.5% of the ground state at 300 K. The cooling effect of the supersonic expansion reduces this ratio to 0.6% at 200 K (the approximate translational temperature measured in the EDGDL when it has operated on CO_2) which aids in creating or enhancing any population inversion.

The results reported are for laser operation at a fixed location 14 cm downstream of the nozzle exit plane. Flow conditions for the highest-power output for each of the laser systems are summarized in Table I. A detailed parametric study of these energy-transfer laser systems (plenum pressure, energy deposition, output coupling, cavity location, etc.) will be reported elsewhere.

The CO-N_2O system was studied using a cavity consisting of a maximum-reflectivity dielectric mirror and a nominally 4% partially transmitting output mirror. Laser output was approximately three-quarters of the power obtained on either a N_2-N_2O or a N_2-CO_2 transfer laser run under similar flow rates and with similar energy deposition. The difference in N_2O laser performance is probably due to the fact that more N_2 ($v \rightarrow v-1$) transitions have energies within kT of N_2O ($00^{o}1$) than do CO transitions.

These preliminary experiments on N_2O transfer lasers were performed at less than optimum output coupling. The laser therefore operated at conditions far from laser threshold. This enables some

comparisons to be made of the potential of N_2O lasers pumped by N_2O, CO, and D_2. The experiments on D_2-N_2O were reported previously[7] and compare unfavorably to either the N_2-N_2O or CO-N_2O lasers.

For the CO-CS_2 laser experiments both a 2% partially transmitting mirror and a maximum-reflectivity mirror with a 0.5-mm hole were used as output couplers. The 0.5-mm hole gave a geometric output coupling of approximately 0.1%. The variation of laser power with CS_2 flow rate is shown in Fig. 2. For the present flow conditions the 2% transmitting mirror gave the best performance. The laser would not operate with a 4% output coupler. From Fig. 2 it can be seen that for the present operating conditions the laser power drops to zero at a CS_2 flow rate of 47 mmoles/sec. This is the result of a "choking" effect caused by excess secondary flow injection.[7] This is not a fundamental limitation and can be overcome by redesigning the secondary injection scheme and/or by increasing the mass flow in the primary gas stream. The CS_2 laser operates near 11.5 μm and most probably occurs between the $(00^{0}1)$ and $(10^{0}0)$ levels in CS_2 but could also occur between the $(01^{1}1)$ and $(11^{1}0)$ levels.[3]

The CO-C_2H_2 experiments were performed using the maximum-reflectivity mirror with the 0.5-mm hole as the laser output coupler. The laser operates on the $(0100^{0}0^{0})$-$(0000^{0}1^{1})$ band at wavelengths slightly above 8 μm. Figure 3 gives laser power versus C_2H_2 flow rate. Note that because of the reflectivity and nonselectivity of the output mirror, the laser operates as a CO laser (for low C_2H_2 flow rates). CO laser power decreases and eventually ceases as vibrational energy

is transferred from CO to C_2H_2. Because the lower laser level in C_2H_2 is also near the ground state, lasing terminates when excessive secondary flow "chokes" the flow and raises the temperature.

Spectral regions of laser action were determined by bandpass filters and confirmed by a monochromator with low resolution. The gases used were all commercial-grade (98% purity), while the CS_2 was vaporized from analytical reagent-grade liquid. Because of the purity of the gases, laser performance could possibly be affected by impurities. In fact, it was observed in the CO-C_2H_2 tests that both CO and C_2H_2 lasing power decreased as the pressure in the gas cylinders dropped. This is possibly due to the deleterious effect of $Fe(CO)_5$[8] which is present in the bottles and which will increase in molar concentration as the bottle pressure decreases. In addition, C_2H_2 is bottled with acetone as a stabilizer. Acetone has a strong absorption band centered at 8.2 μm which could also affect the observed C_2H_2 laser performance.

Operation of the lasers reported here, in addition to the D_2-CO_2 and D_2-N_2O lasers previously reported, demonstrates the potential and versatility of the EDGDL technique.

The authors wish to thank T. McClelland and C. Kyle for their technical assistance, J. Kent Hancock for discussions of vibrational transfer rates and suggestions of potential transfer lasers, and H. Kildal, T. F. Deutsch, F. O'Neill, W. Whitney, and L. Nelson for discussions of their results prior to publication.

References

1. H. Kildal and T. F. Deutsch, Appl. Phys. Lett. 27, 500 (1975).

2. A. B. Peterson and C. Wittig, Chem. Phys. Lett. 32, 274 (1975).

3. L. Y. Nelson, C. H. Fisher, and S. R. Byron, Appl. Phys. Lett. 25, 517 (1974).

4. F. O'Neill and W. T. Whitney (private communication).

5. L. Nelson (private communication).

6. J. K. Hancock, D. F. Starr, and W. H. Green, J. Chem. Phys. 61, 3017 (1974).

7. J. A. Stregack, B. L. Wexler, and G. A. Hart, Appl. Phys. Lett. 27, 670 (1975).

8. R. E. Center, J. Appl. Phys. 44, 3538 (1973).

TABLE I

FLOW CONDITIONS FOR HIGHEST POWER OUTPUT FOR EACH SYSTEM

Laser species	N_2O	CS_2	CS_2	C_2H_2
Fractional molar composition				
X_{He}	0.86	0.85	0.83	0.85
X_{CO}	0.11	0.13	0.15	0.13
X_{lasant}	0.03	0.02	0.02	0.02
Plenum pressure (Torr)	88	129	116	127
Cavity pressure (Torr)	6.2	8	7.8	7
Output coupling	4%	hole (~0.1%)	2%	hole(~0.1%)
Power ouput	3.8 W	130 mW	460 mW	100 mW

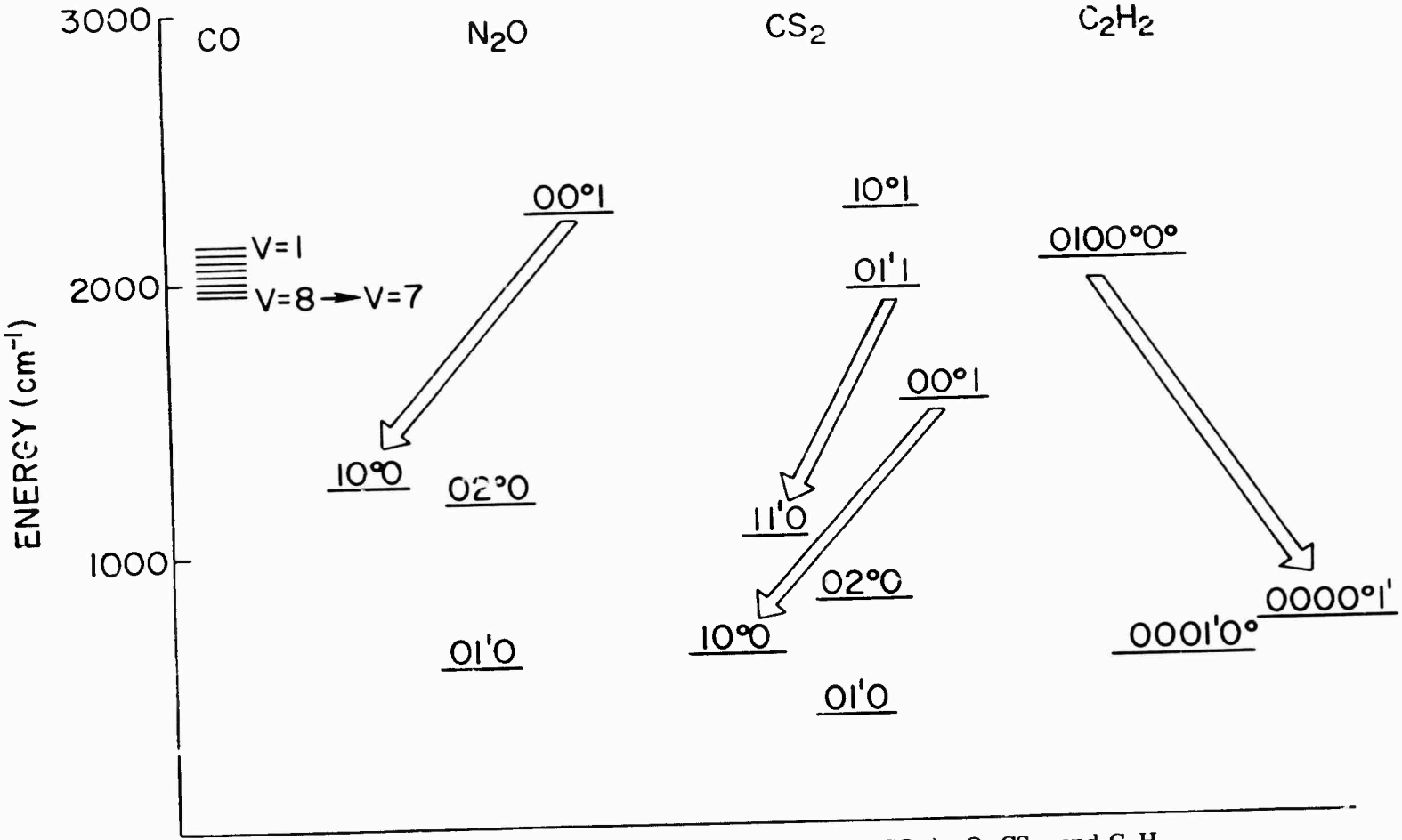

Fig. A2-1 — Partial vibrational energy level diagram for CO, N_2O, CS_2, and C_2H_2

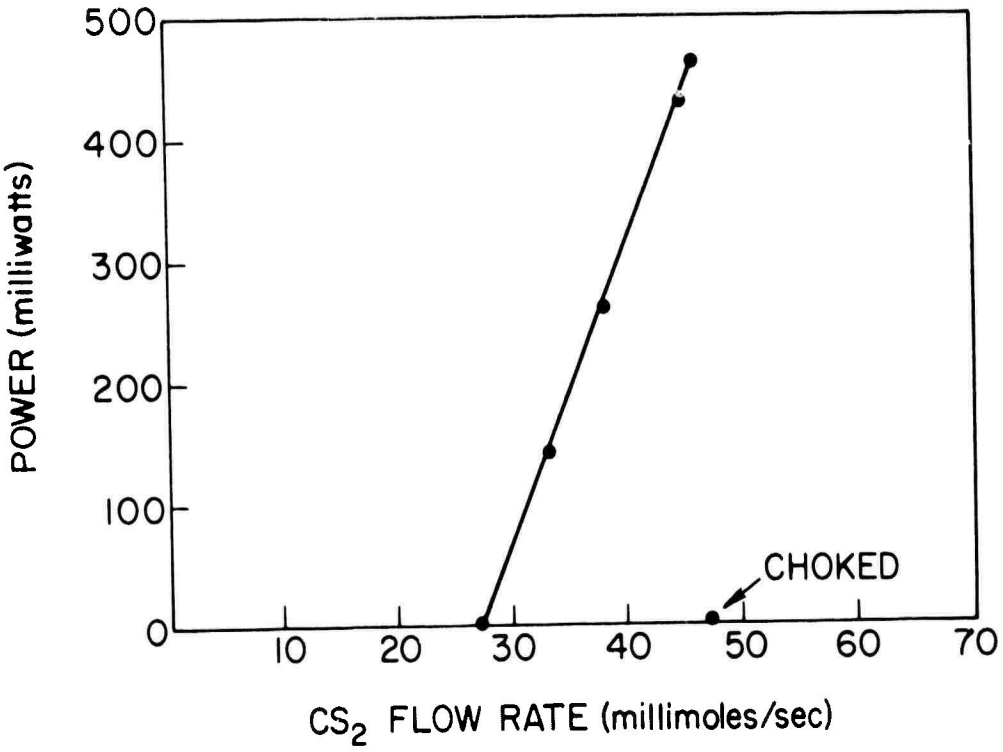

Fig. A2-2 — Laser power vs. CS_2 flow rate for 2% output coupling, 290 mmole/sec CO flow and 1600 mmole/sec He flow. The "choked" condition results from excess CS_2 secondary flow injection causing a loss of supersonic cooling.

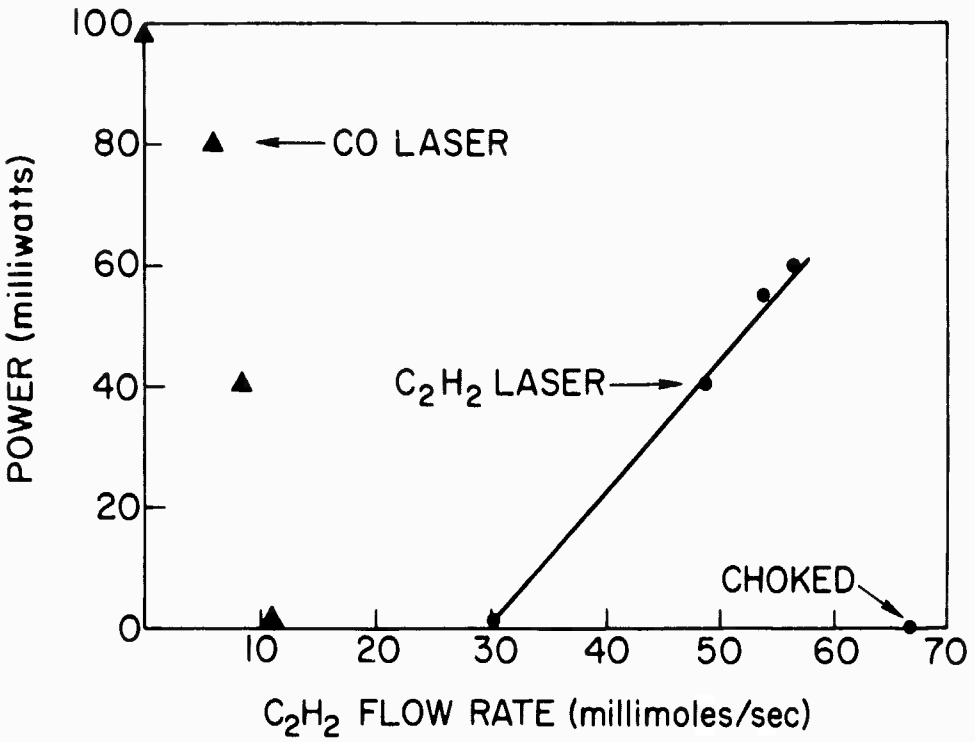

Fig. A2-3 — Laser power vs. C_2H_2 flow rate for 0.1% output coupling, 340 mmole/sec CO flow and 2180 mmole/sec He flow. At C_2H_2 flow rates below 12 mmole/sec the device functions as a CO laser. The "choked" condition results from excess C_2H_2 secondary flow injection causing a loss of supersonic cooling.

APPENDIX 3

XeBr EXCIPLEX LASER*

S. K. Searles

Abstract

Laser emission from the recently discovered XeBr exciplex laser was investigated as a function of the partial pressures of Xe and Br_2. An optical loss process appears to limit high-pressure operation.

---

*Work was supported in part by DARPA.

In a previous publication Searles and Hart reported the first observation of laser emission from a rare-gas monohalide species.[1] The evidence for the XeBr laser action was restricted to a specific Xe-Br_2 mixture at 1 atm total pressure. Our study of the XeBr laser has been continued in an attempt to achieve higher power and efficiency by varying the reagent concentrations. The following advantages of the XeBr laser made it worthy of the further investigation reported here. The XeBr exciplex[2] has an unbound lower laser level and emits at short wavelengths (high quantum efficiency) in contrast to XeF and XeCl lasers.[3-5] Moreover, absorption of laser radiation at 282 nm by Br_2 is negligible.[6]

The experimental apparatus was similar to the one described in references 1 and 7. A 433 kV electron beam was used to deliver a 50-ns-long pulse containing ≃ 55 J of energy to the target gas. 2.8 J of energy was deposited in the gas per cm atm[8] over a volume element of 10 cm^3. Two normal-incidence fused silica windows were used on the laser cell along the optical axis. A low-loss optical cavity was formed by two external > 99.8% R dielectric mirrors. The mirror spacing was 30.5 cm. Thus the maximum number of amplifying passes during the electron beam pulse time was 50.

The relationship between laser emission, fluorescence intensity, and pressure is shown in Fig. 1. The laser operated over a limited pressure range 380-760 Torr. The most interesting feature of the pressure dependence is the high-pressure cutoff. There should be a sufficient population of XeBr* to achieve laser emission at 1280 Torr

in most of the mixtures according to the intense fluorescence signals. Normally the fluorescence of a bound-free transition is a direct measure of the optical gain because the lower laser level population is negligible. For the present case any mixture displaying an emission level greater than a photodiode signal of 26 V, the minimum level for which laser action was recorded, should lase. The absence of stimulated emission at higher pressures where spontaneous emission is strong can be explained if a pressure-dependent loss process becomes important at pressures greater than 1 atm. An optical loss in the gaseous medium would not be apparent in side emission but would profoundly affect the near-threshold laser operation.

Xe_2^* is a plausible candidate for the optical absorber because the nonobservation of laser emission at high pressure is independent of the bromine concentration. Also the Xe_2^* concentration rises dramatically between 760 and 1280 Torr. The fraction of Xe* which undergoes the termolecular dimerization process to Xe_2^* relative to the desired reaction with bromine increases linearly with pressure. Consequently, the generation of Xe_2^* increases with the square of the pressure. Such a nonlinear increase could explain the absence of laser action at 1280 Torr although the apparent gain is 20% greater than at 760 Torr in one case.

The near-threshold nature of the laser referred to earlier is evidenced in Figs. 2 and 3. In Fig. 2 the laser power is seen to be a sensitive function of the electron-beam pump power. The exponential increase of laser power with pumping intensity indicates that

substantially higher laser power and efficiency would be obtained with more powerful electron-beam devices. However, an approximately 10^4 improvement is needed for the laser to be competitive with the XeF laser.[4,5]

A typical laser pulse shown in Fig. 3 also demonstrates the near-threshold characteristics. First, the emission is not apparent until 20 ns after the fluorescence has begun. This delay is the time required for the growth from spontaneous emission to observable laser emission on the oscillogram. The growth time was calculated from the gain of 22%/pass determined from a log plot of normalized laser amplitude versus time. The fluorescence source term was taken to be 35 kW/cm^3. The source term was derived from the calibrated detection system.[8] Second, the laser emission rose until pumping terminated. Clearly, a longer pumping pulse would have generated a more intense laser pulse.

In conclusion, we believe that the XeBr laser can be made to lase much more efficiently by a modest increase in pumping power. However, it is doubtful that this laser will ever compete with the XeF laser.[4,5]

References

1. S. K. Searles and G. A. Hart, Appl. Phys. Lett. 27, 243 (1975).

2. By definition an exciplex is an excited complex with an unbound ground state. An exciplex is formed by two different species in contrast to an excimer.

3. J. J. Ewing and C. A. Brau, Appl. Phys. Lett. 27, 350 (1975).

4. C. A. Brau and J. J. Ewing, Appl. Phys. Lett. 27, 435 (1975).

5. E. R. Ault, R. S. Bradford, and M. L. Bhaumik, Appl. Phys. Lett. 27, 413 (1975).

6. A. A. Passchier, J. D. Christian, and N. W. Gregory, J. Phys. Chem. 71, 938 (1967).

7. G. A. Hart and S. K. Searles, J. Appl. Phys. 47, 2033 (1976).

8. S. K. Searles and G. A. Hart, Appl. Phys. Lett. 28, 384 (1976).

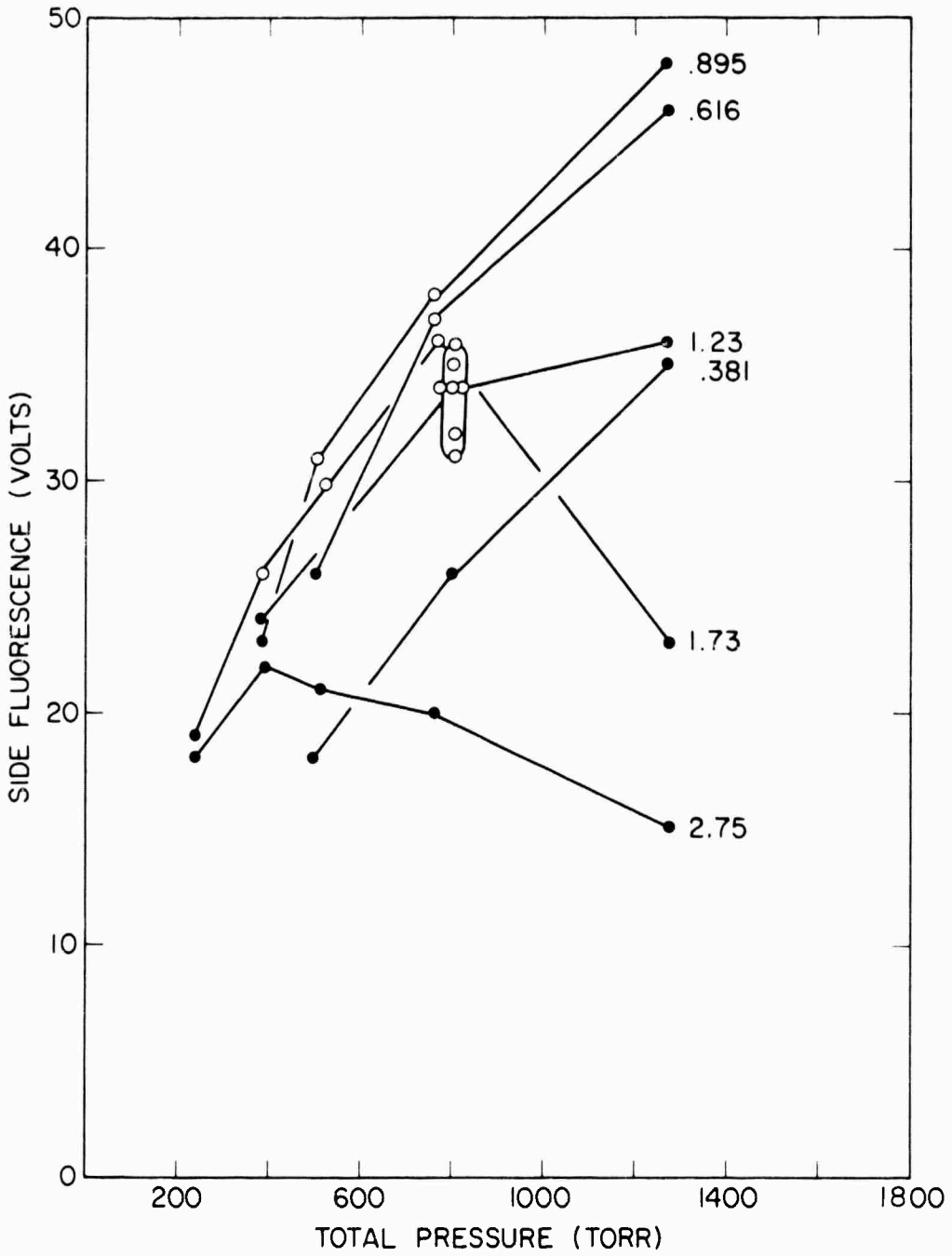

Fig. A3-1 — Relationship between the fluorescence, total pressure, and laser emission as a function of the indicated bromine percentage. Open circles show laser emission while solid circles show absence of laser emission. The laser intensity was quite variable owing to the near-threshold nature of the emission. Peak power ~ 200 W.

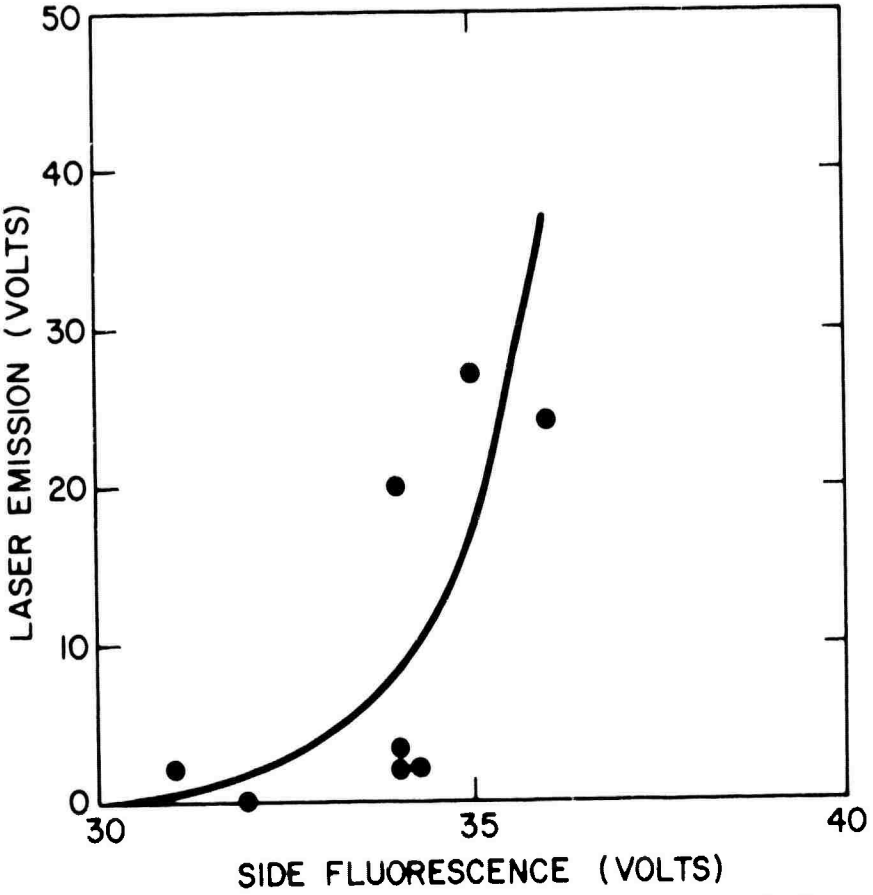

Fig. A3-2 — Dependence of laser emission on variation of the side fluorescence caused by adjustment of the electron-beam intensity. Total pressure 760 torr, 1.23% Br_2.

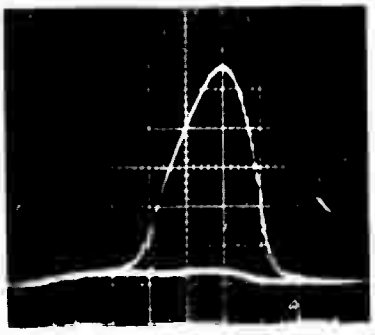

Fig. A3-3 — Typical laser pulse shown with fluorescence background from a previous shot. Time scale: 10 ns/div.

APPENDIX 4

XENON FLUORIDE LASER EXCITATION BY TRANSVERSE ELECTRIC DISCHARGE

R. Burnham*

Science Applications Incorporated, Alexandria, VA 22202

N. W. Harris and N. Djeu

Abstract

Stimulated emission has been produced in mixtures of He, NF_3, and Xe at total pressures between 300 and 1000 Torr. Laser emission was on lines at 3511 and 3531 Å which have been associated with the excited XeF molecule. Excitation of the gas mixture was by a transverse electric discharge which produced pulses with peak currents of approximately 10^4 A and rise times of 20 ns. A maximum laser energy of 7 mJ was obtained from a gas mixture with a ratio of He:Xe:NF_3 of 98.0:1.5:0.5 at a total pressure of 300 Torr.

---

*Work performed in the Laser Physics Branch, Naval Research Laboratory, Washington, D. C. 20375

Recent studies[1,2] of the new class of excimers, the rare-gas monohalides, have led to the very rapid development of high-power lasers operating in the near ultraviolet in at least four of the species.[3,4] To date, lasers in KrF and XeF have produced the highest powers and efficiencies.[5,6] Heretofore, however, these lasers have been obtained only under excitation by electron beams or in electron-beam-sustained discharges.[7] We report here the demonstration of laser action at 3511 and 3531 Å in XeF excited in a transverse electric discharge.

Stimulated emission was obtained in mixtures of He or Ne, Xe, and NF_3 at total pressures between 300 and 1000 Torr excited in a pulsed transverse discharge device similar in design to those commonly used for excitation of lasers on the second positive transitions of N_2.[8] The discharge cell had an active length of 1 m with electrodes made of two band saw blades separated by approximately ½ in. The device was powered by a fast capacitor-dumping circuit which had a storage capacity of up to 10 J. The maximum electric current through the discharge was of the order of 10 kA and the rise time of the discharge pulse was 20 ns. Spectra of the laser pulses showed two components, a stronger line at 3511 Å and a weaker line at 3531 Å. Laser emission was not observed when either NF_3 or Xe was omitted from the gas mixture in the discharge.

Figure 1 shows the performance of the laser for a variety of gas mixtures. The data shown were all taken with He as the major constituent of the mixtures. Comparable performance was obtained when Ne was

substituted for He. The use of argon in the discharge led to severe arcing and laser emission was never observed. Figure 1(a) shows the laser output energy as a function of the mole fraction of Xe in the gas mixture for several concentrations of NF_3. These data show that the maximum laser energy was generally obtained with gas mixtures containing two to three parts Xe to one part NF_3. The decrease in laser energy at higher concentrations of Xe may have been due either to the increase in importance of reaction channels which compete with the formation of the excited molecular state, XeF* (e.g., production of Xe_2^*) or to the effect of higher concentrations of Xe on the conditions of the discharge. It is felt that the latter effect was more important since arcing in the discharge was observed visually for concentrations of Xe above 10%.

Figure 1(b) shows the pulse energy of the laser as a function of the mole fraction of NF_3. These data were taken with a constant ratio of the concentrations of Xe to NF_3 of 2.5 to 1. The decrease in the laser energy for concentrations of NF_3 beyond 0.5% may be attributable to either of the processes mentioned above or to collisional deactivation of XeF* by NF_3. Further studies of the kinetics of formation of the excited molecular state in the discharge as well as studies of the performance of the transverse discharge in the gas mixtures used here are planned.

The total pressure in the discharge at which maximum energy was obtained from the laser varied between 300 and 600 Torr, and depended on the mole fraction of NF_3 in the mixture. However, it was found that

the partial pressure of NF_3 in the discharge cell at which the maximum laser energy was obtained remained constant at about 1 Torr. The most stable operation of the laser was obtained with a pulse repetition rate of about 1 Hz with the gas mixture flowing slowly through the discharge cell. The average pulse energy from the laser was found, however, to decrease rapidly if the pulse repetition rate was increased while the gas flow rate was held constant. Increasing the gas flow rate allowed the pulse repetition rate to be raised from 1 to 10 Hz with no decrease in the average pulse energy. With the discharge cell sealed, the laser energy was found to diminish after about ten shots. We have, however, under conditions of low flow rates produced double and triple laser pulses of equal energy separated by time intervals of 1 ms. It is felt that the decrease in the output of the laser with high repetition rates resulted from depletion of the NF_3 in the gas mixture due to reaction of free fluorine produced in the discharge with materials in the cell.

The time development of a typical laser pulse is shown in Fig. 2. Plotted is the sum of the laser signal from a vacuum photodiode and a voltage proportional to the time derivative of the current in the discharge. The time interval between the maximum and minimum of the current derivative gives the pulse width of the discharge current. The laser pulse may be seen to have a half-width of about 20 ns and to arise only near the end of the current pulse. The delay in the onset of the laser emission indicates that the laser was near threshold for superradiant emission. The limiting process which delays the onset

of laser oscillation has not been identified, but may be either the rate of production of Xe metastables in the discharge, or the rate of reaction of the Xe metastables with NF_3 to form XeF*. The maximum energy was obtained from the laser with an optical cavity composed of a total reflector and an output mirror having a reflectivity of approximately 35% at 3530 Å. Although superradiance was occasionally observed with only the total reflector in place, use of the output coupler increased the laser power by an order of magnitude and decreased the divergence of the beam. The maximum pulse energy obtained from the laser was 7 mJ which corresponded to a peak pulse power of 700 kW. The overall efficiency of the laser based on the energy stored in the charging capacitors was about 0.1%.

An estimate of the ultimate performance which should be obtainable from the XeF laser using excitation by transverse electric discharge may be made from a comparison of the energy emitted by the XeF laser to the energy emitted by an N_2 laser at 3371 Å produced in the same apparatus. Using the discharge device described above we have obtained laser pulses of 2.0 mJ at 3371 Å in N_2 and energies up to 3.5 mJ from N_2 with approximately 1% additive of SF_6. It appears, therefore, that the efficiency obtainable from the XeF laser should be significantly higher than that of the N_2 laser. The results of the present study indicate the feasibility of developing in XeF, and other rare-gas monohalides, lasers of higher efficiency and average power than are presently available in the visible or ultraviolet regions of the spectrum.

References

1. J. E. Valazco and D. W. Setser, J. Chem. Phys. 62, 1991 (1975).

2. J. J. Ewing and C. A. Brau, Phys. Rev. A 12, 129 (1975).

3. S. K. Searles and G. A. Hart, Appl. Phys. Lett. 27, 243 (1975).

4. J. J. Ewing and C. A. Brau, Appl. Phys. Lett. 27, 350 (1975).

5. G. C. Tisone, A. K. Hays, and J. M. Hoffman, Proceedings of the Second Annual Conference on Electronic State Lasers (unpublished).

6. E. R. Ault, R. S. Bradford, and M. L. Bhaumik, Appl. Phys. Lett. 27, 413 (1975).

7. J. A. Mangano and J. H. Jacob (unpublished).

8. Peter Schenck and Harold Metcalf, Appl. Opt. 12, 94 (1973).

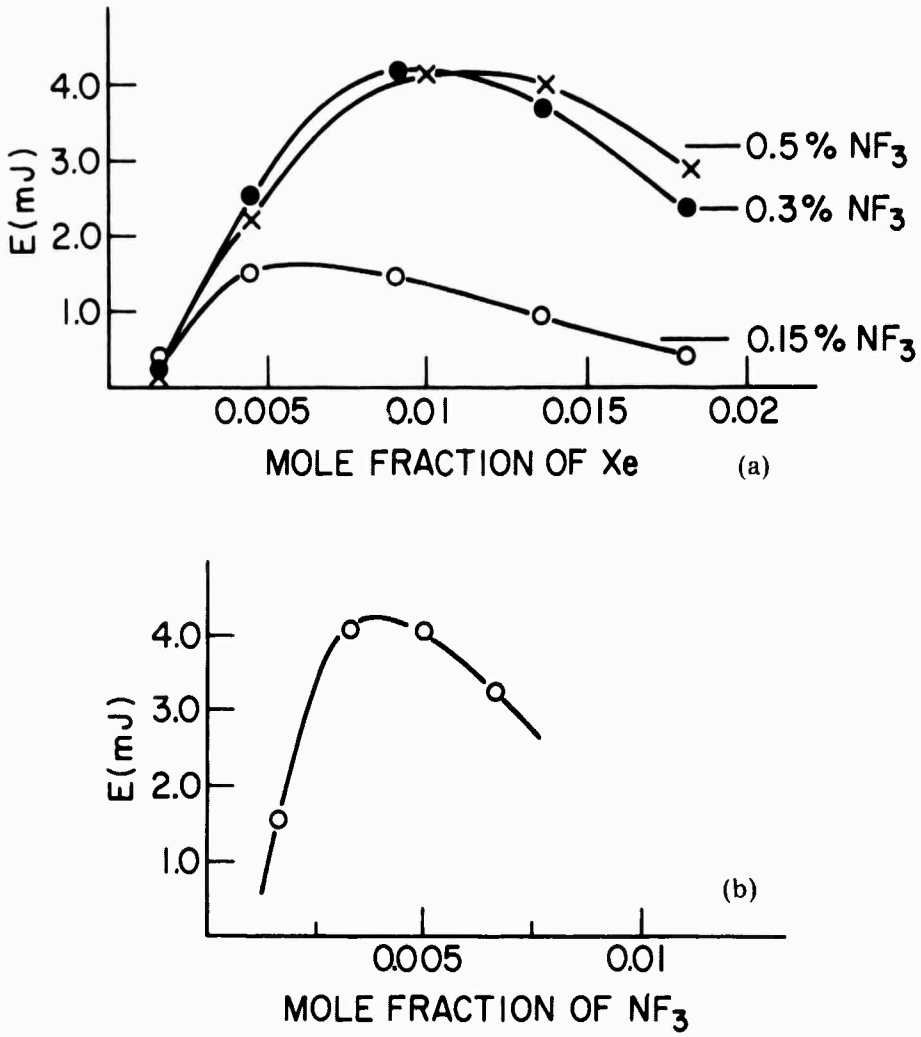

Fig. A4.1 — (a) Pulse energy from the XeF laser at 3511 and 3531 Å vs. concentration of Xe in the gas mixtures for several concentrations of NF_3. The major constituent of the gas mixtures was He. (b) Laser energy vs. concentration of NF_3 for a constant ratio of the concentrations of He to NF_3 of 2.5:1.

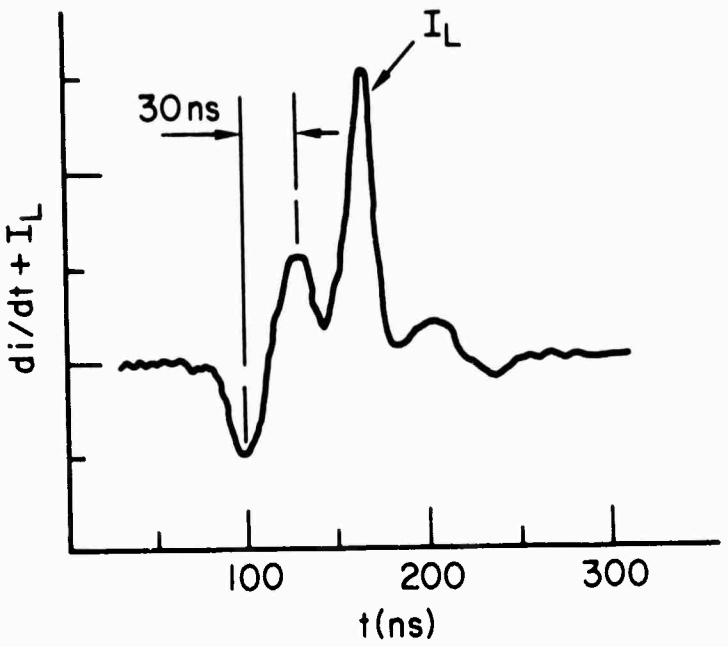

Fig. A4-2 — Discharge current derivative (di/dt) and laser power (I_L) vs. time

APPENDIX 5

TRANSVERSE DISCHARGE METAL VAPOR LASER*

B. L. Wexler

Metal vapor lasers employing transitions from resonance to metastable levels offer high theoretical efficiency. In spite of extensive work however, particularly on the copper vapor laser, reported efficiencies have fallen well short of a target of 5-10%. There also exists a number of atoms with suitable level structure in which lasing has not been reported.

In an effort to explore more efficient devices and to discover new metal vapor lasers, a heatable transverse discharge system with short, fast-rising pulses and high discharge current has been constructed. The transverse discharge geometry should offer significant advantages in scalability and high pressure operation as well. The present device, a schematic of which is shown in Fig. 1, is a flanged, stainless steel enclosure. A row of pins passes through concentric tubing in the top flange to a continuous cathode rod, 3 mm diameter by 20 cm long. Quartz tubes, insulating the pins from the concentric stainless tubes, are joined to a quartz shroud inside the enclosure. In this way the cathode is electrically shielded from the stainless steel enclosure, except for the floor of the box, a raised ridge of which serves as the anode. The discharge volume is 20 cm long, 2.0 cm

high (cathode-anode separation) and 1.25 cm wide. The discharge cell may be heated to 500°C, with the windows and low inductance coaxial lines extending outside of the oven. Depending on the associated circuitry, current rise times as short at 10 ns have been measured, with pulse widths of 20 ns FWHM. Peak current of 10 kiloamps into the 25 cm^2 area parallel to the laser axis have been measured. Since the working temperature of the device is not sufficient for the required metal vapor densities, two thyratron-switched discharges are employed with the tube containing an appropriate metal halide.(1) The discharge circuitry is based on that for a nitrogen laser published by Schenck and Metcalf.(2)

The fast rise time of the discharge is most suitable for investigations of thallium, lead, and a number of other metals with very fast resonance to metastable lifetimes. However, because of the high interest and practical importance of the copper vapor laser, experiments to date have involved only CuCl in the discharge. Previous work in CuCl has involved current rise times extending well beyond the laser pulse, while the highest efficiency will require short discharge pulses. Experiments to date have used helium, neon, or argon as the buffer gas, with neon giving the best results.

With non-optimized cavity configurations, laser output peak powers of 11 kW and total pulse energy of 100 μJ have been measured using an ITT F4018 photodiode and neutral density filters. Laser pulse widths have been observed to vary from 8 to 50 ns depending on operating conditions, and laser output has been observed with neon

pressures of 6 to 100 torr. The laser power is observed to drop as the buffer gas pressure increases from 10 to 100 torr, in conflict with results reported recently by Piper[3] for a larger transverse discharge device. This effect may be due to flashover of the discharge along the quartz liner, in which case enlarging the width of the discharge region should result in a significant improvement in laser output and efficiency. Recent evidence[4] also indicates that in spite of the use of a very large dissociation pulse energy, increasing the energy of the first pulse may be necessary for optimum higher pressure operation using CuCl.

References

*Work supported in part by DARPA.

1. C. J. Chen, N. M. Merhem and G. R. Russell, Appl. Phys. Lett. 23, 514 (1973

2. P. Schenck and H. Metcalf, Appl. Opt. 12, 183 (1973).

3. J. A. Piper, Opt. Comm. 14, 296 (1975).

4. G. R. Russell, private communication.